LUND UNIVERSITY

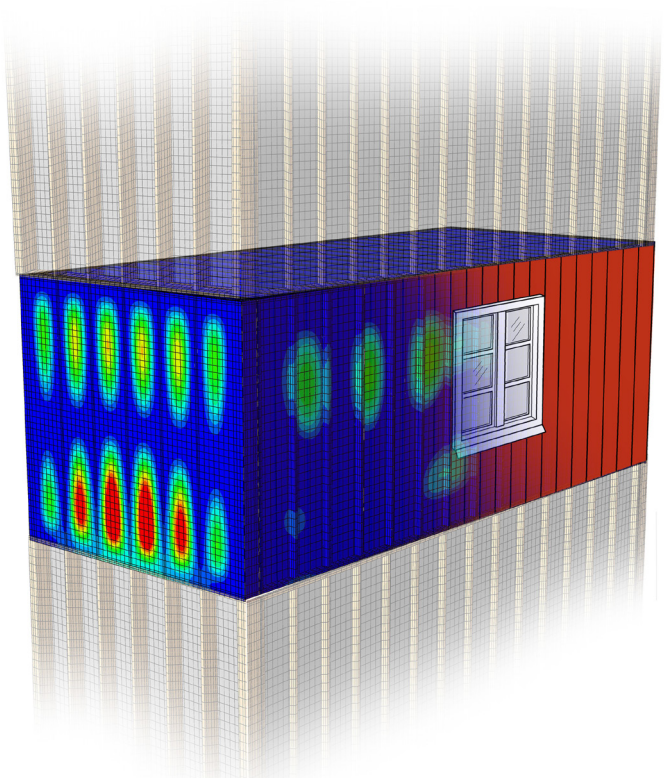

VIBRATIONS IN LIGHTWEIGHT STRUCTURES
Efficiency and Reduction of Numerical Models

OLA FLODÉN

Structural Mechanics

Licentiate Dissertation

DEPARTMENT OF CONSTRUCTION SCIENCES

DIVISION OF STRUCTURAL MECHANICS

ISRN LUTVDG/TVSM--14/3073--SE (1-129) | ISSN 0281-6679

ISBN 978-91-7473-807-0 (print) | 978-91-7473-808-7 (Pdf)

LICENTIATE DISSERTATION

VIBRATIONS IN LIGHTWEIGHT STRUCTURES

Efficiency and Reduction of Numerical Models

OLA FLODÉN

Printed by Media-Tryck LU, Lund, Sweden, January 2014 *(Pl)*.

For information, address:

Div. of Structural Mechanics, LTH, Lund University, Box 118, SE-221 00 Lund, Sweden.
Homepage: http://www.byggmek.lth.se

Acknowledgements

The work presented in this dissertation was carried out at the Department of Construction Sciences at Lund University. The financial support provided by the Silent Spaces project, a part of the EU program Interreg IVA, is gratefully acknowledged.

I would like to thank my supervisors Prof. Göran Sandberg and Ph.D. Kent Persson for their support and guidance during the course of my work and express my gratitude to Mr. Bo Zadig for his great help in the design of certain figures included in the dissertation. I would also like to thank the staff at the Department of Construction sciences for all the entertaining discussion during coffee breaks (and occasionally working hours), covering a wide range of topics such as football, coffee powder and the work rate of Spanish people.

Last but certainly not least, I would like to thank my family, especially my parents Kristina and Ingvar for all of their support during my life and the ups and downs in my eight years here in Lund, and Tiffany for turning a down into an up during the last year.

Lund, January 2014

Ola Flodén

Abstract

Multi-storey wood buildings have been increasing in popularity since a century-old ban on the construction of such buildings was lifted in 1994. Compared to conventional concrete structures, it is more difficult to build lightweight structures in such a way that noise and disturbing vibrations is avoided. To design buildings of high performance regarding sound and vibrations, it is desirable to have tools for predicting the effects of structural modifications prior to construction. The long-term aim of the studies presented in the dissertation is to develop such tools by means of numerical models.

Accurately assessing the dynamic behaviour of multi-storey wood buildings requires use of models representing the geometry in considerable detail, resulting in very large models which easily exceed the limits of computer capacity, at least for computations to be performed within reasonable time. It is therefore desirable to avoid unnecessarily detailed models, while at the same time describing the phenomena of interest accurately. Moreover, the computational efficiency of the models can be improved by employing model order reduction, reducing the size and computational cost of the models without affecting the accuracy appreciably. A common way of employing model order reduction is through substructure modelling, in which full finite element models are divided into smaller parts, or substructures, that are reduced in size and assembled to form reduced global models.

The dissertation includes an investigation into the effect of modelling acoustic media inside cavities of multi-storey wood buildings on the transmission of structural vibrations. Air and insulation inside cavities were modelled as acoustic media in different ways and the resulting finite element models were compared. It was concluded that the acoustic media in cavities close to the source of vibration affect the vibration transmission and that it, therefore, has to be included in the models to some extent.

Furthermore, the efficiency of different methods for reducing substructure models of multi-storey wood buildings are discussed in the dissertation. Comparisons of different methods for model order reduction, applied to substructures of buildings, showed that the frequently employed method of component mode synthesis by Craig & Bampton and the increasingly popular Krylov subspace methods result in efficient reduced order models. In order to improve the efficiency of the reduced order models, interface reduction can be employed. Different methods for interface reduction were found to be the most efficient ones for the interface surfaces of wood components and elastomer materials. Elastomer are used at junctions in wooden buildings in order to reduce the vibration transmission.

Contents

Part I

Introduction and overview of the work

1 Introduction

In 1994, a century-old ban on the construction of wooden buildings more than two storeys in height in Sweden was lifted, leading to the reintroduction of such buildings. The use of wood as a construction material has many advantages, the lightweight properties of wood, for example, reducing the material transportation costs involved and the size of the foundations needed [1]. In addition, the energy consumption which occurs during the construction and the lifecycle of wooden buildings is lower than that of concrete buildings of comparable size [2]. At the same time, however, it is more difficult to build lightweight structures in such a way that noise and disturbing vibrations in the different storeys and rooms are avoided. The vibrations can be caused by, for example, footsteps, airborne sound, vibrating machines and external sources such as railway and road traffic. To design buildings of high performance regarding noise and disturbing vibrations, it is desirable to have tools for predicting the effects of structural modifications prior to construction. Testing prototypes and performing experiments is both time-consuming and expensive, a time and cost effective alternative being to employ numerical models as prediction tools.

Multi-storey wood buildings are often constructed using prefabricated planar or volume elements, often with use of low-stiffness panels mounted on high-stiffness beams. Accurately assessing the dynamic behaviour of these elements when rather high vibration frequencies are involved requires use of models representing the geometry in considerable detail. Having established the models, approximate solutions can be sought employing numerical methods such as the finite element (FE) method. Assembling the individual elements of multi-storey wood buildings within the framework of global models of entire buildings results in very large numerical models, easily exceeding the limits of computer capacity, at least for computations to be performed within reasonable time. The computational efficiency of the numerical models can be improved by employing model order reduction (MOR), reducing the size and the computational cost of the models without affecting the accuracy appreciably.

1.1 Aim of research

The long-term goal is to improve the comfort for residents of multi-storey wood buildings regarding noise and disturbing vibrations. To accomplish this, numerical prediction tools for low-frequency vibrations in such buildings will be developed for use in the design process of the buildings.

The research presented in this dissertation aims at providing knowledge in the process of developing numerical prediction tools. Specifically, the goal is to determine whether or not air and insulation inside cavities of multi-storey wood buildings have to be considered in the numerical models. Moreover, it is investigated how the numerical models can be reduced in size in an efficient manner by comparing different methods for reducing the models.

1.2 Outline

The dissertation is divided into two parts:

In **Part I**, an overview of the dissertation is presented, the aim being to provide a background to the research carried out, present the governing theory and summarise the results obtained in the appended papers. In Chapter 2, it is motivated how the research presented in this dissertation contributes to fulfilling the long-term aim of the project. An overview of the construction of multi-storey buildings in wood is provided and the issues related to noise and disturbing vibrations in such buildings are discussed. In Chapter 3, the FE method, employed here to develop numerical models for the analysis of vibrations in multi-storey wood buildings, is presented. The FE formulation is derived both in the structural domain and in the acoustic fluid domain and it is described how the domains can be coupled. In Chapter 4, the governing theory and some basic concepts in structural dynamics, important for understanding the dynamic behaviour of structures, are presented. The methodology of substructuring, employed here for reducing the size of the FE models, is discussed in Chapter 5. In Chapter 6, the investigations presented in the appended papers are summarised, and in Chapter 7, the conclusions of the research are discussed and further developments suggested.

Part II compiles the three appended papers. In Paper A, an investigation into the effect of modelling air and insulation inside cavities of multi-storey wood buildings is presented. In Paper B, the efficiency of a wide range of MOR methods, applied to substructure FE models of lightweight building structures, is investigated, and in Paper C, the accuracy of different methods for reducing the interfaces of the substructure models are compared.

2 Vibrations in multi-storey wood buildings

In this chapter, the aim is to provide a background to the research presented in the dissertation and to motivate its contributions to the development of prediction tools for vibrations in multi-storey wood buildings. An overview of the construction of multi-storey buildings in wood is presented and the issues related to noise and disturbing vibrations in such buildings are discussed. Moreover, the numerical modelling employed for creating the prediction tools is discussed.

2.1 Building in wood

In 1874, a ban on the construction of wooden buildings more than two storeys in height was introduced in Sweden following a number of urban fires. The ban was maintained for over a century before being lifted in a revision of the building regulations in 1994, leading to the reintroduction of such buildings. In a publication by the Swedish government in 2004 [3], the use of wood as a construction material is promoted, presenting a vision of wood being a natural choice of material for constructions, primarily in Sweden where it is a plentiful resource, but also in the rest of Europe in a longer perspective. Wood is attractive as construction material because of a number of economical and environmental reasons, many related to its lightweight properties. For example, the use of wood as construction material lowers the costs involved in transportation and assembling, as compared to conventional concrete buildings, and can reduce the loads on the foundations by up to 50 % [1]. The environmental advantages of employing wood as construction material were illustrated in [2], where it was found that the energy consumption occurring during the construction and the lifecycle of wooden buildings is lower than that of concrete buildings of comparable size. Moreover, the lightweight properties of wood makes it suitable as construction material for prefabrication of planar and volume elements. Prefabrication has a number of advantages, such as, more time- and cost-effective assembling, better conditions for construction workers, less material waste and lessened sensitivity to weather conditions.

When multi-storey wood buildings re-entered the market in the mid 1990s, research related to such constructions was inadequate. Standards and technical solutions developed for heavier buildings were initially employed also for wooden buildings due to a lack of knowledge and experience [1]. A problematic issue was the one of noise and vibrations, as the dynamic behaviour of lightweight buildings and heavier constructions is fundamen-

tally different. Only frequencies above 100 Hz were considered in standards regulating the noise induced by impact loads, a limitation yielding acceptable sound pressure levels in heavier construction, which are less sensitive to low frequency vibrations. In lightweight buildings, however, the sound isolation is generally poor at low frequencies (20-200 Hz) [4], leading to important information being neglected when designing the buildings according to the standards. The Swedish standards have been updated since, nowadays involving frequencies above 50 Hz. Still, no reliable prediction tools for analysing the issue of low-frequency vibrations in lightweight buildings exist [4], the design of such buildings relying on experience from previous constructions and empirical studies. Testing prototypes and performing experiments is time-consuming and expensive, motivating the need for prediction tools based on numerical calculations.

2.1.1 Wood as construction material

Wood is a natural material, its mechanical properties depending on the way trees grow. Every season, the stem grows outwards, adding a new layer of fibres directed in the lengthwise direction of the stem. This results in a cylindrical orthotropic material structure, having different properties in the different directions as the fibres are much stiffer in the longitudinal direction compared to the radial and tangential directions. In engineering applications, however, the cylindrical structure is usually neglected, employing a transversally isotropic material description where isotropy is assumed in the plane transverse to the fibres. The specific strength, defined as strength divided by density, is high in the fibre direction of wood, as compared to other construction materials such as concrete [5], explaining why wood is referred to as a lightweight material. Wood is often utilised in the form of engineered wood products, structural components manufactured by gluing smaller components. Examples of such products are glue laminated beams, consisting of a number of glued wood beams, and particle boards, created by pressing wood chips or saw dust together with glue under high heat and pressure. Compared to raw sawn timber, engineering wood products have the advantages of creating more homogeneous components, making use of more of the raw material and enabling components of arbitrary size to be produced. They are, however, more expensive to manufacture and have a lower specific strength compared to raw sawn timber.

2.1.2 Construction of wooden buildings

Three main types of building systems can be identified for multi-storey wood buildings [1]:

Column-beam system
Framework of massive timber components.

Plate system
Plate components made of massive wood laminates.

Wood frame system
Low-stiffness panels mounted on frames of high stiffness beams.

The assemblage of a building can be performed by different methods, varying in the degree of prefabrication involved. Three main categories can be identified [1]:

On-site construction
Complete assembling procedure performed at construction site.

Prefabricated planar elements
Industrially produced planar elements assembled at construction site.

Prefabricated volume elements
Industrially produced volume elements assembled at construction site.

Following the update of the Swedish building regulations in 1994, the multi-storey wood buildings were initially constructed on-site, primarily in the form of traditional column-beam systems. However, a trend towards a higher degree of prefabrication has been observed [1], its popularity increasing due to the many advantages compared to on-site construction. The research presented in this dissertation is therefore focused on prefabricated wooden buildings, special care being given to so-called timber volume element (TVE) buildings.

Timber volume element buildings

The conceptual layout of a TVE building is illustrated in Figure 2.1 and a TVE prior to transportation to the construction site is shown in Figure 2.2. A TVE is a prefabricated volume module consisting of wood framed floor-, roof- and wall-elements, each TVE typically constituting a small apartment, one room or part of a larger room. As much of the construction work as possible is performed indoors at a factory, including electrical installations, flooring, cabinets, wardrobes etc. The prefabricated modules are transported to the construction site where they are stacked to form a complete building. In between the TVEs, several elastomer blocks are introduced to reduce vibrations travelling between different storeys as well as rooms. Each elastomer block has an interface area of approximately 0.1×0.1 m^2 and is placed between the walls of two stacked modules. The only additional connection between modules is through a number tie plates, ensuring the global stability of the building. Vibrations transmitted in TVE buildings are, therefore, mainly passing through the elastomer layers or through the air and insulation in cavities of the buildings. Consequently, the vibration transmission in TVE buildings is, to a great extent, controlled by the properties of the elastomer blocks.

2.2 Vibration transmission

Vibrations in buildings can be caused by many different types of sources, such as, footsteps, speakers, vibrating machines or external sources like railway and road traffic. Both the vibrations themselves as well as the sound they induce can cause annoyance for residents. The transmission of vibrations between different storeys and rooms can be divided into two types based on the source of vibration, namely, airborne sound transmission and structure-borne sound transmission [7]. The former involves vibrations caused by sound

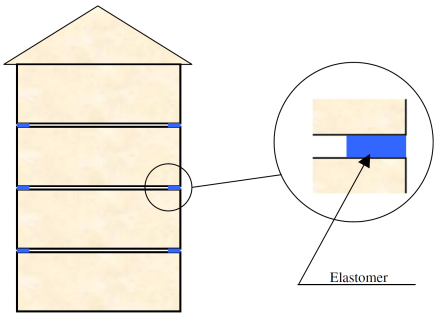

Figure 2.1: Illustration of the TVE building system and the elastomer blocks separating the modules [6].

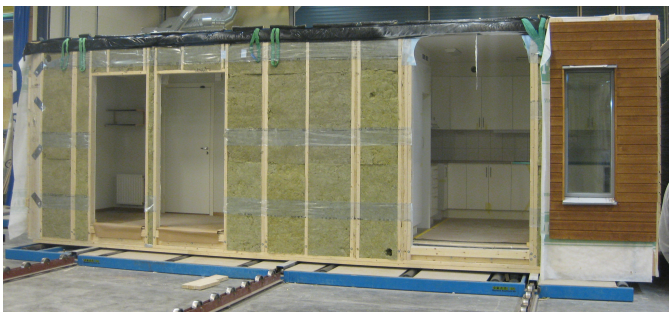

Figure 2.2: A TVE ready for transportation to the construction site.

sources, the latter describing vibrations generated by direct excitation of the structure. The two types of sound transmission are illustrated in Figure 2.3, showing also the possible paths for the transmitted sound and vibrations. The paths can be separated into two types; direct paths, where the sound passes from one room to another directly through a panel, and flanking paths, where the structural vibrations propagate through one or more junctions before reaching the receiver room. The flanking transmission of sound can cause noise in storeys and rooms far away from the source, this being an issue mainly for low-frequency sound as high-frequency vibrations dampen faster.

The annoyance for residents in multi-storey buildings, caused by noise and disturbing vibrations transmitted between different storeys and rooms, can be viewed as a consequence of the following factors:

Load spectrum
Different loads excite a building with varying levels of energy at different frequencies. Speakers, for example, generate vibrations at a wide range of frequencies while vibrating machines typically generate vibrations at specific frequencies.

Sensitivity of buildings
The vibration amplitudes in different parts of a building, caused by a given load, depends on the buildings sensitivity to vibrations at different frequencies. If the load excites the building with high levels of energy at frequencies for which the building is more sensitive to vibrations, it will result in vibrations of high amplitude.

Human perception
Sound and vibrations in residential buildings are, naturally, not a problematic issue until perceived as annoying for residents. The human perception of noise and vibrations in lightweight buildings is not yet quite understood. It is, however, believed that vibrations at very low frequencies, below the 50 Hz limit existing in the Swedish building regulations today, can contribute to annoyance [8].

To design a building perceived as comfortable regarding sound and vibrations, knowledge concerning all of the three aforementioned factors is important. The properties of the loads and the human perception are inputs to the design process while the sensi-

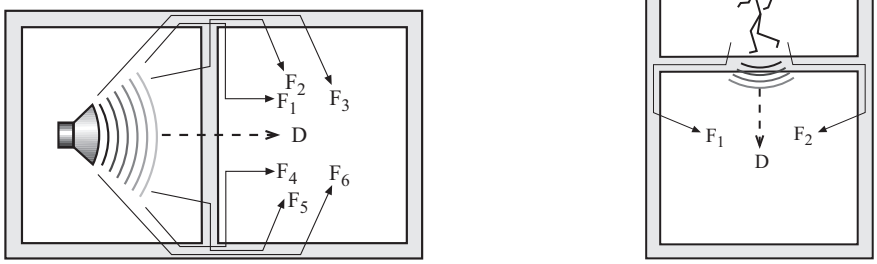

(a) Airborne sound transmission.

(b) Structure-borne sound transmission.

Figure 2.3: Illustration of the two different types of sound transmission in buildings and the possible transmission paths. Direct transmission paths are denoted by 'D' and flanking transmission paths by 'F_i'.

tivity of a building is a consequence of the design itself. Because of the sensitivity of lightweight buildings to low-frequencies vibrations, some sort of technical solution is required to handle the issue, such as, including insulation in panels to reduce the direct sound transmission or involving elastomer layers in junctions to reduce the flanking transmission. The elastomer layers have proved successful in reducing vibrations, but there is room for further improvements [8]. Optimising a technical solution requires a way of predicting its effects, motivating the need for reliable prediction tools.

2.3 Numerical prediction tools

The long-term aim of the research presented in this dissertation is to improve the design of multi-storey wood buildings so that noise and disturbing vibrations can be reduced. To achieve this, numerical tools will be developed in order to predict the effect of structural modifications of the buildings.

The procedure of establishing a numerical model is illustrated in Figure 2.4. The first step in predicting the behaviour of a structure is to establish a mathematical model describing the physical phenomena of interest, often by boundary value differential equations. Having established the mathematical model, an approximate solution can be sought by employing numerical methods that discretise the mathematical model, resulting in a numerical model. Depending on the complexity of the mathematical model and the extent of the discretisations involved, the resulting numerical model can be too large for computations to be performed within reasonable time. The computational efficiency of the model can, in such situations, be improved by employing MOR to create a reduced order model.

A prediction model frequently employed for vibration transmission in buildings is statistical energy analysis (SEA) [7]. In SEA, the structure is represented by a number of coupled subsystems and statistical assumptions are made regarding the flow of kine-

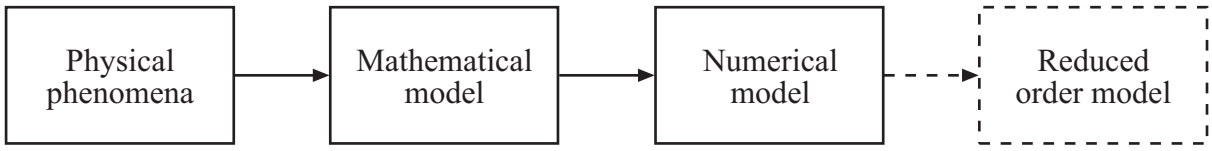

Figure 2.4: The procedure of establishing a numerical model.

matic energy between subsystems. The method is, however, developed for heavy and homogeneous structures, such as concrete buildings, and can in general not be applied to lightweight structures [4]. Moreover, SEA does not take detailed information of the subsystems into consideration and the method is therefore ill-suited for predicting the effect of structural modifications. In order to establish reliable prediction tools for vibrations in lightweight buildings, an alternative methodology has to be adopted. The periodicity of structures within multi-storey wood buildings requires use of methods allowing the geometry to be modelled in a detailed manner. A suitable method is by this means the FE method.

2.3.1 Finite element modelling

The FE method, described in detail in Chapter 3, is a numerical method offering the possibility of calculating approximate solutions for mathematical models of structures having arbitrary geometries. Employing FE models as prediction tools for vibrations in multi-storey wood buildings implies the models to be representing the dynamic characteristics of real buildings accurately, requiring validation of the models by comparisons to measurements. An example of comparisons between analyses of FE models and measurement data can be found in [9], investigating the low-frequency vibrations in a wooden floor-wall structure in terms of FE modelling and full-scale measurements; experimental setup and simulation results being shown in Figure 2.5. Acceptable correlation between the FE model and measurement data was found for the lowest eigenmodes of the system.

In structural dynamic analysis, the FE method is primarily applicable for low-frequency vibrations. The size of the models increases when the response of the buildings is requested

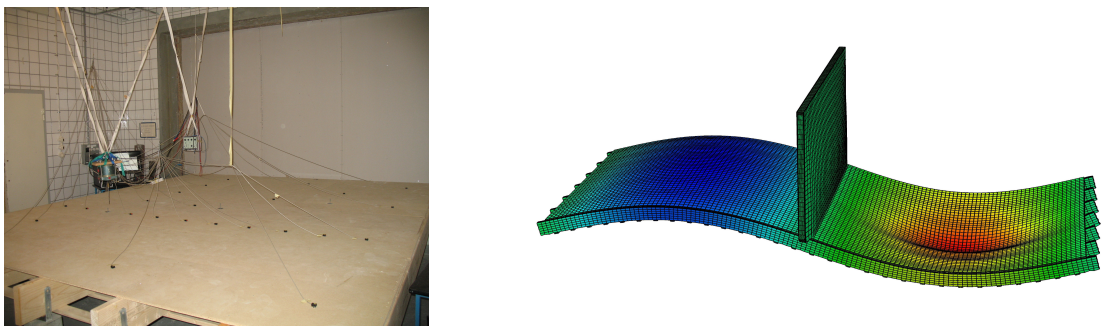

(a) Experimental setup.

(b) Simulation results.

Figure 2.5: Experimental setup and simulation results of the FE model employed in the investigations of a wooden floor-wall structure in [9].

for higher frequencies. Smaller details in the geometry become more important and the geometric discretisation involved in the FE modelling has to be finer in order to resolve the shorter wavelengths. It is a challenging task to model the smaller details in an accurate manner, and for frequencies over a certain limit, it becomes practically impossible to perform the analyses due to the extensive size of the resulting FE models.

The size of the FE models is an issue also for the analyses of vibrations at lower frequencies as fine geometric discretisations are required compared to static analyses. Moreover, large geometries have to be involved in case the transmission of vibrations between distant parts of a building is studied. It is, therefore, important to consider how unnecessarily large models can be avoided. There are a number of issues to be dealt with in achieving this, for example deciding:

- whether or not it is valid to assume linear behaviour, i.e. small deformations and linear material descriptions.
- how many storeys and rooms of the complete building to involve in the model.
- which of the structural components to model in detail and which structures to replace with simplified models, e.g. replacing a wood-framed wall panel with a homogeneous plate.
- if the nails and glue joining structural components has to be modelled in detail or if the interfaces can be regarded as fully connected.
- how fine the discretisation of the geometry has to be.
- if the vibrations transmitted through the air and insulation inside cavities is of importance.

The last of these issues is discussed in Paper A, investigating the effect of modelling air and insulation inside cavities of TVE buildings on the vibration transmission. The air and the insulation are modelled as acoustic media and models including the acoustic media inside cavities in different ways are compared to a model without acoustic media.

By carefully considering issues such as the ones mentioned above, a FE model describing the dynamics of a building can be constructed without including unnecessary information, resulting in the model being as small as possible without a loss of accuracy. The model can, however, still be too large for computations to be performed within reasonable time. In case a model is too large, its computational efficiency can be improved by employing MOR, reducing the size and computation time of the model to the greatest possible extent without affecting the accuracy of the approximate solution appreciably.

2.3.2 Substructure modelling

The MOR is, in this project, performed by employing substructure modelling, described in detail in Chapter 5. Substructure modelling is based on a division of the full geometry into a set of substructures, the FE models of these being reduced in size and coupled to form a reduced global model.

Substructure modelling provides a flexible and practical framework for structural dynamic analysis, enabling a combination of full models and reduced order models of substructures. Furthermore, it is possible to involve experimental substructures in the global model, these being described by frequency response functions obtained from measurements.

As aforementioned, multi-storey wood buildings usually involve elastomer layers. These offer a natural selection for making the substructure division. In spite of their relatively small sizes, the elastomer layers provide the major part of the contact between structural components in the buildings. In TVE buildings, specifically, the large volume modules are coupled by a number of small elastomer blocks, making it natural to consider each TVE as a substructure. Most of the MOR methods available in the literature require the models to be frequency-independent. The elastomer materials possess frequency-dependent properties [10] and, for this reason, they are not involved within the substructures, instead serving as coupling elements.

Many MOR methods are available in the literature and the computational efficiency of the reduced order models will of course depend on the choice of method. In Paper B, the computational efficiency of a wide range of MOR methods, when applied to FE models of lightweight building structures, is compared. Moreover, the efficiency of the reduced order models depends on the size of the interface surfaces connecting the substructures, large interfaces resulting in the reduced models being computationally inefficient. For this reason, it is important to limit the size of the interfaces and in case they are very large, it can be necessary to employ interface reduction. The accuracy of a number of methods for interface reduction is compared in Paper C, employing the methods for the interfaces between elastomer blocks and wooden building structures of the type found in TVE buildings. Furthermore, the development of efficient coupling elements, replacing the elastomer blocks, is presented in Paper C.

3 Finite element method

Various problems encountered in a wide range of engineering fields are described by boundary value differential equations, originating from different types of balance laws. These are often practically impossible to solve analytically, numerical methods therefore being employed in order to calculate approximate solutions. The FE method is an example of such a method, used for problems involving, for example, heat conduction, electromagnetics or solid mechanics. The FE method approximates the sought field variables through a division of the geometric domain into elements, assuming the variables to vary according to some shape functions, usually polynomials of various degrees, within each element. The field variables are discretised into a number of dofs, defined at nodes of the elements, the shape functions being used for interpolating the variables between the nodes. The elements and nodes, defined in the domain of interest, form an FE mesh, its size determining the size of the resulting system of equations. A very fine mesh, i.e. small elements, results in a good approximation of the field variables at the expense of obtaining a large discretised system. Employing the FE method involves a consideration for the practising engineer, weighing the accuracy of the approximations to the computational cost of the model.

In this chapter, an FE formulation for the dynamics of a three-dimensional linear elastic solid is derived. Two equivalent formulations of the problem, the strong and weak formulations, are presented before arriving at the FE formulation. Moreover, an FE formulation for a coupled structure-acoustic system is derived, involving the coupling between an elastic solid and an acoustic fluid. For a more detailed derivation of the FE method, see for example [11, 12]. The derivations in this chapter follow the notation employed in [12].

3.1 Strong formulation

By considering Newton's second law of motion for the continuum formulation of a solid, the differential equation of motion, for a body occupying the domain Ω, can be obtained as [13]

$$\tilde{\boldsymbol{\nabla}}^T \boldsymbol{\sigma} + \mathbf{b} = \rho \frac{\partial^2 \mathbf{u}}{\partial t^2}, \tag{3.1}$$

$$\tilde{\boldsymbol{\nabla}}^T = \begin{bmatrix} \frac{\partial}{\partial x} & 0 & 0 & \frac{\partial}{\partial y} & \frac{\partial}{\partial z} & 0 \\ 0 & \frac{\partial}{\partial y} & 0 & \frac{\partial}{\partial x} & 0 & \frac{\partial}{\partial z} \\ 0 & 0 & \frac{\partial}{\partial z} & 0 & \frac{\partial}{\partial x} & \frac{\partial}{\partial y} \end{bmatrix}, \quad \boldsymbol{\sigma} = \begin{bmatrix} \sigma_{xx} \\ \sigma_{yy} \\ \sigma_{zz} \\ \sigma_{xy} \\ \sigma_{xz} \\ \sigma_{yz}, \end{bmatrix}, \quad \mathbf{b} = \begin{bmatrix} b_x \\ b_y \\ b_z \end{bmatrix}, \quad \mathbf{u} = \begin{bmatrix} u_x \\ u_y \\ u_z \end{bmatrix}, \tag{3.2}$$

where $\boldsymbol{\sigma}$ is the vector representation of the stress tensor, $\mathbf{b}$ and $\mathbf{u}$ are the body force and displacement vectors, respectively, ρ is the mass density and t is the time. If the deformations of the body are assumed to be small, the vector representation of the strains are given by

$$\boldsymbol{\epsilon} = \begin{bmatrix} \epsilon_{xx} & \epsilon_{yy} & \epsilon_{zz} & \epsilon_{xy} & \epsilon_{xz} & \epsilon_{yz} \end{bmatrix}^T = \mathbf{D}\tilde{\boldsymbol{\nabla}}\mathbf{u}, \tag{3.3}$$

where $\mathbf{D}$ is the constitutive matrix. Moreover, if linear elastic material behaviour is assumed, the stresses are given by

$$\boldsymbol{\sigma} = \mathbf{D}\boldsymbol{\epsilon} = \mathbf{D}\tilde{\boldsymbol{\nabla}}\mathbf{u}. \tag{3.4}$$

A surface traction $\mathbf{t}$ acts on the boundary of Ω, $\partial\Omega$, and is related to the stresses according to

$$\mathbf{t} = \begin{bmatrix} t_x \\ t_y \\ t_z \end{bmatrix} = \begin{bmatrix} \sigma_{xx}n_x + \sigma_{xy}n_y + \sigma_{xz}n_z \\ \sigma_{xy}n_x + \sigma_{yy}n_y + \sigma_{yz}n_z \\ \sigma_{xz}n_x + \sigma_{yz}n_y + \sigma_{zz}n_z \end{bmatrix}, \tag{3.5}$$

where n_x, n_y and n_z are the components of the boundary normal vector $\mathbf{n}$, pointing outwards from $\partial\Omega$. Boundary conditions has to be assigned at $\partial\Omega$, prescribing the displacement and surface traction according to

$$\begin{aligned} \mathbf{u} &= \mathbf{u}_{bc} \qquad \text{on } \partial\Omega_u, \\ \mathbf{t} &= \mathbf{t}_{bc} \qquad \text{on } \partial\Omega_t, \end{aligned} \tag{3.6}$$

where $\mathbf{u}_{bc}$ and $\mathbf{t}_{bc}$ are known quantities on $\partial\Omega_u$ and $\partial\Omega_t$, separated parts of the boundary adding up to the complete boundary $\partial\Omega$. Eq. (3.1) in combination with Eq. (3.6) constitute the strong formulation, stating a fully defined problem in three-dimensional solid mechanics.

3.2 Weak formulation

The FE method is a variational method and the weak formulation, based on the use of test functions, is introduced in order to derive the FE formulation. Starting from Eq. (3.1), the first step in obtaining the weak formulation is to pre-multiply the equation with the vector of arbitrary weight functions $\mathbf{v}$ and integrate over the region Ω, resulting in

$$\int_\Omega \mathbf{v}^T \left(\tilde{\boldsymbol{\nabla}}^T \boldsymbol{\sigma} + \mathbf{b} - \rho \frac{\partial^2 \mathbf{u}}{\partial t^2} \right) \mathrm{d}V = 0, \tag{3.7}$$

$$\mathbf{v}^T = \begin{bmatrix} v_x & v_y & v_z \end{bmatrix}. \tag{3.8}$$

Applying Green-Gauss theorem to the first term in the integral results in

$$\int_\Omega \mathbf{v}^T \tilde{\boldsymbol{\nabla}}^T \boldsymbol{\sigma} \mathrm{d}V = \int_{\partial\Omega} \mathbf{v}^T \mathbf{t} \mathrm{d}S - \int_\Omega (\tilde{\boldsymbol{\nabla}} \mathbf{v})^T \boldsymbol{\sigma} \mathrm{d}V, \tag{3.9}$$

and an insertion of this expression into Eq. (3.7) gives

$$\int_\Omega \mathbf{v}^T \rho \frac{\partial^2 \mathbf{u}}{\partial t^2} \mathrm{d}V + \int_\Omega (\tilde{\boldsymbol{\nabla}} \mathbf{v})^T \boldsymbol{\sigma} \mathrm{d}V = \int_{\partial\Omega} \mathbf{v}^T \mathbf{t} \mathrm{d}S + \int_\Omega \mathbf{v}^T \mathbf{b} \mathrm{d}V, \tag{3.10}$$

which is the weak formulation of the problem subject to the boundary conditions in Eq. (3.6), the prescribed surface tractions being inserted in the integral equation.

3.3 Finite element formulation

So far, no approximations of Eq. (3.1) have been introduced, the strong and weak formulations being equivalent descriptions of the problem. In the FE formulation, however, the displacements are approximated by

$$\mathbf{u} = \mathbf{N}\mathbf{a}, \tag{3.11}$$

with the matrix $\mathbf{N}(x, y, z) \in \mathbb{R}^{3 \times n}$ containing the global shape functions, used to obtain the displacement field by interpolating the nodal displacements $\mathbf{a}(t) \in \mathbb{R}^{n \times 1}$, n being the number of nodal displacements. Adopting Galerkin's method, the shape functions $\mathbf{N}$ are employed also for the arbitrary weight functions

$$\mathbf{v} = \mathbf{N}\mathbf{c}, \tag{3.12}$$

$\mathbf{c}$ being an arbitrary constant vector. Inserting Eqs. (3.4), (3.11) and (3.12) into Eq. (3.10), using that $\ddot{\mathbf{a}}$ and $\mathbf{a}$ are independent of spatial coordinates and $\mathbf{c}$ is arbitrary, results in the FE formulation for a linear elastic solid

$$\int_\Omega \mathbf{N}^T \rho \mathbf{N} \mathrm{d}V \ddot{\mathbf{a}} + \int_\Omega (\tilde{\boldsymbol{\nabla}} \mathbf{N})^T \mathbf{D} \tilde{\boldsymbol{\nabla}} \mathbf{N} \mathrm{d}V \mathbf{a} = \int_{\partial\Omega} \mathbf{N}^T \mathbf{t} \mathrm{d}S + \int_\Omega \mathbf{N}^T \mathbf{b} \mathrm{d}V, \tag{3.13}$$

which can be rewritten in the more compact form

$$\mathbf{M}\ddot{\mathbf{a}} + \mathbf{K}\mathbf{a} = \mathbf{f}_l + \mathbf{f}_b, \tag{3.14}$$

$$\begin{aligned} \mathbf{M} &= \int_\Omega \mathbf{N}^T \rho \mathbf{N} \, \mathrm{d}V, & \mathbf{K} &= \int_\Omega (\tilde{\boldsymbol{\nabla}} \mathbf{N})^T \mathbf{D} \tilde{\boldsymbol{\nabla}} \mathbf{N} \, \mathrm{d}V, \\ \mathbf{f}_l &= \int_\Omega \mathbf{N}^T \mathbf{b} \, \mathrm{d}V, & \mathbf{f}_b &= \int_{\partial\Omega} \mathbf{N}^T \mathbf{t} \, \mathrm{d}S, \end{aligned} \tag{3.15}$$

where the mass matrix $\mathbf{M}$, the stiffness matrix $\mathbf{K}$, the body force vector $\mathbf{f}_l$ and the boundary force vector $\mathbf{f}_b$ have been introduced. The boundary conditions in Eq. (3.6) are imposed in Eq. (3.14) by prescribing an element in either $\mathbf{a}$ or $\mathbf{f}_b$ for the equations describing the equilibrium for the dofs at the domain boundary. The system obtained in Eq. (3.14) is a linear equation of motion of the form in Eq. (4.3). A damping matrix can be added to the system by employing, for example, Rayleigh damping, as described in Section 4.4.1.

3.4 Structure-acoustic analysis

Vibrating structures can interact with surrounding fluids, inducing acoustic pressure waves, and vice versa. For heavier structures, the influence of the acoustic pressure waves on the structural vibrations is usually negligible. It is, therefore, possible to analyse the acoustic pressure field by applying the structural displacements, obtained from a precedent analysis of the structural domain, as boundary conditions. For lightweight structures, however, it is more likely to have a two-way interaction between the domains, demanding simultaneous analyses of the domains to yield correct results.

The FE method can be employed also for analysing the acoustic pressure field in a fluid. By imposing conditions of continuity for the displacements and the pressures at boundaries separating the two domains, they can be coupled to form an interacting FE system of equations. In the derivations below, a subscript F is adopted for quantities in the acoustic fluid domain Ω_F, whereas the subscript S is used for quantities in the structural domain Ω_S, so that Eq. (3.14) is rewritten as

$$\mathbf{M}_S\ddot{\mathbf{a}}_S + \mathbf{K}_S\mathbf{a}_S = \mathbf{f}_{l,S} + \mathbf{f}_{b,S} = \mathbf{f}, \tag{3.16}$$

3.4.1 Acoustic fluid domain

In addition to the assumption of small displacements, the equations governing the acoustic fluid domain are derived assuming the fluid to be inviscid and irrotational. The motion of an acoustic fluid can be described using different primary variables, such as, the fluid displacement or a fluid displacement potential. In the FE formulation presented here, the acoustic pressure is used as primary variable. A detailed description of the FE formulation for an acoustic fluid and the structure-acoustic coupling can be found in for example [14]. The pressure field in an acoustic fluid is governed by the equation of motion

$$\rho_{0,F}\frac{\partial^2\mathbf{u}_F}{\partial t^2} + \boldsymbol{\nabla}p_F = 0, \tag{3.17}$$

and the continuity equation

$$\frac{\partial p_F}{\partial t} + \rho_{0,F}c_{0,F}^2\boldsymbol{\nabla}\cdot\frac{\partial\mathbf{u}_F}{\partial t} = 0, \tag{3.18}$$

where $\rho_{0,F}$ is the static density, $c_{0,F}$ is the speed of sound, p_F is the acoustic pressure and $\boldsymbol{\nabla}$ is the gradient operator. By differentiating Eq. (3.18) with respect to time and

inserting it in Eq. (3.17), the wave equation in the acoustic fluid domain is obtained as

$$\frac{1}{c_{0,F}^2}\frac{\partial^2 p_F}{\partial t^2} - \boldsymbol{\nabla}^2 p_F = 0. \tag{3.19}$$

Derivations corresponding to those for a linear elastic solid results in the FE formulation for an acoustic fluid

$$\mathbf{M}_F\ddot{\mathbf{p}}_F + \mathbf{K}_F\mathbf{p}_F = \mathbf{f}_{b,F}, \tag{3.20}$$

$$\begin{aligned} &\mathbf{M}_F = \frac{1}{c_{0,F}^2}\int_{\Omega_F} \mathbf{N}_F^T\mathbf{N}_F \,\mathrm{d}V, \quad \mathbf{K}_F = \int_{\Omega_F} (\boldsymbol{\nabla}\mathbf{N}_F)^T\boldsymbol{\nabla}\mathbf{N}_F \,\mathrm{d}V, \\ &\mathbf{f}_{b,F} = \int_{\partial\Omega_F} \mathbf{N}_F^T\mathbf{n}_F^T\boldsymbol{\nabla}p_F \,\mathrm{d}S, \end{aligned} \tag{3.21}$$

where $\mathbf{n}_F^T$ is the boundary normal vector, pointing outwards from the acoustic fluid domain.

3.4.2 Coupling of domains

At interfaces connecting an acoustic fluid domain and a structural domain, denoted $\partial\Omega_{SF}$, there will naturally be a continuity in displacement and pressure

$$\mathbf{u}_S\mathbf{n}_F = \mathbf{u}_F\mathbf{n}_F, \tag{3.22}$$

$$\boldsymbol{\sigma}_S|_{n_F} = -p_F, \tag{3.23}$$

where $\boldsymbol{\sigma}_S|_{n_F}$ is the stress normal to $\partial\Omega_{SF}$. By introducing the spatial coupling matrix

$$\mathbf{H}_{SF} = \int_{\partial\Omega_{SF}} \mathbf{N}_S^T\mathbf{n}_F\mathbf{N}_F \,\mathrm{d}S, \tag{3.24}$$

and using Eq. (3.17), the boundary force vectors, at $\partial\Omega_{SF}$, may be rewritten as

$$\mathbf{f}_{b,S} = \mathbf{H}_{SF}\mathbf{p}_F, \tag{3.25}$$

$$\mathbf{f}_{b,F} = -\rho_{0,F}\mathbf{H}_{SF}^T\ddot{\mathbf{a}}_S, \tag{3.26}$$

Introducing the coupling terms, Eq. (3.25) and Eq. (3.26), in the FE equation systems, Eq. (3.16) and Eq. (3.20), results in the coupled structure-acoustic system of equations

$$\begin{bmatrix} \mathbf{M}_S & \mathbf{0} \\ \rho_{0,F}\mathbf{H}_{SF}^T & \mathbf{M}_F \end{bmatrix} \begin{bmatrix} \ddot{\mathbf{a}}_S \\ \ddot{\mathbf{p}}_F \end{bmatrix} + \begin{bmatrix} \mathbf{K}_S & -\mathbf{H}_{SF} \\ \mathbf{0} & \mathbf{K}_F \end{bmatrix} \begin{bmatrix} \mathbf{a}_S \\ \mathbf{p}_F \end{bmatrix} = \begin{bmatrix} \mathbf{f}_{l,S} \\ \mathbf{0} \end{bmatrix} + \begin{bmatrix} \mathbf{f}_{b,S} \\ \mathbf{f}_{b,F} \end{bmatrix}, \tag{3.27}$$

where $\mathbf{f}_{b,S}$ and $\mathbf{f}_{b,F}$ contain contributions from the parts of the domain boundaries $\partial\Omega_S$ and $\partial\Omega_F$, respectively, that are separated from the interface boundary $\partial\Omega_{SF}$.

4 Structural dynamics

In this chapter, the aim is to provide a theoretical background to structural dynamics and introduces the concept of eigenfrequencies and eigenmodes of a system and the closely related phenomena of resonance for harmonic vibrations. Moreover, it is discussed how the dynamic behaviour of structures is affected by the introduction of damping. Only free vibration and the response to harmonic excitation are considered here as it is sufficient for providing a basic understanding. A dynamic load described by its time history can be Fourier transformed to obtain its frequency content and knowledge about the systems response to harmonic excitations can thereby be used to predict the response. The theory presented in this chapter is based on assumptions of linearity, neglecting any non-linear behaviour of the structures. Such assumptions are valid for loads having magnitudes that are sufficiently low for the system in question. This is normally the case for structural vibrations in buildings, caused by common load-cases.

Further reading about structural dynamics can be found in, for example, [15, 16].

4.1 Equation of motion

Employing a single degree of freedom (sdof) system is the simplest way of modelling the dynamics of a structure. In Figure 4.1 an example of such a system is shown. It consists of a mass m connected to a wall by a spring with stiffness k and a viscous damper with damping coefficient c. The mass moves frictionless along the horizontal axis and the sdof is, in this example, the displacement $u(t)$ from the static equilibrium position, caused by a time-dependent load $f(t)$. Applying Newton's second law of motion for the system results in

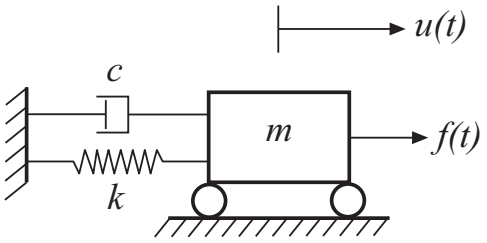

Figure 4.1: Example of an sdof system.

$$f(t) - c\dot{u}(t) - ku(t) = m\ddot{u}(t). \tag{4.1}$$

Rearranging the terms gives the linear equation of motion for an sdof system

$$m\ddot{u}(t) + c\dot{u}(t) + ku(t) = f(t). \tag{4.2}$$

More complex structures require multiple degrees of freedom (dofs) to describe the dynamic behaviour accurately, resulting in multi degree of freedom (mdof) systems. The equation of motion for an mdof system is given by

$$\mathbf{M}\ddot{\mathbf{u}}(t) + \mathbf{C}\dot{\mathbf{u}}(t) + \mathbf{K}\mathbf{u}(t) = \mathbf{f}(t), \tag{4.3}$$

where $\mathbf{M,\ C,\ K} \in \mathbb{R}^{n\times n}$ are the mass, damping and stiffness matrices, respectively, $\mathbf{f}(t) \in \mathbb{R}^{n\times 1}$ is the load vector and $\mathbf{u}(t) \in \mathbb{R}^{n\times 1}$ is the displacement vector. The equation of motion for an mdof system can be derived by, for example, employing the FE method, described in Chapter 3.

4.2 Free vibration

The free vibration of a structure are studied by assuming that no external loads are present, resulting in the motion being determined by the initial conditions, i.e. the prescribed displacements and velocities at $t = 0$. In the following derivations, the undamped case is considered, damping being introduced in Section 4.4. Eq. (4.3) is, for free undamped vibrations, reduced to a homogeneous differential equation

$$\mathbf{M}\ddot{\mathbf{u}}(t) + \mathbf{K}\mathbf{u}(t) = 0, \tag{4.4}$$

which can be solved by assuming the harmonic solution

$$\mathbf{u}(t) = \hat{C}e^{iwt}\Phi, \tag{4.5}$$

where $\hat{C}$ is the complex amplitude, i is the complex number, ω is the angular frequency and $\Phi \in \mathbb{R}^{n\times 1}$ is a constant vector. Differentiation of Eq. (4.5) and insertion into Eq. (4.4) results in the eigenvalue problem

$$(\mathbf{K} - \omega^2\mathbf{M})\Phi = 0, \tag{4.6}$$

with non-trivial solutions given by

$$\det(\mathbf{K} - \omega^2\mathbf{M}) = 0. \tag{4.7}$$

For a system containing n dofs, there will be n solutions $\omega_j = \omega_1, ..., \omega_n$, referred to as the eigenfrequencies of the system, each eigenfrequency having a corresponding eigenvector, or eigenmode, Φ_j given by Eq. (4.6). The set of n eigenmodes form an orthogonal basis, meaning that the solution to Eq. (4.4) can be expressed as a sum of the eigenmodes as

$$\mathbf{u}(t) = \sum_{j=1}^{n} q_j(t)\Phi_j, \tag{4.8}$$

$$q_j(t) = \hat{q}_j e^{iwt}, \tag{4.9}$$

where $q_j(t)$ describes the amplitude of the jth eigenmode and $\hat{q}_j$ is the complex amplitude, determined by use of the initial conditions. Eq. (4.8) is referred to as the modal decomposition of $\mathbf{u}(t)$.

4.3 Harmonic excitation

A system exposed to harmonic excitation will, after an initial transient phase, respond by oscillating with the frequency of the load. Assuming harmonic load and harmonic displacements

$$\mathbf{f}(t) = \hat{\mathbf{f}}e^{iwt}, \qquad \mathbf{u}(t) = \hat{\mathbf{u}}e^{iwt}, \tag{4.10}$$

where $\hat{\mathbf{f}}$ and $\hat{\mathbf{u}}$ are the complex load and complex displacement amplitudes, respectively, results in the equation of motion for an undamped mdof system

$$\mathbf{D}(\omega)\hat{\mathbf{u}} = \hat{\mathbf{f}}, \tag{4.11}$$

$$\mathbf{D}(\omega) = -\omega^2\mathbf{M} + \mathbf{K}. \tag{4.12}$$

Employing the modal decomposition of $\mathbf{u}(t)$ and pre-multiplying the system of equations in Eq. (4.11) with Φ_k^T results in

$$-\omega^2 \sum_{j=1}^{n} \Phi_k^T \mathbf{M}\Phi_j \ddot{\hat{q}}_j + \sum_{j=1}^{n} \Phi_k^T \mathbf{K}\Phi_j \hat{q}_j(t) = \Phi_k^T \hat{\mathbf{f}}, \tag{4.13}$$

for $k = 1, ..., n$. The eigenmodes are orthogonal in the scalar products $\Phi_k^T\mathbf{M}\Phi_j$ and $\Phi_k^T\mathbf{K}\Phi_j$, resulting in the term with $j = k$ being the only non-zero term in the summations. This results in n uncoupled sdof systems given by

$$-\omega^2 \bar{M}_j \hat{q}_j(t) + \bar{K}_j \hat{q}_j(t) = \bar{f}_j, \tag{4.14}$$

$$\bar{M}_j = \Phi_j^T\mathbf{M}\Phi_j, \quad \bar{K}_j = \Phi_j^T\mathbf{K}\Phi_j, \quad \bar{f}_j = \Phi_j^T\hat{\mathbf{f}}, \quad j = 1, ..., n, \tag{4.15}$$

where each sdof system describes the amplitude of an eigenmode. The sdof systems have the solutions

$$\hat{q}_j = \frac{\bar{f}_j}{\bar{K}_j} \frac{1}{1 - (\omega/\omega_j)^2}, \tag{4.16}$$

$$\omega_j = \sqrt{\frac{\bar{K}_j}{\bar{M}_j}}. \tag{4.17}$$

The ratio between the response $\hat{q}_j$ to a harmonic load and a static load of the same magnitude becomes

$$R_d = \frac{1}{1 - (\omega/\omega_j)^2}, \tag{4.18}$$

and is referred to as the deformation response factor. It can be observed in Eq. (4.18) that a harmonic excitation will, in case the excitation frequency is equal to an eigenfrequency ($\omega = \omega_j$), result in an infinite response amplitude, a phenomenon referred to as resonance. This can of course not occur in a real structure since any damping present in the structure will prevent such behaviour. If the level of damping is relatively low, however, the deformation response factor will be large for excitation frequencies close to an eigenfrequency.

4.4 Damped systems

Damping is included in numerical models to represent the energy dissipation occurring during dynamical processes and is always present to some extent because of, for example, friction in joints or internal losses in materials. Identifying the damping properties of a structure is a challenging task and damping is often included in models as a rough approximation by smearing global damping properties of the structure based on its mass and stiffness distributions. By assuming free vibration for the sdof system in Eq. 4.2, it can be rewritten as

$$\ddot{u}(t) + 2\zeta\omega_n\dot{u}(t) + \omega_n^2 u(t) = 0, \tag{4.19}$$

$$\omega_n = \sqrt{\frac{k}{m}},\ \zeta = \frac{c}{2m\omega_n}, \tag{4.20}$$

where ω_n is the eigenfrequency for the undamped case and the damping ratio ζ is introduced. The resulting free vibrations of a damped sdof system are given by

$$u(t) = e^{-\zeta\omega_n t}[u(0)cos(\omega_D t) + \frac{\dot{u}(0) + \zeta\omega_n u(0)}{\omega_D} sin(\omega_D t)], \tag{4.21}$$

$$\omega_D = \omega_n\sqrt{1 - \zeta^2}, \tag{4.22}$$

where ω_D is the eigenfrequency for the damped system and the initial conditions $u(0)$ and $\dot{u}(0)$ are used. For relatively small damping ratios, $\zeta < 0.2$ (common in many engineering structures), $\omega_D \approx \omega_n$.

The deformation response factor for harmonic vibrations of a damped sdof system is given by

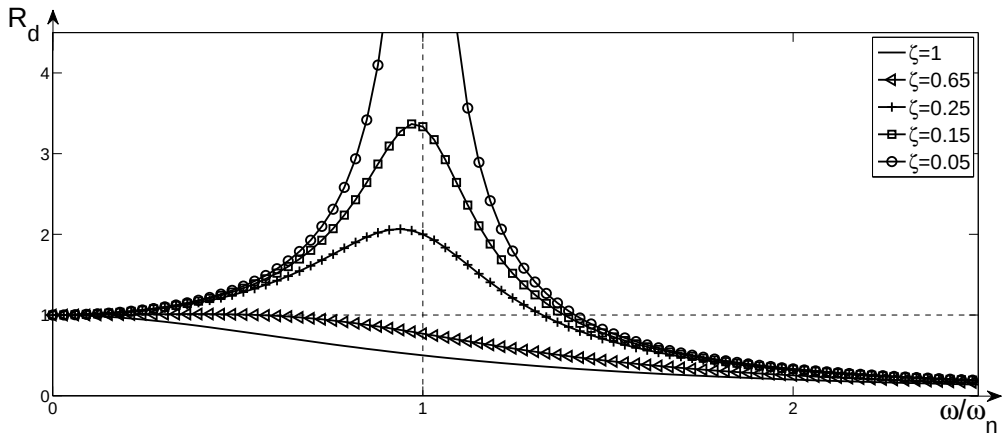

Figure 4.2: The deformation response factor R_d as a function of excitation frequency divided by eigenfrequency (ω/ω_n) for different damping ratios.

$$R_d = \frac{1}{\sqrt{\left(1-(\omega/\omega_n)^2\right)^2 + \left(2\zeta\,(\omega/\omega_n)\right)^2}}. \tag{4.23}$$

In Figure 4.2, the deformation response factor for different values of the damping ratio is shown. It can be observed how a lower value of the damping ratio results in a more distinct resonance peak in the frequency spectra, while a very high value eliminates the resonant behaviour.

In a damped mdof system, a damping matrix needs to be constructed. It is not as straightforward as constructing the stiffness matrix, built by considering the stiffness properties of individual structural components. The damping properties of materials are not as well established and the energy dissipation in connections is difficult to measure and, consequently, difficult to model. As an alternative, the damping matrix can be constructed using modal damping ratios of the structure, obtained by, for example, measuring the free vibration of the structure at certain eigenmodes and fitting the measured data to Eq. (4.21). In case measurement data is unavailable, damping properties of similar structures may be used. Damping matrices can be divided into two types, classical and non-classical. Classical damping matrices are, in contrast to non-classical matrices, diagonalised in case of a modal decomposition of the system, enabling the system of equations in Eq. (4.3) to be separated into n uncoupled equations as was done in Eq. (4.14) for the undamped case.

4.4.1 Rayleigh damping

A method frequently employed for constructing damping matrices is Rayleigh damping, producing classical damping matrices. Rayleigh damping uses a linear combination of the mass and stiffness matrices to construct the damping matrix

$$\mathbf{C} = a_0\mathbf{M} + a_1\mathbf{K}, \tag{4.24}$$

where a_0 and a_1 are the weighting coefficients. With use of Eq. 4.20, it can be shown that the damping ratio of the nth mode is given by

$$\zeta_n = \frac{a_0}{2\omega_n} + \frac{a_1\omega_n}{2}. \tag{4.25}$$

The coefficients a_0 an a_1 can be obtained if the damping ratios ζ_i and ζ_j for the eigenmodes i and j are known. Assume $\zeta_i = \zeta_j = \zeta$, then a_0 and a_1 are given by

$$a_0 = \zeta\frac{2\omega_i\omega_j}{\omega_i + \omega_j}, \tag{4.26}$$

$$a_1 = \zeta\frac{2}{\omega_i + \omega_j}. \tag{4.27}$$

In Figure 4.3, the damping ratio ζ_n as a function of angular frequency ω_n, assuming $\zeta_i = \zeta_j = \zeta$, is shown. The two dashed curves illustrate the contributions from the mass and stiffness matrices, the mass matrix dominating at lower frequencies and the stiffness matrix providing the major contribution at higher frequencies.

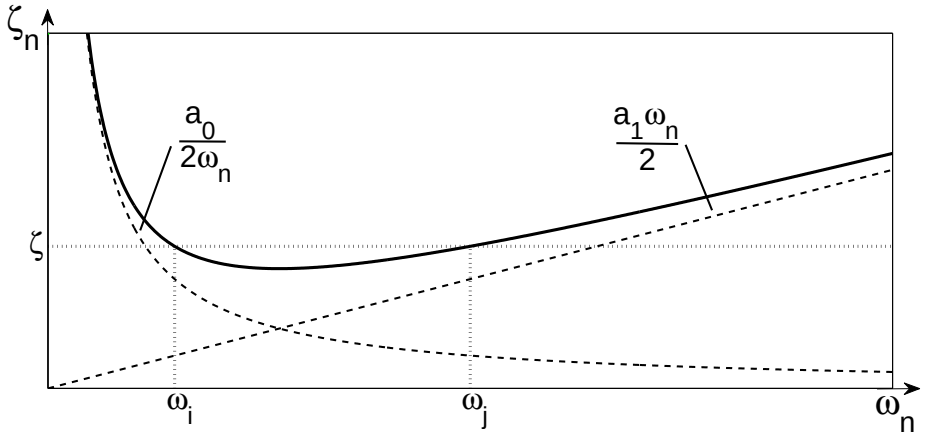

Figure 4.3: The damping ratio ζ as a function of angular frequency ω when employing Rayleigh damping.

5 Substructure modelling

The concept of substructure modelling is discussed in this chapter. The theory behind a wide range of MOR and interface reduction is taken up and some basic features of the methods are demonstrated in a numerical example consisting of an FE model of a wooden beam. For a review of the historic development of substructuring and a classification of substructuring technique, see [17].

Substructure modelling is a methodology frequently adopted for the reduction of large numerical models. Even though the computational resources available for engineers and researchers are continuously increasing, MOR is still a topic attracting a lot of interest as larger and more complex problems are dealt with. Moreover, it is in many cases important to solve a certain problem in a time efficient manner, real time applications being a typical example. The substructuring procedure is illustrated in Figure 5.1. It is based on a division of the structure into components, or substructures, which are reduced in size and assembled to form reduced global models. Substructuring is suitable for structures which in a natural way are divided into components, such as engines or wind turbines, when the flexibility of each component has to be accounted for.

In structural dynamic analysis, substructure modelling provides a flexible and practical framework, enabling a combination of full numerical models and reduced order models of the substructures. Using a floating frame of reference for each substructure, the methodology of substructuring can be employed for systems with large rigid body translations and rotations, while assuming small strains within each substructure. Moreover, problem-specific substructures, developed by considering for example a certain load-case, can easily be integrated within a reduced global model of a building. Assume, for example, that a substructure model of a building exists and that a load is applied on one of its floor structures, requiring the floor in question to be modelled in great detail. The substructure containing the floor can then be replaced with a refined model without having to modify the reduced order models of the remaining parts of the building. Furthermore, it is possible to involve experimental substructures in the global model, these being described by frequency response functions obtained from measurements.

After a substructure division of a FE model has been performed, each substructure is described by an equation of motion of the form in Eq. (3.14). In order to reduce the size of a certain substructure, the transformation $\mathbf{u} = \mathbf{T}\mathbf{a}_R$ is introduced, $\mathbf{u}_R \in \mathbb{R}^{m\times 1}$ being the reduced state vector, $\mathbf{T} \in \mathbb{R}^{n\times m}$ the transformation matrix and $m << n$. This results in a reduced system given by

$$\mathbf{M}_R\ddot{\mathbf{u}}_R + \mathbf{K}_R\mathbf{u}_R = \mathbf{f}_R, \tag{5.1}$$

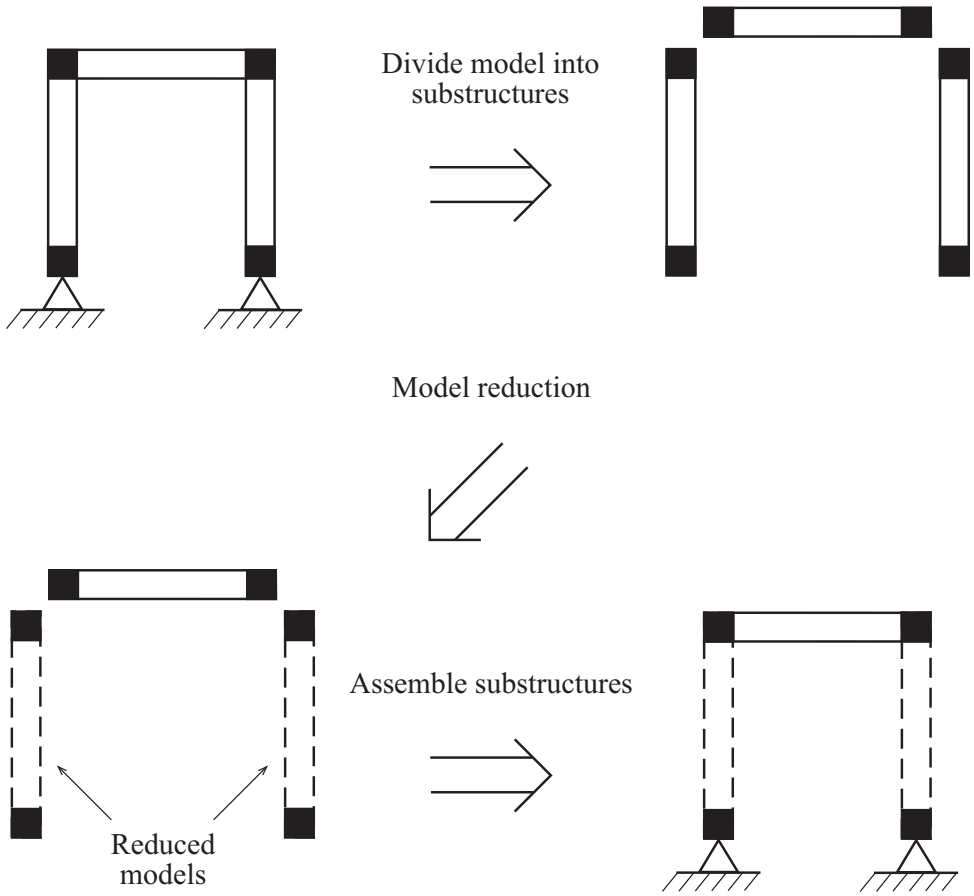

Figure 5.1: Illustration of substructure modelling.

$$\mathbf{M}_R = \mathbf{T}^T\mathbf{M}\mathbf{T}, \quad \mathbf{K}_R = \mathbf{T}^T\mathbf{K}\mathbf{T}, \quad \mathbf{f}_R = \mathbf{T}^T\mathbf{f}, \tag{5.2}$$

where $\mathbf{M}_R, \mathbf{K}_R \in \mathbb{R}^{m\times m}$ are the reduced mass and stiffness matrices, respectively, and $\mathbf{f}_R \in \mathbb{R}^{m\times 1}$ is the reduced load vector. In recent decades, many MOR methods, involving procedures of varying types for establishing the transformation matrix and the reduced state vector involved, have been proposed in the literature. All of the methods can be understood as Rayleigh-Ritz procedures [11], differing in the selection of Ritz basis vectors constituting the columns of the transformation matrix. Each dof in the reduced state vector represents the amplitude of a Ritz basis vector and the dofs can be divided into two categories: physical dofs, being dofs of the full system that are retained in the reduction process, and generalised coordinates. The reduction methods can be categorised according to the type of dofs generated in the reduction process, where *condensation methods* involve only physical dofs, *generalised coordinate methods* are based solely on generalised coordinates, and *hybrid reduction methods* employ a combination of dofs of both types.

In commercial FE software, generalised coordinates are often treated as internal dofs in the substructures and, usually, the coupling of substructures is realised by use of La-

grange multipliers [11], tying the nodes of two interface surfaces to each other by imposing constraints on the displacement dofs. Consequently, if a global substructure model is to be analysed and post-processed in commercial FE software, any reduction methods based solely on generalised coordinates are excluded as physical dofs are required for coupling.

A set of interface nodes, used for the coupling of substructures, is identified for the FE model of each substructure. The dofs of the interface nodes are retained in the reduction process whilst the remaining dofs of the full model are eliminated. The reduced system matrices are in general fully populated, making reduced order models containing more than a few thousand dofs infeasible to analyse. It is therefore important to restrict the number of interface dofs of each substructure, which can be rather large in case the substructure is in contact with the surroundings at surfaces having dense node distribution. For substructures having a large number of interface dofs, interface reduction can be applied to improve the efficiency of the reduced order model. In this dissertation, a frequently employed methodology for interface reduction, based on the use of condensation nodes [18], is employed.

5.1 Methods for model order reduction

In this section, a number of condensation methods and hybrid methods are presented. The hybrid methods presented here are referred to as component mode synthesis methods. The name originates from the 1960s when a number of methods for the reduction of dynamic systems, involving component modes of different kinds, were developed [17]. Generalised coordinate methods are excluded here as the substructures produced by such methods are incompatible with commercial FE software. The generalised coordinate methods are not to be confused with the generalised methods presented below, based on reformulations of the condensation processes employed in the different methods.

5.1.1 Condensation methods

In the condensation methods, the dofs are separated into masters (m) and slaves (s), the slave dofs being condensed in the reduction process, resulting in a reduced state vector containing only the master dofs. Partitioning the state vector in terms of masters and slaves enables the system matrices in Eq. (3.14) to be partitioned into sub-blocks as follows

$$\begin{bmatrix} \mathbf{M}_{mm} & \mathbf{M}_{ms} \\ \mathbf{M}_{sm} & \mathbf{M}_{ss} \end{bmatrix} \begin{bmatrix} \ddot{\mathbf{u}}_m \\ \ddot{\mathbf{u}}_s \end{bmatrix} + \begin{bmatrix} \mathbf{K}_{mm} & \mathbf{K}_{ms} \\ \mathbf{K}_{sm} & \mathbf{K}_{ss} \end{bmatrix} \begin{bmatrix} \mathbf{u}_m \\ \mathbf{u}_s \end{bmatrix} = \begin{bmatrix} \mathbf{f}_m \\ \mathbf{f}_s \end{bmatrix}. \tag{5.3}$$

It is assumed in the following derivations that no loads are acting on the slave dofs, i.e. $\mathbf{f}_s = \mathbf{0}$.

Guyan reduction [19]

Solving the equation in the second row in Eq. (5.3) for $\mathbf{u}_s$ results in

$$\mathbf{u}_s = -\mathbf{K}_{ss}^{-1} \left(\mathbf{M}_{sm} \ddot{\mathbf{u}}_m + \mathbf{M}_{ss} \ddot{\mathbf{u}}_s + \mathbf{K}_{sm} \mathbf{u}_m \right), \tag{5.4}$$

which, if the inertia terms are neglected, results in the transformation of the state vector for Guyan reduction

$$\begin{bmatrix} \mathbf{u}_m \\ \mathbf{u}_s \end{bmatrix} = \begin{bmatrix} \mathbf{I} \\ -\mathbf{K}_{ss}^{-1}\mathbf{K}_{sm} \end{bmatrix} \mathbf{u}_m = \mathbf{T}_{\text{Guyan}}\mathbf{u}_m, \tag{5.5}$$

where the transformation matrix $\mathbf{T}_{\text{Guyan}}$ can be used in Eq. (5.2) to obtain the reduced system matrices and the reduced load vector. Guyan reduction is often referred to as static condensation since models reduced with Guyan reduction do not result in any errors in static analysis. Due to its static nature, Guyan reduction can be expected to only produce acceptable results for frequencies close to the lowest eigenfrequencies of the system. At higher frequencies, the neglected inertia terms have a stronger influence, resulting in errors of larger size. The performance of this method is highly dependent upon the approach for selecting master dofs. In the numerical examples studied here, only the dofs needed to connect the substructures to the surroundings serve as masters, although additional dofs can be employed as master dofs as well, various methods for selecting such dofs having been proposed [20, 21].

Dynamic reduction [22]

A harmonic time-dependent load, $\mathbf{f} = \hat{\mathbf{f}}e^{i\omega t}$, and response, $\mathbf{u} = \hat{\mathbf{u}}e^{i\omega t}$, is assumed, $i = \sqrt{-1}$ being the imaginary unit, ω the angular frequency and $\hat{\mathbf{f}}$ and $\hat{\mathbf{u}}$ the complex load and displacement amplitudes, respectively. Introducing this assumption into Eq. (5.3) results in the equation of motion applying to the frequency domain

$$\begin{bmatrix} \mathbf{D}_{mm}(\omega) & \mathbf{D}_{ms}(\omega) \\ \mathbf{D}_{sm}(\omega) & \mathbf{D}_{ss}(\omega) \end{bmatrix} \begin{bmatrix} \hat{\mathbf{u}}_m \\ \hat{\mathbf{u}}_s \end{bmatrix} = \begin{bmatrix} \hat{\mathbf{f}}_m \\ \mathbf{0} \end{bmatrix}, \tag{5.6}$$

$$\mathbf{D}(\omega) = -\omega^2\mathbf{M} + \mathbf{K}. \tag{5.7}$$

Solving the equation in the lower row in Eq. (5.6) for $\hat{\mathbf{u}}_s$ results in

$$\hat{\mathbf{u}}_s = -\mathbf{D}_{ss}^{-1}(\omega)\,\mathbf{D}_{sm}(\omega)\,\hat{\mathbf{u}}_m, \tag{5.8}$$

and, consequently, the transformation of the state vector for dynamic reduction is given by

$$\begin{bmatrix} \hat{\mathbf{u}}_m \\ \hat{\mathbf{u}}_s \end{bmatrix} = \begin{bmatrix} \mathbf{I} \\ -\mathbf{D}_{ss}^{-1}(\omega)\,\mathbf{D}_{sm}(\omega) \end{bmatrix} \hat{\mathbf{u}}_m = \mathbf{T}_{\text{dynamic}}\hat{\mathbf{u}}_m, \tag{5.9}$$

where the transformation matrix $\mathbf{T}_{\text{dynamic}}$ requires a selection of ω in order to be established. The special case of dynamic reduction in which $\omega = 0$ results in the transformation of Guyan reduction shown in Eq (5.5). For harmonic load cases with the excitation frequency having the same value as ω, dynamic reduction provides exact results. This suggests dynamic reduction to be an effective scheme for analysing a structure subjected to load cases having narrow frequency content. For steady-state analyses, fully accurate reduced models can be obtained by reducing the system matrices at each discrete frequency. This is, however, a costly procedure that requires the availability of large memory resources for storing the resulting matrices.

Improved reduction system (IRS) [23, 24]

The term improved in the name improved reduction system (IRS) refers to a perturbation of the transformation taking place in Guyan reduction, Eq. (5.5). The previously neglected inertia terms are then included as pseudo-static forces. Assuming free undamped vibrations of a system reduced by means of a Guyan reduction results in the following expression for the acceleration of the master dofs

$$\ddot{\mathbf{u}}_m = -\mathbf{M}_{\text{Guyan}}^{-1}\mathbf{K}_{\text{Guyan}}\mathbf{u}_m, \tag{5.10}$$

where $\mathbf{M}_{\text{Guyan}}$ and $\mathbf{K}_{\text{Guyan}}$ are the reduced stiffness- and mass matrices obtained by employing Guyan reduction. Differentiating Eq. (5.5) and making use of the relationship expressed in Eq. (5.10) results in the acceleration of the slave dofs being given by

$$\ddot{\mathbf{u}}_s = -\mathbf{K}_{ss}^{-1}\mathbf{K}_{sm}\ddot{\mathbf{a}}_m = \mathbf{K}_{ss}^{-1}\mathbf{K}_{sm}\mathbf{M}_{\text{Guyan}}^{-1}\mathbf{K}_{\text{Guyan}}\mathbf{u}_m. \tag{5.11}$$

Inserting Eq. (5.10) and Eq. (5.11) into Eq. (5.4) results in the following approximation of the slave dofs

$$\mathbf{u}_s = \mathbf{K}_{ss}^{-1}\left(\mathbf{M}_{sm}\mathbf{M}_{\text{Guyan}}^{-1}\mathbf{K}_{\text{Guyan}} - \mathbf{M}_{ss}\mathbf{K}_{ss}^{-1}\mathbf{K}_{sm}\mathbf{M}_{\text{Guyan}}^{-1}\mathbf{K}_{\text{Guyan}} - \mathbf{K}_{sm}\right)\mathbf{u}_m. \tag{5.12}$$

This rather complicated expression can be written in more compact form, resulting in the transformation matrix for IRS being given by

$$\mathbf{T}_{\text{IRS}} = \mathbf{T}_{\text{Guyan}} + \mathbf{S}\mathbf{M}\mathbf{T}_{\text{Guyan}}\mathbf{M}_{\text{Guyan}}^{-1}\mathbf{K}_{\text{Guyan}}, \tag{5.13}$$

$$\mathbf{S} = \begin{bmatrix} \mathbf{0} & \mathbf{0} \\ \mathbf{0} & \mathbf{K}_{ss}^{-1} \end{bmatrix}. \tag{5.14}$$

In the IRS transformation, the reduced system matrices that Guyan reduction provides are utilised so as to produce updated reduced matrices. As a further extension of this, the updated matrices can be used to create an iterative scheme, the transformation matrix for the ith iteration being given by

$$\mathbf{T}_{\text{IRS},i+1} = \mathbf{T}_{\text{Guyan}} + \mathbf{S}\mathbf{M}\mathbf{T}_{\text{IRS},i}\mathbf{M}_{\text{IRS},i}^{-1}\mathbf{K}_{\text{IRS},i}, \tag{5.15}$$

and the iterations being started by calculating $\mathbf{T}_{\text{IRS},1}$ according to Eq. (5.13). The iterative scheme converges to form the transformation matrix of SEREP [25], creating a reduced system that reproduces exactly the lowest eigenfrequencies and eigenmodes of the full system, the rate of convergence depending upon the selection of master dofs. In contrast to Guyan reduction, however, IRS does not reproduce the static behaviour of the full system exactly.

5.1.2 Component mode synthesis methods

Component mode synthesis methods are developed for use in substructure modelling, its name referring to the creation of a global system by using different kinds of structural

modes for components of the full model. In general, a component mode synthesis method is a hybrid method which is obtained by combining a condensation method with a generalised coordinate method.

Craig–Bampton (CMS) [26, 15]

Use of component mode synthesis by Craig–Bampton, here denoted CMS, compensates for the neglected inertia terms in Guyan reduction through its including a set of generalised coordinates $\boldsymbol{\xi}$. These generalised coordinates represent the amplitudes of a set of eigenmodes for the slave structure, calculated with the master dofs being fixed. Setting $\mathbf{u}_m = \mathbf{0}$ and $\mathbf{f}_s = \mathbf{0}$ in Eq. (5.3) and assuming a harmonic solution with angular frequency ω results in the following eigenvalue problem

$$\mathbf{K}_{ss}\Phi = \lambda \mathbf{M}_{ss}\Phi, \tag{5.16}$$

which can be solved for the eigenvalues $\lambda = \omega^2$ and the eigenmodes Φ. A number of the eigenmodes, referred to as retained eigenmodes, are selected as additional basis vectors to the approximation of the slave dofs in Eq. (5.5), resulting in

$$\mathbf{u}_s = -\mathbf{K}_{ss}^{-1}\mathbf{K}_{sm}\mathbf{u}_m + \sum \Phi_i \xi_i = \boldsymbol{\Psi}\mathbf{u}_m + \boldsymbol{\Phi}\boldsymbol{\xi}. \tag{5.17}$$

This results in the transformation of the state vector for CMS

$$\begin{bmatrix} \mathbf{u}_m \\ \mathbf{u}_s \end{bmatrix} = \begin{bmatrix} \mathbf{I} & \mathbf{0} \\ \boldsymbol{\Psi} & \boldsymbol{\Phi} \end{bmatrix} \begin{bmatrix} \mathbf{u}_m \\ \boldsymbol{\xi} \end{bmatrix} = \mathbf{T}_{\text{CMS}} \begin{bmatrix} \mathbf{u}_m \\ \boldsymbol{\xi} \end{bmatrix}, \tag{5.18}$$

defining the transformation matrix $\mathbf{T}_{\text{CMS}}$. As for Guyan reduction, the accuracy of CMS depends upon the selection of master dofs, affecting the static modes as well as the eigenmodes of the slave structure. Moreover, the accuracy depends upon the selection of retained eigenmodes, certain eigenmodes having a larger influence than others on the solution of a specific problem. To obtain a reduced model with as great accuracy for general load distributions as possible, however, all the eigenmodes up to some given limit that is chosen should be included.

Krylov subspace method (KCMS) [27, 28]

In recent years, methods originating from control theory have become increasingly popular among researchers in computational mechanics. Such methods can be divided into two main categories, Krylov subspace methods and balanced truncation [29], both being generalised coordinate methods. Here, the eigenmodes employed in CMS are exchanged for Ritz basis vectors obtained from Krylov subspace projections. The Krylov subspace is defined as

$$K_q\left(\mathbf{A}, \mathbf{b}\right) = span\left\{\mathbf{b}, \mathbf{A}\mathbf{b}, ..., \mathbf{A}^{q-1}\mathbf{b}\right\}, \tag{5.19}$$

where $\mathbf{A} \in \mathbb{R}^{n\times n}$ is a constant matrix, $\mathbf{b} \in \mathbb{R}^{n\times 1}$ a constant vector and q a positive integer. $\mathbf{b}$ can also be a block of vectors, in which case each Krylov projection generates a new block of vectors. Since methods originating from control theory are ones developed for

systems of an input-output form, the equation of motion is rewritten here as such a system in the following form

$$\mathbf{M}\ddot{\mathbf{u}} + \mathbf{K}\mathbf{u} = \mathbf{B}\mathbf{x}, \tag{5.20}$$

$$\mathbf{y} = \mathbf{C}^T\mathbf{u}, \tag{5.21}$$

where $\mathbf{x} = \mathbf{x}(t) \in \mathbb{R}^{x\times 1}$ is the input vector, $\mathbf{y} = \mathbf{y}(t) \in \mathbb{R}^{y\times 1}$ the output vector, $\mathbf{B} \in \mathbb{R}^{n\times x}$ a matrix describing the spatial load distributions and $\mathbf{C} \in \mathbb{R}^{n\times y}$ a matrix relating the state vector to the output vector. Laplace transformation of the input-output system yields the transfer function $\mathbf{G}(s)$

$$\mathbf{G}(s) = \mathbf{C}^T\left(s^2\mathbf{M} + \mathbf{K}\right)^{-1}\mathbf{B}. \tag{5.22}$$

where s is a complex variable. Krylov subspace methods are based on so-called moment matching. The moments involved are defined as the coefficients of a Taylor series expansion of $\mathbf{G}(s)$ around $s = 0$. It can be shown that the first q moments of the full system and of a reduced system match if the reduced basis is selected as the Krylov subspace generated by $\mathbf{A} = \mathbf{K}^{-1}\mathbf{M}$ and $\mathbf{b} = \mathbf{K}^{-1}\mathbf{B}$ [28]. In the present study it is required that the reduction methods employed are structure-preserving, i.e. retains the physical dofs at the interfaces. Accordingly, the approach of using Krylov subspace vectors in a component mode synthesis manner, as described in [30, 31], here denoted KCMS, is adopted. Inserting $\mathbf{u}_m = 0$ and $\mathbf{f}_s = \mathbf{B}_s\mathbf{x}_s\,(\neq \mathbf{0})$ into Eq. (5.3) results in the following equation of motion for the slave structure

$$\mathbf{M}_{ss}\ddot{\mathbf{u}}_s + \mathbf{K}_{ss}\mathbf{u}_s = \mathbf{B}_s\mathbf{x}_s. \tag{5.23}$$

A Krylov subspace is generated for the slave structure by selecting $\mathbf{A} = \mathbf{K}_{ss}^{-1}\mathbf{M}_{ss}$ and $\mathbf{b} = \mathbf{K}_{ss}^{-1}\mathbf{B}_s$:

$$K_q\left(\mathbf{K}_{ss}^{-1}\mathbf{M}_{ss}, \mathbf{K}_{ss}^{-1}\mathbf{B}_s\right) = span\left\{\underbrace{\mathbf{K}_{ss}^{-1}\mathbf{B}_s}_{V_\mathrm{k}^1}, \underbrace{\left(\mathbf{K}_{ss}^{-1}\mathbf{M}_{ss}\right)\mathbf{K}_{ss}^{-1}\mathbf{B}_s}_{V_\mathrm{k}^2}, ..., \underbrace{\left(\mathbf{K}_{ss}^{-1}\mathbf{M}_{ss}\right)^{q-1}\mathbf{K}_{ss}^{-1}\mathbf{B}_s}_{V_\mathrm{k}^q}\right\}, \tag{5.24}$$

and the approximation of the slave dofs is given by

$$\mathbf{u}_s = -\mathbf{K}_{ss}^{-1}\mathbf{K}_{sm}\mathbf{u}_m + \sum V_\mathrm{k}^i\xi_i = \mathbf{\Psi}\mathbf{u}_m + \mathbf{V}_\mathrm{k}\boldsymbol{\xi}, \tag{5.25}$$

one which is similar to that of CMS, shown in Eq. (5.17), but with the eigenmodes of the slave structure exchanged for the Krylov subspace vectors as defined in Eq. (5.24). This results in the transformation of the state vector

$$\begin{bmatrix}\mathbf{u}_m\\ \mathbf{u}_s\end{bmatrix} = \begin{bmatrix}\mathbf{I} & \mathbf{0}\\ \mathbf{\Psi} & \mathbf{V}_\mathrm{k}\end{bmatrix}\begin{bmatrix}\mathbf{u}_m\\ \boldsymbol{\xi}\end{bmatrix} = \mathbf{T}_{\mathrm{KCMS}}\begin{bmatrix}\mathbf{u}_m\\ \boldsymbol{\xi}\end{bmatrix}, \tag{5.26}$$

defining the transformation matrix $\mathbf{T}_{\mathrm{KCMS}}$. In order to avoid numerical issues, the Krylov subspace is generated by using the Arnoldi algorithm with modified Gram-Schmidt orthogonalization [27], creating a set of linearly independent vectors. Calculating the starting vector $\mathbf{b}$ of the Krylov subspace projections requires that $\mathbf{B}_s$, describing the load distribution on the slave structure, be selected. In the studies presented in this dissertation, where a substructuring approach is adopted for the modelling of multi-storey buildings, smaller parts of the buildings are considered as substructures. In most cases, these have no loads that act upon the slave structure ($\mathbf{f}_s = \mathbf{0}$). Accordingly, a fictitious load needs to be selected, a random distribution being used here.

Improved component mode synthesis [30]

The two component mode synthesis methods described above, CMS and KCMS, are obtained by complementing Guyan reduction by a set of Ritz basis vectors for the slave structure, these being either eigenmodes or Krylov subspace vectors. IRS can be seen as representing an improvement as compared to Guyan reduction, an improvement that can also be applied to the component mode synthesis methods employed here. The transformation matrices of the improved component mode synthesis methods, improved CMS (ICMS) and improved KCMS (IKCMS), can be obtained by simply replacing the basis vectors of Guyan reduction by the basis vectors of IRS:

$$\mathbf{T}_{\mathrm{ICMS}} = \begin{bmatrix} \mathbf{T}_{\mathrm{IRS}} & \hat{\mathbf{\Phi}} \end{bmatrix}; \quad \hat{\mathbf{\Phi}} = \begin{bmatrix} \mathbf{0} \\ \mathbf{\Phi} \end{bmatrix}, \tag{5.27}$$

$$\mathbf{T}_{\mathrm{IKCMS}} = \begin{bmatrix} \mathbf{T}_{\mathrm{IRS}} & \hat{\mathbf{V}}_{\mathrm{k}} \end{bmatrix}; \quad \hat{\mathbf{V}}_{\mathrm{k}} = \begin{bmatrix} \mathbf{0} \\ \mathbf{V}_{\mathrm{k}} \end{bmatrix}, \tag{5.28}$$

where $\mathbf{T}_{\mathrm{IRS}}$ can be either the original form of IRS, Eq. (5.13), or its iterated version, Eq. (5.15). The use of IRS instead of Guyan reduction can be expected to improve the dynamic behaviour of the reduced models, at the expense of introducing errors in static analyses.

5.1.3 Generalised methods

The generalised versions of the reduction methods (denoted here by a "*g*-" in the method names) are obtained by re-formulating the equation of motion [32]. Instead of using the block-partitioning of the system matrices in Eq. (5.3), the following partitioning is employed

$$\begin{bmatrix} \mathbf{M}_m & \mathbf{M}_s \end{bmatrix} \begin{bmatrix} \ddot{\mathbf{u}}_m \\ \ddot{\mathbf{u}}_s \end{bmatrix} + \begin{bmatrix} \mathbf{K}_m & \mathbf{K}_s \end{bmatrix} \begin{bmatrix} \mathbf{u}_m \\ \mathbf{u}_s \end{bmatrix} = \begin{bmatrix} \mathbf{f}_m \\ \mathbf{f}_s \end{bmatrix}, \tag{5.29}$$

with the non-square submatrices $\mathbf{K}_m, \mathbf{M}_m \in \mathbb{R}^{n \times m}$ and $\mathbf{K}_s, \mathbf{M}_s \in \mathbb{R}^{n \times s}$. The generalised methods incorporate more of the information in the stiffness matrix as compared to the condensation methods presented in Section 5.1.1, which were derived from the partitioning of the system matrices employed in Eq. (5.3). The efficiency of the methods is therefore expected to improve by employing their generalised versions.

Generalised Guyan reduction

In the same manner as in Eq. (5.4) and Eq. (5.5), the inertia terms in Eq. (5.29) are neglected when solving for the slave dofs, resulting in the following transformation of the state vector for generalised Guyan (g-Guyan) reduction

$$\begin{bmatrix} \mathbf{u}_m \\ \mathbf{u}_s \end{bmatrix} = \begin{bmatrix} \mathbf{I} \\ -\mathbf{K}_s^+ \mathbf{K}_m \end{bmatrix} \mathbf{u}_m = \mathbf{T}_{\text{g-Guyan}} \mathbf{u}_m, \tag{5.30}$$

where $\mathbf{K}_s^+ = \left(\mathbf{K}_s^T \mathbf{K}_s\right)^{-1} \mathbf{K}_s^T$ is the generalised left-inverse of $\mathbf{K}_s$ and $\mathbf{T}_{\text{g-Guyan}}$ is the transformation matrix. Note that in the approximation of the slave dofs, it is assumed that there are no loads that act on either the master dofs or the slave dofs ($\mathbf{f}_m = \mathbf{0}$ and $\mathbf{f}_s = \mathbf{0}$, respectively, in contrast to the original Guyan reduction, in which only $\mathbf{f}_s = \mathbf{0}$ needs to be assumed.

Generalised dynamic reduction

Through use of an approach corresponding to the derivation of g-Guyan reduction, the transformation matrix of generalised dynamic (g-dynamic) reduction, $\mathbf{T}_{\text{g-Dynamic}}$, can be defined according to

$$\begin{bmatrix} \hat{\mathbf{u}}_m \\ \hat{\mathbf{u}}_s \end{bmatrix} = \begin{bmatrix} \mathbf{I} \\ -\mathbf{D}_s^+ \mathbf{D}_m \end{bmatrix} \hat{\mathbf{u}}_m = \mathbf{T}_{\text{g-Dynamic}} \hat{\mathbf{u}}_m. \tag{5.31}$$

Generalised IRS

The transformation matrix of generalised IRS (g-IRS) is obtained by including the inertia terms found in Eq. (5.29) as pseudo-static forces, using approximations corresponding to those employed in Eq. (5.10) and Eq. (5.11), resulting in

$$\mathbf{T}_{\text{g-IRS}} = \mathbf{T}_{\text{g-Guyan}} + \hat{\mathbf{S}}\mathbf{M}\mathbf{T}_{\text{g-Guyan}}\mathbf{M}_{\text{g-Guyan}}^{-1}\mathbf{K}_{\text{g-Guyan}}, \tag{5.32}$$

$$\hat{\mathbf{S}} = \begin{bmatrix} \mathbf{0} \\ \mathbf{K}_s^+ \end{bmatrix}, \tag{5.33}$$

where $\mathbf{M}_{\text{Guyan}}$ and $\mathbf{K}_{\text{Guyan}}$ are the reduced stiffness- and mass matrices obtained by employing g-Guyan reduction. g-IRS can also be extended to produce an iterative scheme in the same manner as in the original IRS, where the transformation matrix for the ith iteration is given by

$$\mathbf{T}_{\text{g-IRS},i+1} = \mathbf{T}_{\text{g-Guyan}} + \hat{\mathbf{S}}\mathbf{M}\mathbf{T}_{\text{g-IRS},i}\mathbf{M}_{\text{g-IRS},i}^{-1}\mathbf{K}_{\text{g-IRS},i}. \tag{5.34}$$

and the iterations are started by calculating $\mathbf{T}_{\text{g-IRS},1}$ according to Eq. (5.32).

Generalised component mode synthesis

The generalised versions of Guyan reduction and IRS can be used to obtain the transformation matrices for the generalised versions of CMS, KCMS, ICMS and IKCMS (g-CMS, g-KCMS, g-ICMS and g-IKCMS, respectively)

Condensation methods	
Method name	**Abbrevation**
Guyan reduction	–
Dynamic reduction	–
Improved reduction system	IRS
Generalised Guyan reduction	g-Guyan reduction
Generalised dynamic reduction	g-dynamic reduction
Generalised IRS	g-IRS
Component mode synthesis methods	
Method name	**Abbrevation**
Component mode synthesis by Craig–Bampton	CMS
Improved CMS	ICMS
Krylov subspace component mode synthesis	KCMS
Improved KCMS	IKCMS
Generalised CMS	g-CMS
Generalised ICMS	g-ICMS
Generalised KCMS	g-KCMS
Generalised IKCMS	g-IKCMS

Table 5.1: The MOR methods presented and investigated in this chapter.

$$\mathbf{T}_{\text{g-CMS}} = \begin{bmatrix} \mathbf{T}_{\text{g-Guyan}} & \hat{\mathbf{\Phi}} \end{bmatrix}, \tag{5.35}$$

$$\mathbf{T}_{\text{g-KCMS}} = \begin{bmatrix} \mathbf{T}_{\text{g-Guyan}} & \hat{\mathbf{V}}_{\text{k}} \end{bmatrix}, \tag{5.36}$$

$$\mathbf{T}_{\text{g-ICMS}} = \begin{bmatrix} \mathbf{T}_{\text{g-IRS}} & \hat{\mathbf{\Phi}} \end{bmatrix}, \tag{5.37}$$

$$\mathbf{T}_{\text{g-IKCMS}} = \begin{bmatrix} \mathbf{T}_{\text{g-IRS}} & \hat{\mathbf{V}}_{\text{k}} \end{bmatrix}, \tag{5.38}$$

where $\hat{\mathbf{\Phi}}$ and $\hat{\mathbf{V}}_{\text{k}}$ are defined in Eq. (5.27) and Eq. (5.28), respectively.

5.1.4 Summary of methods

In Table 5.1, the MOR methods that are presented above and investigated in the numerical example are summarised.

5.2 Interface reduction

The reduced order models of substructures can be inefficient in case the number of interface dofs is large. To improve the efficiency, interface reduction can be employed, resulting in the coupling of substructures being realised at a reduced number of dofs. A frequently

employed methodology for interface reduction involves the introduction of a condensation node for each interface surface [18]. A condensation node has six dofs, three translational and three rotational, and represents the motion of the complete interface surface it is connected to. The coupling between two substructures is then realised by connecting their condensation nodes.

There are two main types of coupling employed for the connection between a condensation node and an interface surface: rigid coupling and distributed coupling. The former is obtained by assuming a rigid body motion of the interface surface, the condensation node following its motion. The latter distributes the forces and moments acting on the condensation node to the nodes of the interface surface by certain weight factors, resulting in the motion of the condensation node being a weighted average of the motion of the interface dofs. The introduction of rigid body constraints results in an overestimation of the stiffness whilst a distributed coupling can result in an underestimation.

5.2.1 Rigid coupling

By assuming rigid coupling between the interface surface and the condensation node, the displacements of node i at the interface surface is, considering small displacements, described by [33]:

$$\mathbf{u}_i = \mathbf{u}_c + \boldsymbol{\Theta}_c \times \mathbf{r}_{ci}, \tag{5.39}$$

where $\mathbf{u}_c$ and $\boldsymbol{\Theta}_c$ are the displacements and rotations of the condensation node, respectively, and $\mathbf{r}_{ci}$ is the vector from the condensation node to node i at the interface surface.

5.2.2 Distributed coupling

Distributed coupling is obtained by distributing the forces and moments acting on the condensation node to the nodes of the interface surface according to [33]:

$$\mathbf{f}_i = \hat{\omega}_i \left(\mathbf{f}_c + \left(\mathbf{T}^{-1} \left(\mathbf{m}_c + \mathbf{r}_c \times \mathbf{f}_c \right) \right) \times \mathbf{r}_i \right), \tag{5.40}$$

$$\mathbf{T} = \sum_i \hat{\omega}_i \left((\mathbf{r}_i \cdot \mathbf{r}_i) \, \mathbf{I} - (\mathbf{r}_i \mathbf{r}_i) \right), \tag{5.41}$$

$$\mathbf{r}_i = \mathbf{x}_i - \bar{\mathbf{x}}, \qquad \mathbf{r}_c = \mathbf{x}_c - \bar{\mathbf{x}}, \tag{5.42}$$

$$\bar{\mathbf{x}} = \sum_i \hat{\omega}_i \mathbf{x}_i, \qquad \hat{\omega}_i = \frac{\omega_i}{\sum_i \omega_i}, \tag{5.43}$$

where $\mathbf{f}_i$ is the force acting on node i of the interface surface, $\mathbf{f}_c$ and $\mathbf{m}_c$ are the force and moment acting on the condensation node, $\mathbf{x}_i$ and $\mathbf{x}_c$ are the coordinates of node i and the condensation node respectively and ω_i is the weight factor assigned to node i. The method of distributing the forces and moments results in the motion of the condensation node being a weighted average of the displacements at the interface surface, given by

$$\mathbf{u}_c = \sum_i \hat{\omega}_i \mathbf{u}_i, \tag{5.44}$$

$$\boldsymbol{\Theta}_c = \sum_i \hat{\omega}_i \frac{\mathbf{r}_{ci}}{|\mathbf{r}_{ci}|^2} \times \mathbf{u}_i. \tag{5.45}$$

Since the weight factors can be selected arbitrarily, distributed coupling can be defined in an infinite number of ways. Four methods for determining the weight factors are presented below. The most straightforward method is uniform weighting, distributing equal load to all nodes at the interface surface. The remaining three methods employ decreasing weight at farther distance from the condensation node, using polynomials of different degrees.

Uniform weighting

$$\omega_i = 1. \tag{5.46}$$

Linearly decreasing weighting

$$\omega_i = 1 - \left| \frac{\mathbf{r}_{ci}}{\mathbf{r}_{c0}} \right|, \tag{5.47}$$

where $\mathbf{r}_{c0}$ is the vector from the condensation node to the most distant node of the interface surface.

Quadratically decreasing weighting

$$\omega_i = 1 - \left| \frac{\mathbf{r}_{ci}}{\mathbf{r}_{c0}} \right|^2. \tag{5.48}$$

Cubically decreasing weighting

$$\omega_i = 1 - 3\left| \frac{\mathbf{r}_{ci}}{\mathbf{r}_{c0}} \right|^2 + 2\left| \frac{\mathbf{r}_{ci}}{\mathbf{r}_{c0}} \right|^3. \tag{5.49}$$

5.3 Numerical example

A numerical example is presented here to demonstrate some characteristics of the different MOR methods and interface reduction methods. An FE model of a wooden beam, modelled with three-dimensional solid elements, employing quadratic interpolation, was studied. The mesh, shown in Figure 5.2, consisted of 2,476 nodes, resulting in 8,238 dofs. An orthotropic material model was used for the wood, having the properties shown in Table 5.2. The 4 m long beam had a cross-section of 45×220 mm^2 and was divided into two equally large substructures. The substructures division is shown in Figure 5.2,

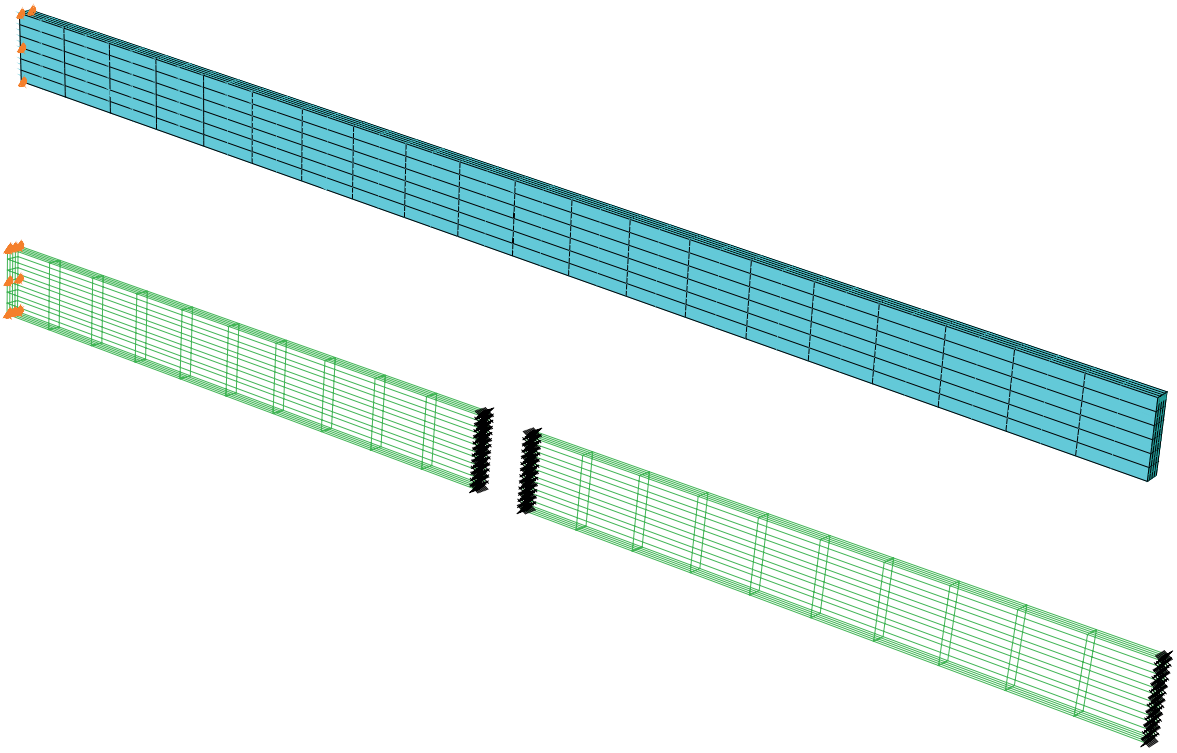

Figure 5.2: The model of the wooden beam studied in the numerical example; the mesh employed (above) and the division into substructures (below).

E_1	E_2	E_3	G_{12}	G_{13}	G_{23}	ν_{12}	ν_{13}	ν_{23}	ρ
8500	350	350	700	700	50	0.2	0.2	0.3	432

Table 5.2: The material parameters used for the wooden beam [9], the stiffness parameters (E,G) being given in terms of MPa and the density (ρ) in kg/m^3.

illustrating the 93 interface nodes of each interface surface with black crosses. Cantilever boundary conditions were applied, the one end of the beam being fixed, the other end being free.

First, the MOR methods and interface reduction methods were investigated separately, employing one type of reduction at a time. Subsequently, the most efficient methods for both types of reduction were employed simultaneously, as it will be for the substructure models of multi-storey wood buildings.

The accuracy of the reduced models was compared by studying the eigenfrequencies of the beam as well as the steady-state response to harmonic loading. The load in the steady-state analyses was distributed equally over all nodes at the free end of the beam, a vertical unit load being applied in each node.

The eigenfrequencies were compared using the normalised relative frequency difference (NRFD), defined, for the ith eigenfrequency, as

$$\text{NRFD} = \frac{\left| f_i^{red} - f_i^{full} \right|}{f_i^{full}} \cdot 100, \tag{5.50}$$

where f_i^{full} and f_i^{red} are the eigenfrequencies of the full model and a reduced model, respectively. The quotient is multiplied by 100 to obtain the NRFD value as a percentage. The analyses were restricted to frequencies below 200 Hz, resulting in the 12 eigenfrequencies of the full model below 200 Hz being included in the results and compared to the 12 first eigenfrequencies of the reduced models (possibly at frequencies over 200 Hz).

The steady-state analyses were evaluated by studying the magnitude of the complex vertical displacements in the node at the middle of the free end of the beam. A normalised error was, for each reduced model, calculated according to

$$u_{\text{error}}(\omega) = \frac{|u_{red}(\omega) - u_{full}(\omega)|}{u_{full}(\omega)} \cdot 100, \tag{5.51}$$

where u_{full} and u_{red} are the magnitude of the complex displacement amplitudes for the full model and the reduced model, respectively. Calculating the error for a number of harmonic excitation frequencies enables an error spectrum to be obtained. Since the error spectra typically fluctuate to a marked degree, the result plots used for comparing the different reduced models make use of averaged error spectra. The errors were averaged by sweeping a 10 Hz wide window over the frequency range and calculating the mean value of the spectrum inside the window for each point in the frequency range. Frequencies up to 200 Hz were analysed in steps of 2 Hz.

The green, yellow and red dashed lines in the result plots (cf. Figure 5.3–5.15) represent the levels of error 0.1 %, 1 % and 10 %, respectively.

5.3.1 Model order reduction

In the MOR carried out, all dofs at the interface surfaces connecting the two substructures were retained as physical dofs in the reduced models, no interface reduction being employed. In addition, the dofs of the 93 nodes at the free end of the beam were retained in the reduced models, resulting in a total of $93 \times 3 \times 3 = 837$ retained physical dofs. The reduced models created by employing the eight different component mode synthesis methods included 10 generalised coordinates per substructure, resulting in the models having a total of 847 dofs.

In the comparisons of the different methods, it is not only the accuracy of the reduced models which is of interest, but also the extent to which the computation time is reduced. The computation times for the models obtained by employing the different MOR methods were, however, very similar. This is a consequence of the reduced models having similar sizes and the band width of the system matrices being very large for all reduced models. The computation times for the reduced models were approximately 2 % of the time required for the analyses of the full model.

Condensation methods

The three condensation methods, namely Guyan reduction, dynamic reduction and IRS, were investigated first, employing them in their oridinal versions as described in Section 5.1.1. The dynamic reduction involved a frequency shift of 90.173 Hz, this being the eigenfrequency of the full model closest to 100 Hz, the centre of the frequency range. IRS was employed in its iterated version, using three iterations.

The eigenfrequencies obtained when employing the condensation methods are shown in Table 5.3 and the NRFD values are shown in Figure 5.3. For the Guyan reduction, only the lowest eigenfrequencies of the full model were approximated with an acceptable level of accuracy. The NRFD values obtained for dynamic reduction indicate poor accuracy for all eigenfrequencies, a result which is misguiding as a change in order of the eigenmodes has occurred. The third eigenmode obtained with dynamic reduction approximates the sixth eigenmode of the full model with very good precision, a consequence of the frequency shift being 90.173 Hz. The accuracy of dynamic reduction was, however, poor for the remaining eigenfrequencies. Iterated IRS proved to be a more reliable method, yielding errors between 1-10 % for most eigenfrequencies, an illustration of the previously mentioned fact that iterated IRS converges to reproduce the eigenfrequencies of the full model exactly.

In Figure 5.4, the errors obtained in the steady-state analysis are shown. In agreement with the results of the eigenvalue analysis, Guyan reduction was found to produce acceptable levels of error only at frequencies close to the lowest eigenfrequencies, the levels of error converging to zero as the frequency goes to zero. The frequency shift employed in the dynamic reduction is manifested in the results, a distinct minimum in the level of error being observed at 90 Hz, while large errors were obtained in the rest of the frequency range. High levels of error were obtained for IRS as well, in particular at the middle of the frequency range. IRS was, however, the condensation method yielding the most accurate results at higher frequencies.

Component mode synthesis methods

The four variants of component mode synthesis presented in Section 5.1.2, namely CMS, KCMS, ICMS and IKCMS, were investigated next. The eigenfrequencies obtained when employing the methods are shown in Table 5.4 and the NRFD values are shown in Figure 5.5. In general, the accuracy in eigenfrequencies was significantly improved when employing the component mode synthesis methods as compared to the condensation methods, although they add only 10 generalised coordinates to each of the substructures, taking the total number of dofs in the reduced systems from 837 to 857. The accuracy of CMS and KCMS was high at the lower eigenfrequencies, as compared to ICMS and IKCMS. This can be explained by the two former methods having Guyan reduction as condensation method and the two latter having IRS, similar observations being made for those methods. At higher eigenfrequencies, the accuracy of the four component mode synthesis methods was similar with CMS producing the lowest levels of error.

Full model	Guyan-reduction	Dynamic-reduction	IRS
2.0148	2.0674	60.987	2.6060
9.9828	10.261	68.099	10.216
12.598	16.900	90.173	13.991
29.918	32.716	118.43	30.225
35.150	78.906	169.10	35.217
59.363	261.57	214.08	65.849
68.531	305.70	300.56	76.774
90.173	862.95	901.63	91.542
112.57	1710.7	1684.3	126.54
151.67	2482.9	2556.6	154.99
154.52	2574.1	2573.0	155.85
166.90	2711.8	2915.7	227.73

Table 5.3: Eigenfrequencies (Hz) obtained for the condensation methods applied to the numerical example.

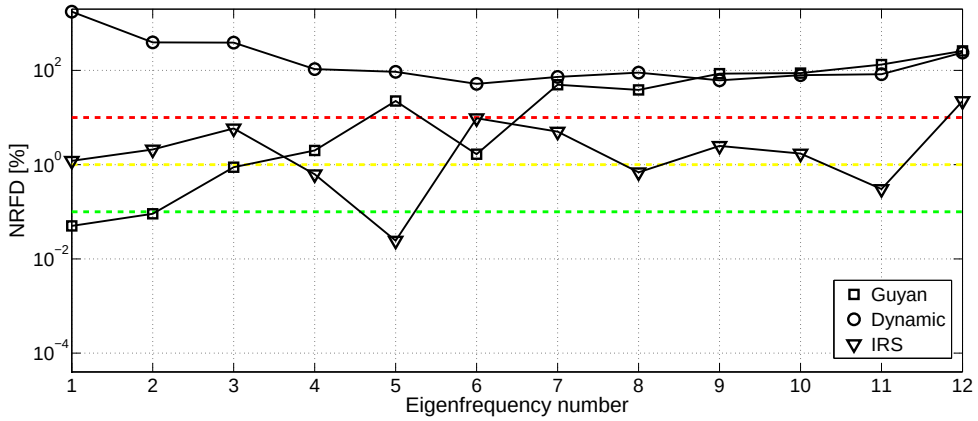

Figure 5.3: NRFD values for the condensation methods applied to the numerical example.

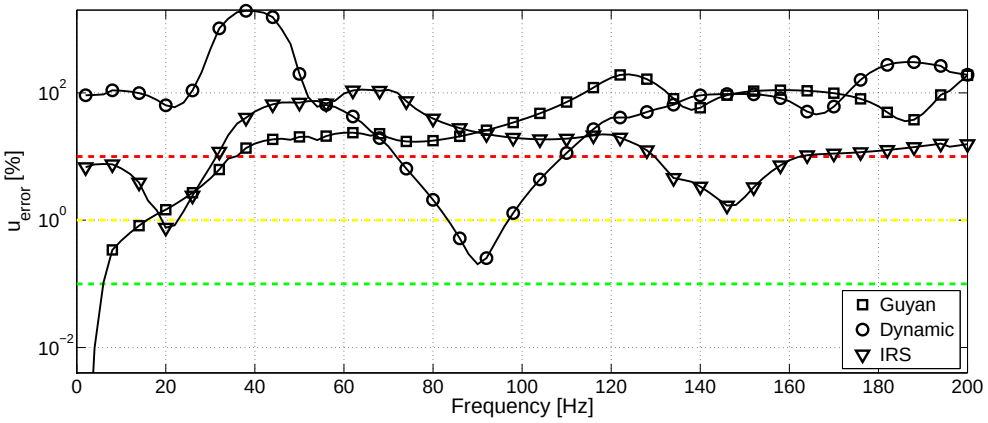

Figure 5.4: Errors in the steady-state analysis of the numerical example when employing the condensation methods.

Full model	CMS	KCMS	ICMS	IKCMS
2.0148	2.0148	2.0148	2.4382	2.4382
9.9828	9.9829	9.9829	9.9948	9.9936
12.598	12.598	12.598	12.948	12.948
29.918	29.920	29.934	30.100	30.125
35.150	35.150	35.150	35.152	35.152
59.363	59.411	59.442	59.533	59.501
68.531	68.552	68.577	68.606	68.610
90.173	90.211	90.663	90.520	90.748
112.57	112.58	112.60	112.58	112.58
151.67	151.86	154.63	152.40	153.48
154.52	154.61	164.10	154.63	154.62
166.90	167.22	167.67	167.07	167.17

Table 5.4: Eigenfrequencies (Hz) obtained for the component mode synthesis methods applied to the numerical example.

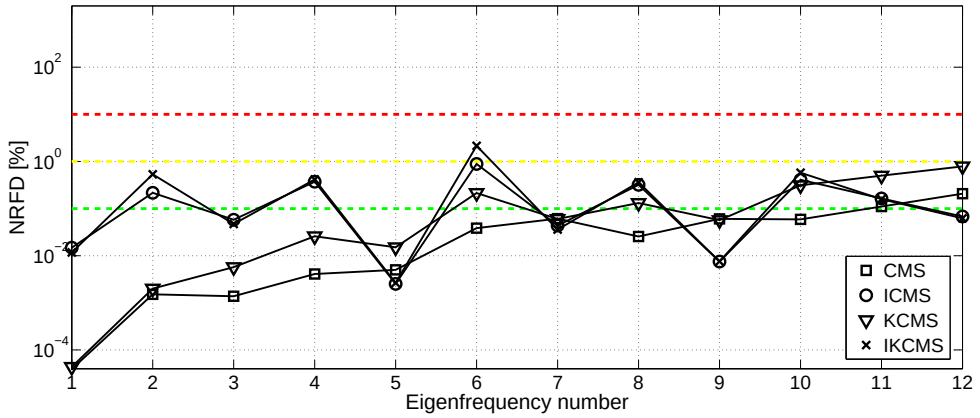

Figure 5.5: NRFD values for the component mode synthesis methods applied to the numerical example.

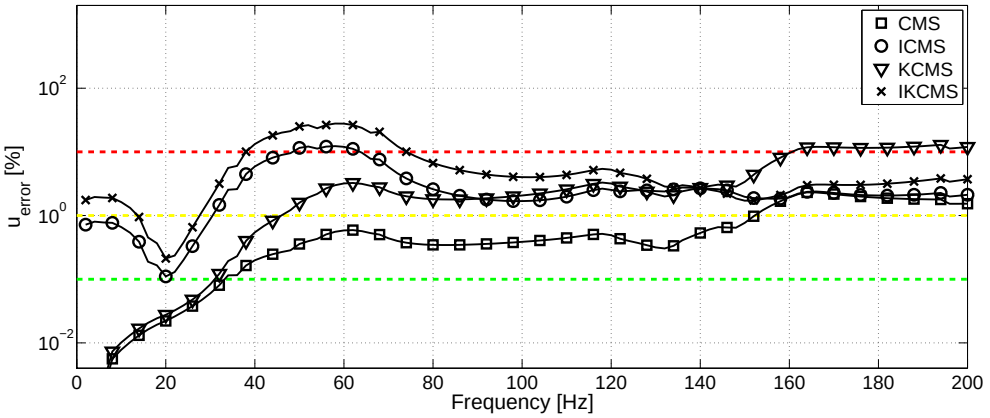

Figure 5.6: Errors in the steady-state analysis of the numerical example when employing the component mode synthesis methods.

In Figure 5.6, the errors obtained in the steady-state analyses are shown. It can be observed, by comparing the errors to those of the condensation methods, shown in Figure 5.4, that the results of ICMS and IKCMS are strongly correlated to those of IRS, all three methods resulting in large errors at lower frequencies and more accurate results at higher frequencies. It was only for the highest frequencies that the improved variants of the component mode synthesis methods offered an actual improvement. Among the different methods, CMS provided the most accurate results.

It should be noted that the results obtained by employing KCMS and IKCMS varies for different reduced systems constructed with the same method as the additional Ritz basis vectors are calculated for a random load distribution at the slave dofs. The variance in results due to the random distribution is, however, expected to be low in the numerical example since the number of slave dofs is relatively large.

Generalised methods

Next, all of the condensation methods and component mode synthesis methods were investigated in their generalised versions. The eigenfrequencies obtained are shown in Table 5.5 and Table 5.6, respectively, and the NRFD values in Figure 5.7 and Figure 5.9, respectively. For Guyan reduction and dynamic reduction, there was an overall improvement in accuracy when employed in their generalised versions, the exception being the lowest eigenfrequencies for Guyan reduction. g-IRS, however, did not offer an improvement compared to IRS, the two methods producing very similar results. Due to the decreased accuracy for the lowest eigenfrequencies when employing Guyan reduction in its generalised version, the same applies for CMS and KCMS, while the accuracy was similar between the original and generalised versions for the higher eigenfrequencies. Moreover, it can be observed that the errors obtained for ICMS and IKCMS were nearly unaffected by employing the methods in their generalised versions, an observation to be expected as the same was observed for IRS, utilised as condensation method in KCMS and IKCMS.

In Figure 5.8 and Figure 5.10, the levels of error obtained in the steady-state analyses are shown. It can be observed that the levels of error obtained for the generalised version of Guyan reduction do not converge to zero as the frequency goes to zero. Similarly, the levels of error obtained for the generalised version of dynamic reduction do not display a local minimum around the frequency shift of 90.173 Hz. For most frequencies, however, g-Guyan reduction and g-dynamic reduction improved the levels of error compared to their original versions. IRS and g-IRS, however, provided very similar levels of error. The errors obtained when employing g-CMS and g-KCMS were increased, as compared to CMS and KCMS, for lower frequencies.

Although the difference in accuracy between the condensation methods and the component mode synthesis methods was reduced when employing the methods in their generalised versions, the component mode synthesis methods were, in general, still more accurate.

Full model	g-Guyan-reduction	g-Dynamic-reduction	g-IRS
2.0148	2.0310	12.767	2.0412
9.9828	10.133	25.086	10.072
12.598	13.118	36.387	13.664
29.918	29.979	50.536	30.214
35.150	35.176	63.363	35.174
59.363	63.420	71.296	61.644
68.531	72.476	90.383	74.815
90.173	90.949	112.89	91.246
112.57	134.19	138.73	128.05
151.67	155.52	154.03	155.12
154.52	165.81	155.11	160.76
166.90	263.69	217.22	224.17

Table 5.5: Eigenfrequencies (Hz) obtained for the generalised condensation methods applied to the numerical example.

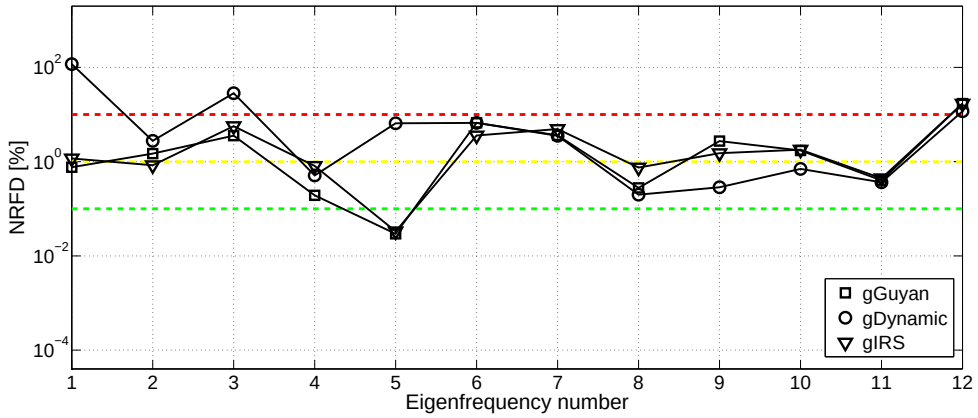

Figure 5.7: NRFD values for the generalised condensation methods applied to the numerical example.

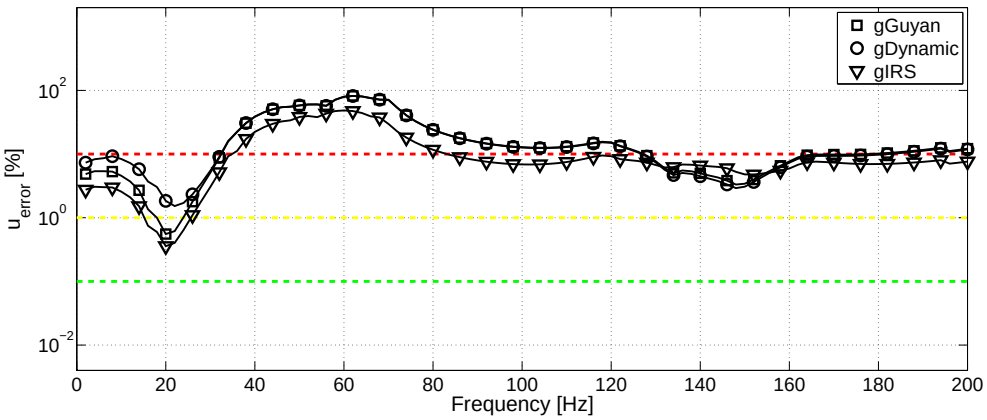

Figure 5.8: Errors in the steady-state analysis of the numerical example when employing the generalised condensation methods.

Full model	g-CMS	g-KCMS	g-ICMS	g-IKCMS
2.0148	2.0149	2.0149	2.0151	2.0175
9.9828	9.9891	9.9887	9.9941	9.9921
12.598	12.602	12.602	12.600	12.603
29.918	29.964	29.965	30.126	30.268
35.150	35.154	35.154	35.152	35.154
59.363	59.466	59.455	59.482	59.474
68.531	68.548	68.554	68.545	68.553
90.173	90.313	90.634	90.670	91.133
112.57	112.58	112.58	112.57	112.58
151.67	151.98	154.60	152.88	153.99
154.52	154.62	158.02	154.74	154.72
166.90	167.10	167.21	167.03	167.15

Table 5.6: Eigenfrequencies (Hz) obtained for the generalised component mode synthesis methods applied to the numerical example.

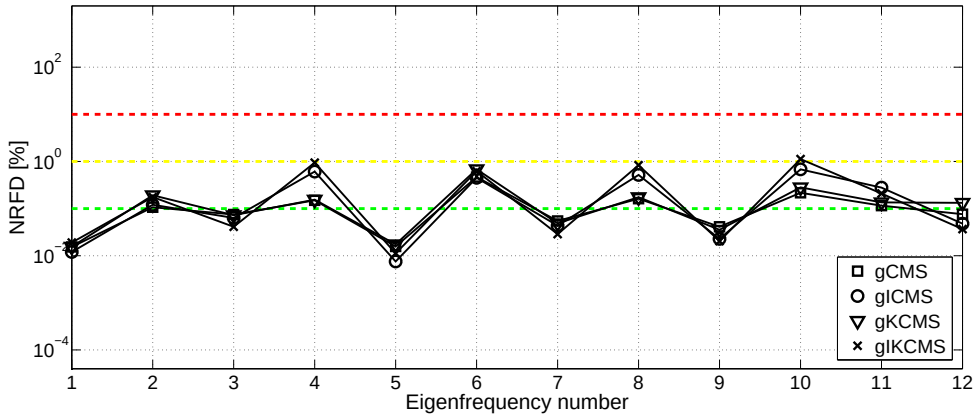

Figure 5.9: NRFD values for the generalised component mode synthesis methods applied to the numerical example.

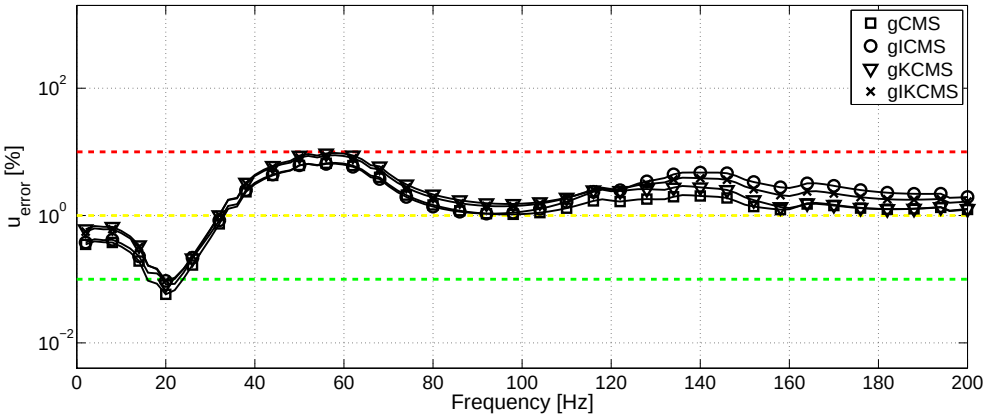

Figure 5.10: Errors in the steady-state analysis of the numerical example when employing the generalised component mode synthesis methods.

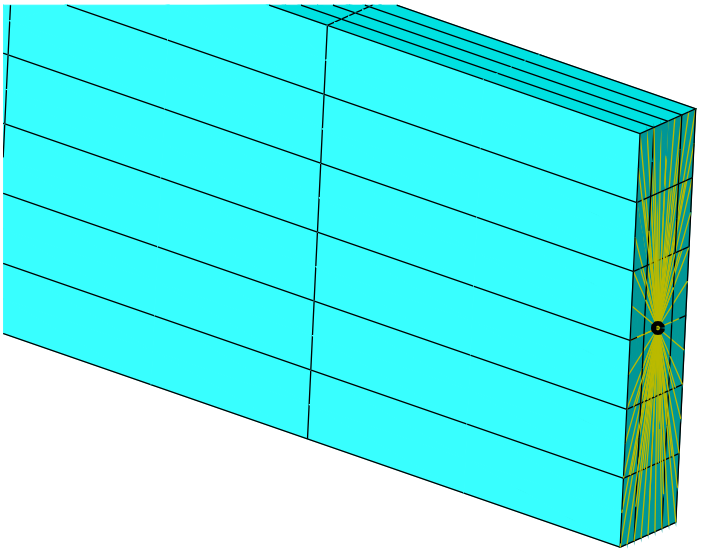

Figure 5.11: Coupling between a condensation node and the nodes located at an interface surface in the numerical example.

5.3.2 Interface reduction

The coupling between a condensation node and nodes of an interface surface is shown in Figure 5.11. All three interface surfaces, illustrated with the black crosses in Figure 5.2, were coupled to condensation nodes. At the free end of the beam, uniform weighting was employed since the load applied in the steady-state analyses was distributed equally over the nodes of the surface. Hence, the interface reduction at the free end does not introduce any errors for this load distribution. At the surfaces coupling the two substructures, rigid coupling and distributed coupling in its four versions were employed and compared. In each analysis, the same type of coupling was used for the two interface surfaces.

The eigenfrequencies obtained when employing the different methods for interface reduction are shown in Table 5.4 and the NRFD values are shown in Figure 5.5. Rigid coupling was the method resulting in the most accurate eigenfrequencies. At certain eigenfrequencies, however, the NRFD value is high also when employing rigid coupling, these being the eigenfrequencies having torsional eigenmodes. Compared to bending modes, the torsional eigenmodes involve larger deformations of the cross-section, these deformations being constrained at the interface surfaces when employing rigid coupling. As expected, the additional stiffness introduced in the system by a rigid coupling resulted in an overestimation of the eigenfrequencies. The opposite applied for the different types of distributed coupling, which resulted in an underestimation of the eigenfrequencies that in general increased when rising the degree of the weighting polynomial, cubic weighting providing in the least accurate results.

In Figure 5.13, the errors obtained in the steady-state analyses are shown. It is evident that rigid coupling provided the most accurate results, the levels of error being below 1.5 % for all frequencies. The different types of distributed coupling resulted in high levels of

Full model	Rigid coupling	Uniform weighting	Linear weighting	Quadratic weighting	Cubic weighting
2.0148	2.0149	2.0109	2.0048	2.0073	2.0007
9.9828	9.9835	9.9444	9.8768	9.9005	9.7912
12.598	12.600	12.492	12.333	12.399	12.230
29.918	30.714	29.424	29.100	29.138	28.953
35.150	35.151	35.146	35.118	35.128	35.105
59.363	59.366	58.503	56.902	57.418	55.159
68.531	68.538	67.984	67.178	67.508	66.674
90.173	92.192	88.892	88.091	88.187	87.722
112.57	112.58	112.53	112.26	112.36	112.13
151.67	154.65	148.91	147.25	147.45	146.48
154.52	156.35	154.08	154.34	154.38	154.21
166.90	166.91	165.62	163.78	164.52	162.66

Table 5.7: Eigenfrequencies (Hz) obtained for the different interface reduction methods applied to the numerical example.

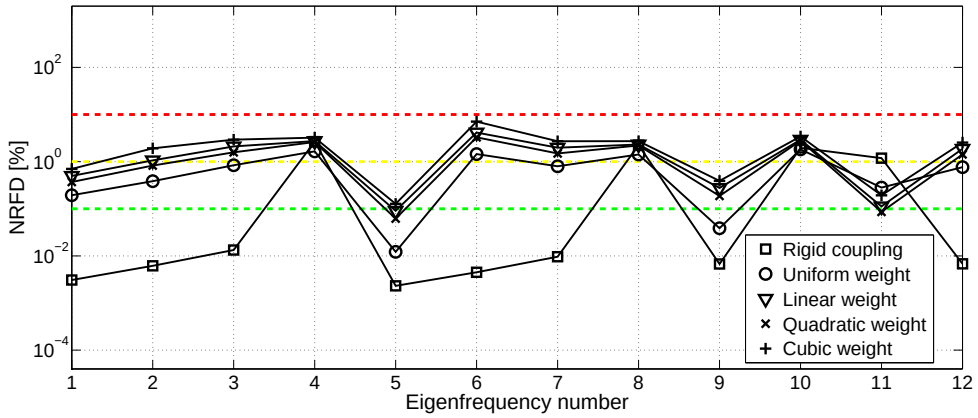

Figure 5.12: NRFD values obtained for the different interface reduction methods applied to the numerical example.

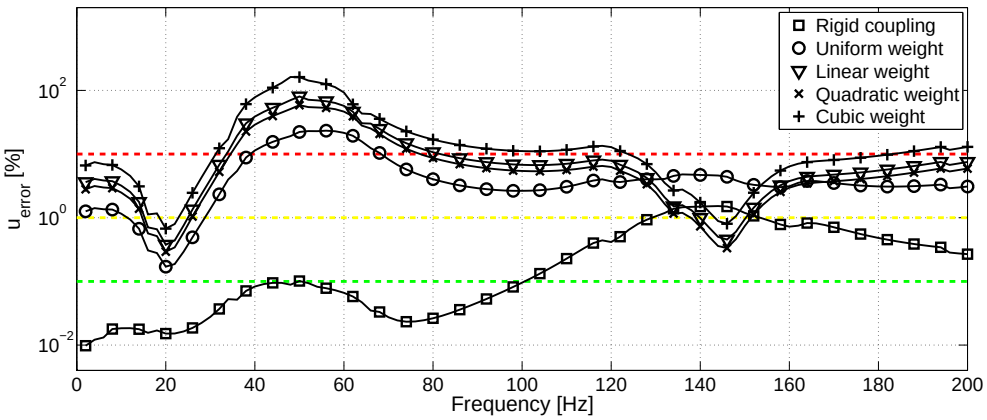

Figure 5.13: Errors in the steady-state analysis of the numerical example when employing the different interface reduction methods.

error with cubic weighting being the least accurate method. The accuracy of rigid coupling would be likely to decrease when applying a load causing torsional deformations of the beam.

In the numerical example, the two connecting interfaces are equally stiff. In case an interface surface, however, is much stiffer than the surface it is connected to, a distributed coupling is likely provide more accurate results for the stiffer surface than a rigid coupling would do. A rigid coupling is fully accurate in case the other surface is infinitely stiff, but can lead to large errors in case the other surface has a much lower stiffness.

5.3.3 Combining model order reduction and interface reduction

Finally, MOR was employed for a model with reduced interfaces. The MOR method and interface reduction method found to be most accurate in Sections 5.3.1 and 5.3.2, CMS and rigid coupling, respectively, were used. The number of eigenmodes retained in the CMS reduction was varied, the smallest system retaining 10 eigenmodes in each of the two substructures, the same number of eigenmodes as the model reduced by employing CMS without interface reduction, investigated in Section 5.3.1. Moreover, a model retaining 100 eigenmodes in each of the two substructures was investigated, as well as a model retaining 273 eigenmodes in the substructure containing the fixed end and 546 eigenmodes in the other, resulting in a total of 837 dofs, the same number of dofs as in the model reduced by employing the condensation methods without interface reduction. The computation time of the model retaining 10 eigenmodes in each substructure was approximately 0.2 % of the time required for the analysis of the full model.

The eigenfrequencies obtained when employing MOR in combination with interface reduction are shown in Table 5.8 and the NRFD values are shown in Figure 5.14. The model with 10 eigenmodes retained in each substructure, containing as few as 38 dofs in total, resulted in the levels of error being relatively low as compared with, for example, the model created by employing Guyan reduction without interface reduction, see Figure 5.3. The model retaining 100 eigenmodes in each substructure resulted in eigenfrequencies similar to those obtained when employing rigid coupling without MOR, see Figure 5.12, indicating that it is sufficient to retain 100 eigenmodes in each substructure. This observation is enhanced by the fact that the retaining of 273 and 546 eigenmodes in the two substructures, respectively, resulted in very similar eigenfrequencies as well. The additional retained eigenmodes did, therefore, not affect the dynamic characteristics of the reduced model.

In Figure 5.15, the levels of error obtained in the steady-state analyses are shown. The model retaining 10 eigenmodes provided relatively accurate results also in this analysis as compared to many of the models investigated in Section 5.3.1, which contained far more dofs. The two remaining models provided very similar levels of error, confirming the conclusion that the retaining of more than 100 eigenmodes in each substructure does not improve the accuracy.

Full model	CMS: 2×10 retain. eig.	CMS: 2×100 retain. eig.	CMS: 273+546 retain. eig.
2.0148	2.0149	2.0149	2.0149
9.9828	9.9836	9.9835	9.9835
12.598	12.600	12.600	12.600
29.918	30.719	30.717	30.717
35.150	35.152	35.151	35.151
59.363	59.389	59.366	59.366
68.531	68.580	68.538	68.538
90.173	92.315	92.289	92.289
112.57	112.65	112.58	112.58
151.67	154.82	154.65	154.65
154.52	156.78	156.69	156.69
166.90	167.26	166.92	166.91

Table 5.8: Eigenfrequencies (Hz) obtained when employing both interface reduction and MOR in the numerical example.

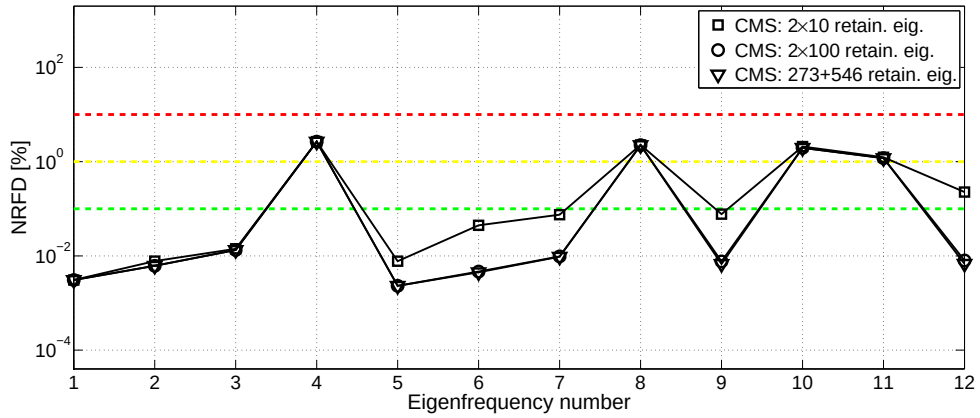

Figure 5.14: NRFD values obtained when employing both interface reduction and MOR in the numerical example.

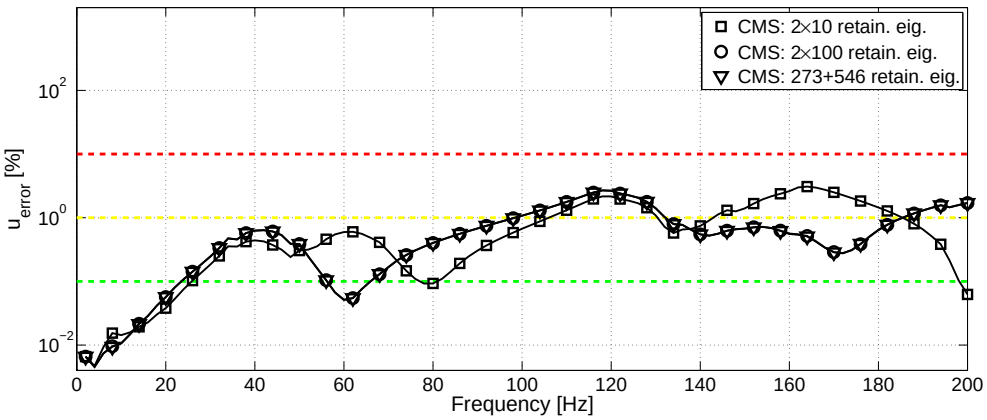

Figure 5.15: Errors in the steady-state analysis of the numerical example when employing both interface reduction and MOR in the numerical example.

5.3.4 Conclusions

The numerical example illustrated the limitations of Guyan reduction and dynamic reduction, the methods being reliable only close to their frequency shifts, namely 0 Hz in the Guyan reduction and 90.173 Hz in the dynamic reduction. In situations where an FE model is exposed to loads with narrow frequency content, dynamic reduction can, however, be a suitable alternative as it provides fully accurate results for steady-state analyses at its frequency shift. IRS provided relatively accurate results in terms of eigenfrequencies, but resulted in higher levels of error in the steady-state analysis. This illustrates the importance of exposing the reduced models to realistic loads and boundary conditions, and not only performing free-free eigenvalue analyses, when comparing different MOR methods.

To obtain an, in general, more accurate reduced order model, one of the component mode synthesis methods can be employed. CMS proved to be the method most accurate method in the numerical example, providing a significantly increased precision compared to Guyan reduction while increasing the size of the reduced system by no more than a few percent through the inclusion of a set of 10 additional Ritz basis vectors in each of the two substructures. This demonstrates the efficiency of CMS, the method most frequently employed among structural and mechanical engineers.

The use of KCMS resulted in acceptable levels of error for most frequencies, but was less accurate compared to CMS. KCMS can, however, be the most suitable method in situations where it is important to construct the reduced model in an efficient manner, avoiding the eigenvalue extraction carried out when employing CMS. The possible loss in accuracy of the reduced model can in such cases be compensated for by increasing the number of Krylov basis vectors included in the reduced model. Model order reduction always involves a consideration regarding the number of Ritz basis vectors to include, weighing the accuracy of the reduced model to its computational cost. Moreover, the Krylov subspace methods cannot be used to their full potential in the substructure modelling employed here as the aim is to establish models valid for general load-cases. The basis vectors in Krylov subspace methods are constructed by considering the load distribution on the structure, an advantage compared to other methods. The KCMS method presented in this chapter, however, uses a random load distribution for this, aiming at constructing reduced order models that perform well for varying load cases.

In the case of the numerical example, the name *improved* component mode synthesis methods proved to be misleading, these methods being less accurate compared to conventional CMS and KCMS.

Employing the generalised versions of Guyan reduction and dynamic reduction improved their accuracy significantly. The generalised formulation of the component mode synthesis methods did, however, not offer any considerable improvements and led to increased levels of error in the case of CMS. Overall, the results were more homogeneous among the condensation methods and component mode synthesis methods, respectively, when employed in their generalised versions.

Rigid coupling was the most accurate method for interface reduction, resulting in the lowest levels of error considering both eigenfrequencies and steady-state response. The distributed coupling methods displayed increasing levels of error for an increasing degree of

the weighting polynomial. The accuracy of the different methods are, however, dependent on the type of deformation the interface surface is exposed to, rigid coupling resulting in larger errors for the eigenmodes with torsional deformations in the numerical example.

The efficiency of models created by combining MOR and interface reduction (employing CMS and rigid coupling, respectively) was demonstrated, the resulting errors being kept at relatively low levels as compared to models created by employing either of the reductions. The size of the reduced systems was decreased substantially, the smallest model containing only 38 dofs, reducing the computation time to approximately 0.2 % of the time required for analysis of the full model, while resulting in low errors. The combination of MOR and interface reduction will be of great importance in the modelling of multi-storey wood buildings, resulting in reduced models of small size that are able to preserve the dynamic characteristics of the full model.

6 Summary of appended papers

6.1 Paper A

The effect of modelling acoustic media in cavities of lightweight building structures on the transmission of structural vibrations

O. Flodén, J. Negreira, K. Persson, G. Sandberg.

Submitted for publication.

Summary

It was investigated here if modelling air and insulation inside cavities of multi-storey wood buildings affects the transmission of low-frequency structural vibrations and, hence, has to be considered when performing numerical analyses. Two numerical examples, both being FE models of TVEs, were employed. The vibration transmission from loads acting on floor structures to surrounding panels was investigated for different models of air and insulation inside the cavities. Models including both air and insulation as acoustic media were compared to models including air alone and models including neither air nor insulation.

It was concluded that air and insulation inside cavities affect the vibration transmission and, to some extent, has to be considered in numerical models for vibration analyses of multi-storey wood buildings.

Contributions by O. Flodén

O. Flodén contributed to the work by being the main author of the paper and planning research tasks. He created FE models, performed calculations and drew conclusions that were presented.

6.2 Paper B

Reduction methods for the dynamic analysis of substructure models of lightweight building structures

O. Flodén, K. Persson, G. Sandberg.

Submitted for publication.

Summary

Different MOR methods were compared here in terms of their effects on the dynamic characteristics of FE models of wooden building structures in order to analyse their efficiency when employed in substructure modelling of multi-storey wood buildings. A wide variety of reduction methods were employed and compared in two numerical examples, both being models of wooden floor structures. The reduced models were compared in terms of eigenfrequencies and eigenmodes as well as the vibrations transmitted in the floors when exposing them to realistic boundary conditions, achieved by coupling the reduced models of the floor structures to models of wood-framed wall panels.

Conclusions were drawn regarding the relative efficiency of the reduction methods, the frequently employed method of CMS by Craig–Bampton providing good results. Moreover, the need for realistic boundary conditions and load cases when comparing the reduced order models was pointed out, concluding that free-free eigenvalue analyses of the models is insufficient.

Contributions by O. Flodén

O. Flodén contributed to the work by being the main author of the paper and writing it, as well planning the research tasks. He developed the FE models, implemented the MOR methods employed, performed the calculations and drew conclusions that were presented.

6.3 Paper C

Coupling elements for substructure modelling of lightweight multi-storey buildings

O. Flodén, K. Persson, G. Sandberg.

Accepted for the proceedings of *IMAC XXXII*, Orlando, USA, February 2014.

Summary

Different methods for reducing the interfaces between elastomer layers and wooden building structures were investigated here in order to analyse their efficiency when employed in substructure modelling of multi-storey wood buildings. The methodology of introducing condensation nodes was employed, involving different methods for coupling the condensation nodes to the interface surfaces of elastomer layers and wooden building structures. The methods were compared for a test model consisting of a floor-ceiling structure in wood, having the floor and the ceiling separated by elastomer blocks.

It was concluded that a rigid coupling is the most accurate method for the interface surfaces of elastomer blocks, while a distributed coupling is the most accurate method for the interfaces of wooden building structures.

Contributions by O. Flodén

O. Flodén contributed to the work by being the main author of the paper and writing it, as well planning the research tasks. He developed the FE models, performed the calculations and drew conclusions that were presented.

7 Concluding remarks

Numerical modelling of vibrations in multi-storey wood buildings requires the use of models representing the geometry involved in great detail, resulting in large models and, consequently, long computation times. It is, therefore, important to include only the relevant information and no more than a sufficient level of details in the models by considering, for example, to which extent the air and insulation inside cavities has to be included. Moreover, it is necessary to reduce the size of the resulting models to improve their computational efficiency, the methodology of substructuring being introduced for this purpose. Different MOR methods and interface reduction can be employed in substructure modelling, resulting in reduced models representing the dynamic characteristics of the full model with varying accuracy.

7.1 Conclusions

The acoustic media, air and insulation, in cavities of multi-storey wood buildings was found to affect the vibration transmission. It was observed that the vibrations in the ceiling and walls of a TVE, originating from a load acting on the floor structure of the TVE above, were affected by modelling the acoustic media inside the cavity between the floor and the ceiling and in the cavities in the surrounding walls. Including only air as acoustic media resulted in a more resonant system while the inclusion of both air and insulation introduced a dampening effect, particularly at higher frequencies. It was observed, for frequencies above 100 Hz, that modelling both air and insulation inside the wall cavities had no effect on the vibration transmission from the floor to the wall panels of the storey below. It is, therefore, sufficient to include acoustic media only in the cavity between the floor and the ceiling for higher frequencies. In such situations, it can be preferable to use different models for different frequency ranges. At higher frequencies, less acoustic media has to be included in the model while a finer mesh is required for resolving the wavelengths. At lower frequencies, more acoustic media have to be included whilst a coarser mesh can be adopted.

In the comparison of the different MOR methods, employed for substructures of multi-storey wood buildings, the condensation methods Guyan reduction and dynamic reduction proved to be insufficient. More accurate reduced models can be obtained by employing one of the component mode synthesis methods investigated, the frequently employed method by Craig–Bampton as well as the Krylov subspace based KCMS providing good results. Moreover, the need for realistic boundary conditions and load cases when comparing

the reduced models was pointed out, concluding that free-free eigenvalue analyses of the models is insufficient.

In the reduction of interfaces between wooden building structures and elastomer blocks, different methods for coupling the interfaces to condensation nodes was found to be most accurate for the wooden structures and the elastomer blocks. The interior of an elastomer block undergoes large deformations compared to its interface surfaces as the interfaces are coupled to the stiffer wooden structures, resulting in a rigid coupling providing the most accurate results for the elastomer blocks. For the wooden structures, however, uniformly distributed coupling provided the most accurate results. This can be explained by the fact that no considerable constraints are imposed on the deformation of their interface surfaces by the softer elastomer blocks they are coupled to.

7.2 Proposals for future work

In the modelling of insulation inside cavities, different porous material models were investigated. These are, however, only a few of many methods available in the literature. As it was concluded that acoustic media has to be considered inside cavities of lightweight buildings, it should be validated that the insulation is modelled in an accurate manner.

It was observed that the effect of including acoustic media inside cavities of wooden buildings was decreasing at further distances from the load. A future development is to investigate how far from the load the acoustic media has to be considered in order to avoid models including an excessive amount of acoustic media.

The comparisons of the different methods for MOR and interface reduction have provided knowledge concerning their relative efficiency when employed for models of wooden building structures. The aim is to utilise this knowledge in establishing a framework for constructing computationally efficient models of multi-storey wood buildings. Initially, substructure models reduced by employing both MOR and interface reduction can be investigated. Subsequently, the assembling of the substructures to form reduced models of entire buildings can be studied.

Once a framework for establishing the models is created, the models have to be validated to measurements on real buildings. This is the most challenging task in the process of obtaining reliable prediction tools. Ideally, the models of entire buildings will represent the dynamic characteristics of real buildings, a first step in achieving this being to validate the model of each substructure, such as, floors, walls and TVEs.

As air and insulation inside cavities of wooden buildings has to be considered in the models, it has to be involved in the substructure framework as well. The global FE model should, however, not be divided into substructures so that they have acoustic media at the interface surfaces as this results in very large interfaces, destroying the efficiency of the model order reduction. Consequently, the acoustic media has to be included inside the substructures, requiring an alternative division of TVE buildings into substructures, no longer considering each TVE as a substructure. Depending on the extent to which the acoustic media has to be considered, the substructures including acoustic media can be included locally in a model of an entire building in the parts of the building where it is required.

Bibliography

[1] Stehn L., Rask L.O., Nygren I. Östman B., Byggandet av flervåningshus i trä – Erfarenheter efter tre års observation av träbyggandets utveckling. Technical Report, Luleå University of Technology, Sweden, 2008.

[2] Gustavsson L., Pingoud K., Sathre R. Carbon dioxide balance of wood substitution: comparing concrete- and wood-framed buildings. Mitig Adapt Strateg Glob Change, 2006;11:667–691.

[3] Swedish Ministry of Enterprise, Energy and Communications. Mer trä i byggandet – Underlag för en nationell strategi att främja användning av trä i byggande, Ds 2004:1. Stockholm, 2004.

[4] Forssén J., Kropp W., Brunskog J., Ljunggren S., Bard D., Sandberg G., Ljunggren F., Ågren A., Hallström O., Dybro H., Larsson K., Tillberg K., Sjökvist L.G., Östman B., Hagberg K., Bolmsvik Å., Olsson A., Ekstrand C.G., Johansson M. Acoustics in wooden buildings – State of the art 2008. Vinnova project 2007-01653, Report 2008:16, SP Trätek, Stockholm, 2008.

[5] Labonnote N. Damping in timber structures. PhD thesis, Department of Structural Engineering, Norwegian University of Science and Technology, Trondheim, Norway, 2005.

[6] Ljunggren F., Ågren A.. Potential solutions to improved sound performance of volume based lightweight multi-storey timber buildings. Appl Acoust, 2011;72:231–240.

[7] Vigran T.E. Building acoustics. Taylor & Francis, New York, 2008.

[8] Ågren A. Acoustic highlights in Nordic light weight building tradition – Focus on ongoing development in Swedish. Proc of BNAM, Bergen, Norway, 2010.

[9] Flodén O., Ejenstam J., Vibration analyses of a wooden floor-wall structure – Experimental and finite element studies. Masters dissertation, Division of Structural Mechanics, Lund University, Sweden, 2011.

[10] Negreira J. Vibrations in lightweight buildings – Perception and prediction. Licentiate dissertation, Division of Engineering Acoustics, Lund University, Sweden, 2013.

[11] Bathe K.J. Finite element procedures. Prentice Hall, New York, 1996.

[12] Ottosen N., Petersson H. Introduction to the finite element method. Pearson Education Ltd., Harlow, United Kingdom, 1992.

[13] Holzapfel G.A. Nonlinear solid mechanics: a continuum approach for engineering. John Wiley & Sons Ltd., Chichester, United Kingdom, 2000.

[14] Sandberg G. Finite element modelling of fluid-structure interaction. PhD thesis, Division of Structural Mechanics, Lund University, Sweden, 1986.

[15] Craig R.R. Structural dynamics – An introduction to computer methods. John Wiley & sons Inc., New York, 1981.

[16] Chopra A.K. Dynamics of structures: theory and application to earthquake engineering 3d ed. Prentice Hall, New Jersey, 2007.

[17] de Klerk D., Rixen D.J., Voormeeren S.N. General framework for dynamic substructuring: history, review and classification of techniques. AIAA J, 2008;46(5):1169–1181.

[18] Heirman G.H.K., Desmet W. Interface reduction of flexible bodies for efficient modeling of body flexibility in multibody dynamics. Multibody Syst Dyn, 2010;24(2):219–234.

[19] Guyan R.J. Reduction of stiffness and mass matrices. AIAA J 1965;3:380.

[20] Bouhaddi N., Fillod R. A method for selecting master dof in dynamic substructuring using the Guyan condensation method. Comput Struct, 1992;45(5):941–946.

[21] Shah V., Raymund M. Analytical selection of masters for the reduced eigenvalue problem. Int J Numer Methods Eng, 1982;18(1):89–98.

[22] Leung A.Y.T. An accurate method of dynamic condensation in structural analysis, Int J Numer Methods Eng, 1978;12:1705–1715.

[23] O'Callahan J. A procedure for an improved reduced system (IRS) model. Proc 7th Int Modal Anal Conf, 1989;17–21.

[24] Friswell M.I., Garvey S.D., Penny J.E.T. Model reduction using dynamic and iterated IRS techniques. J Sound Vib, 1995;186:311–323.

[25] O'Callahan J., Avitabile P., Riemer R. System equivalent reduction expansion process (SEREP). Proc 7th Int Modal Anal Conf, 1989;29–37.

[26] Craig R.R., Bampton M. Coupling of substructures in dynamic analysis. AIAA J, 1968;6:1313–1319.

[27] Lohmann B., Salimbahrami B. Introduction to Krylov subspace methods in model order reduction. Methods Appl Autom, 2003;1–13.

[28] Salimbahrami B., Lohmann B. Order reduction of large scale second-order systems using Krylov subspace methods. Linear Algebra Appl, 2006;415(2):385–405.

[29] Reis T., Stykel T. Balanced truncation model reduction of second-order systems. Math Comput Model Dyn Syst, 2008;14(5):391–406.

[30] Koutsovasilis P., Beitelschmidt M. Model order reduction of finite element models: improved component mode synthesis. Math Comput Model Dyn Syst, 2010;16(1):57–73.

[31] Häggblad B., Eriksson L. Model reduction methods for dynamic analyses of large structures. Comput Struct, 1993;47(4):735–749.

[32] Koutsovasilis P. Improved component mode synthesis and variants. Multibody Syst Dyn, 2013;29(4):343–359.

[33] Dassault Systèmes, Abaqus theory manual – Version 6.12, 2012.

Part II

Appended publications

Paper A

The effect of modelling acoustic media in cavities of lightweight buildings on the transmission of structural vibrations

O. Flodén, J. Negreira, K. Persson, G. Sandberg

Lund University
Department of Construction Sciences
P.O. Box 118, SE-22100 Lund, Sweden

Submitted for publication

The effect of modelling acoustic media in cavities of lightweight buildings on the transmission of structural vibrations

Ola Flodén, Juan Negreira, Kent Persson, Göran Sandberg
Lund University, Department of Construction Sciences, P.O. Box 118, SE-22100 Lund, Sweden

Abstract

Determining the dynamic behaviour of lightweight buildings by means of finite element analyses requires models representing the geometry involved in great detail, this resulting in systems having many millions of degrees of freedom. It is, therefore, important to avoid unnecessarily detailed models by carefully considering what is necessary to include in the models, and the level of details required for describing the phenomena of interest accurately. In the study presented here, it was investigated whether or not air and insulation inside cavities of multi-storey wood buildings affect the transmission of low-frequency structural vibrations. It was concluded from the numerical studies carried out that including air and insulation inside cavities, modelled as acoustic media, affects the transmission from a floor to the underlying ceiling and surrounding walls.

Keywords: Air inclusion; Porous materials; Vibration transmission; Lightweight buildings; Finite element method

1 Introduction

In 1994, a century-old ban on the construction of wooden buildings more than two storeys in height in Sweden was lifted, leading to the reintroduction of such structures. It is difficult to construct multi-storey wood buildings in such a way that noise and disturbing vibrations in the different storeys and rooms are avoided, this being one of the major drawbacks of such buildings. The vibrations can be caused by, for example, footsteps, airborne sound, vibrating machines and external sources such as railway and road traffic. To design buildings of high performance regarding vibrations and structure-borne sound, it is desirable to have tools for predicting the effects of structural modifications prior to construction. Testing prototypes and performing experiments is both time-consuming and expensive, the long-term aim therefore being to develop prediction tools making use of finite element (FE) models that are valid for general load-cases.

Accurately assessing the dynamic behaviour of multi-storey lightweight buildings, even at lower frequencies, requires FE models representing the geometry in considerable detail, resulting in the models being very large. The number of degrees of freedom of such models easily exceeds the limits of computer capacity, at least for computations to be performed within reasonable lengths of time. It is, therefore, important to avoid unnecessarily detailed models by carefully considering what is necessary to include in the models, and the level of details required for describing the phenomena of interest accurately. The issue considered here is whether or not air and insulation inside cavities of multi-storey wood buildings affect the transmission of low-frequency structural vibrations.

The acoustic pressure field in a room can interact with the vibrations in the floor, ceiling and walls. For heavier structures, the influence of the acoustic pressure waves on the structural vibrations is usually negligible. It is, therefore, possible to analyse the acoustic pressure field by applying the structural displacements, obtained from a precedent analysis of the structural domain, as boundary conditions. It was concluded in [1] that this procedure is valid also for lightweight buildings; studies on a 2D FE model of a two-storey wood building showing that the inclusion of air in the rooms has a negligible effect on the displacements of the building for frequencies below 250 Hz, the air being modelled to have a realistic acoustic damping (present in buildings due to objects and porous materials such as curtains and carpets). In multi-storey wood buildings, there are acoustic media not only in the rooms, but also inside the many cavities containing both air and insulation. The effect of modelling air inside cavities of lightweight double-plate wall panels was investigated in [2, 3]. In [2], the vibration transmission was investigated for a model including two double-plate wall panels connected in an L-shape, with and without air inside the cavities. Both eigenvalue and steady-state analyses showed that the inclusion of air in the cavities of the structure has a large influence on its dynamic characteristics at high frequencies and a noticeable effect already at the first eigenfrequency. In [3], the response of a double-plate wall panel, with and without air inside the cavities, to diffuse field excitation was investigated. Simulations in terms of eigenvalue and steady-state analyses showed that the air has a negligible effect on the dynamic characteristics of the structure.

1.1 Objective

The studies presented here aim at determining whether or not air and insulation inside cavities have to be considered when performing numerical vibration analyses of multi-storey lightweight buildings. The studies are limited to the low-frequency range, defined here as frequencies below 200 Hz. As a first step, different porous material models for modelling of the insulation were compared, a frame of a double-plate wall panel being employed as a test model. Subsequently, numerical studies were carried out for a section of a multi-storey wood building constructed with so-called timber volume elements (TVEs), such buildings being described in section 1.2. The response of a floor exposed to a harmonic point load and the vibration transmission to the underlying ceiling and the surrounding walls were investigated by comparing FE models including the acoustic media in terms of air and insulation inside cavities to models without acoustic media. An additional objective with the numerical studies is to provide knowledge regarding the effect of modelling the insulation, and how this changes the response of the models compared to considering the air alone.

1.2 Timber volume element buildings

The conceptual layout of a TVE building is illustrated in Figure 1. A TVE is a prefabricated volume module consisting of wood framed floor-, roof- and wall-elements, each TVE typically constituting a small apartment, one room or part of a larger room. As much of the construction work as possible is performed indoors at a factory, including electrical installations, flooring, cabinets, wardrobes etc. The prefabricated modules are transported to the construction site where they are stacked to form a complete building. In between the TVEs, several elastomer blocks are introduced to reduce flanking transmission of vibrations. Each elastomer block has an interface area of approximately 0.1×0.1 m^2 and is placed between the walls of two stacked modules. The only additional connection between modules is through a number tie plates, ensuring the global stability of the building. Vibrations transmitted in TVE buildings are, therefore, mainly passing through the elastomer layers or through the air and insulation in cavities of the buildings. The FE models employed in the numerical studies presented here were constructed according to the drawings shown in Figure 2.

2 Governing theory

2.1 Structure-acoustic analysis

Vibrating structures can interact with surrounding fluids, inducing acoustic pressure waves, and vice versa. This phenomenon can be analysed by deriving FE formulations both for the structural domain and the acoustic fluid domain. By imposing continuity conditions for displacements and pressures at domain-separating boundaries, the domains form a coupled FE equation system. Vibrations in lightweight buildings are usually of such amplitudes that any non-linear behaviour can be neglected and, therefore, linear behaviour is assumed here for both domains. In the following derivations, a subscript S denotes a quantity in the structural domain, whereas a subscript F indicates a quantity in the acoustic fluid domain.

2.1.1 Structural domain

The equations describing the structural domain follow the notation in [5]. For a detailed derivation of the FE formulation of a solid, see e.g. [5, 6]. The differential equation of motion for the continuum formulation of a three-dimensional solid, occupying the domain Ω_S, is given as [7]

$$\tilde{\boldsymbol{\nabla}}^T \boldsymbol{\sigma}_S + \mathbf{b}_S = \rho_S \frac{\partial^2 \mathbf{u}_S}{\partial t^2}, \tag{1}$$

where $\boldsymbol{\sigma}_S$ is the matrix representation of the stress tensor, $\mathbf{b}_S$ is the body force vector, ρ_S is the mass density, $\mathbf{u}_S$ is the displacement vector, $\tilde{\boldsymbol{\nabla}}$ is a differential operator matrix and t is the time. A FE discretisation and use of Galerkin's method results in a FE formulation in the structural domain, given by

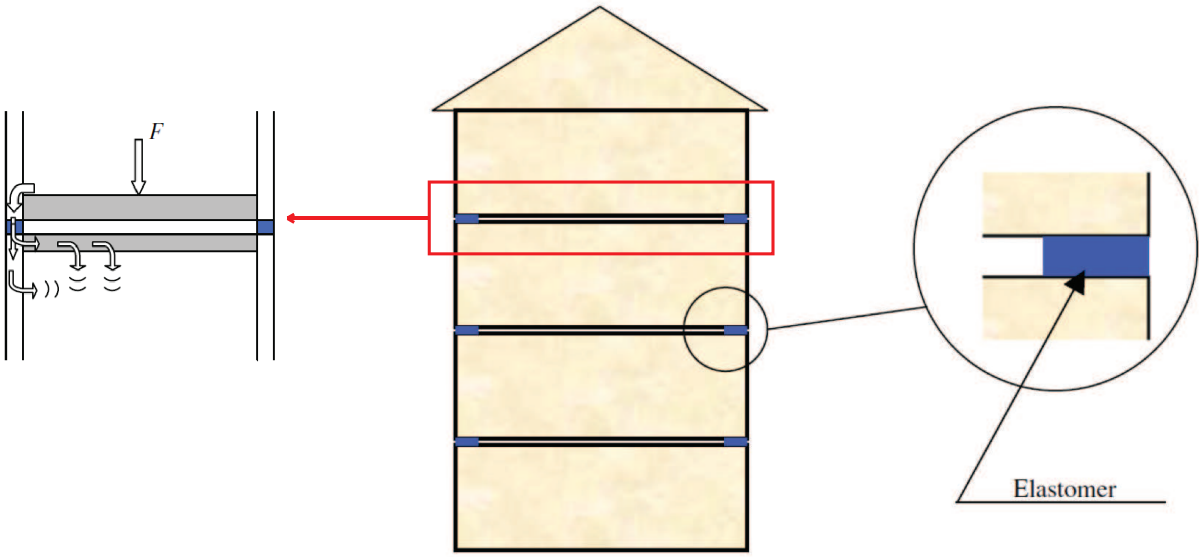

Figure 1: Sketch of a TVE building [4]. The path of structural vibrations between storeys is illustrated in the figure to the left and an elastomer block is illustrated in the figure to the right.

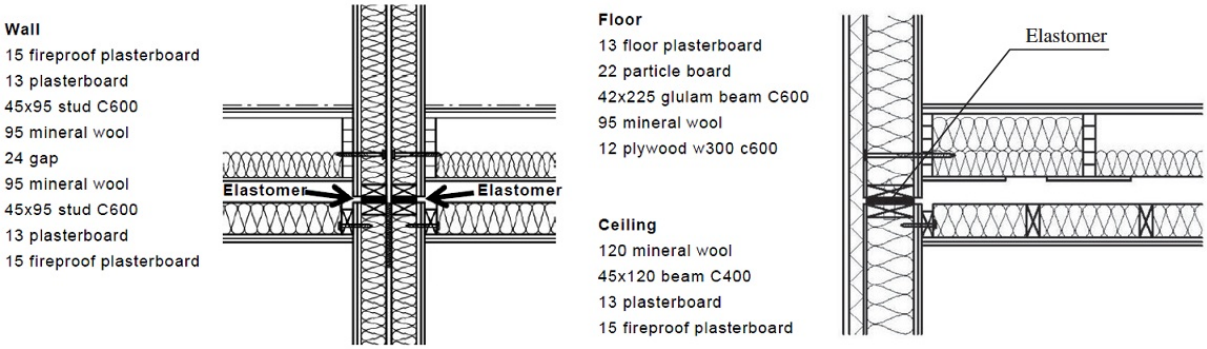

Figure 2: Drawings of the TVE building system, showing sections of the floor and ceiling structures and the junctions with apartment separating wall (left) and façade wall (right).

$$\mathbf{M}_S\ddot{\mathbf{a}}_S + \mathbf{K}_S\mathbf{a}_S = \mathbf{f}_{l,S} + \mathbf{f}_{b,S}, \tag{2}$$

$$\begin{aligned} \mathbf{M}_S &= \int_{\Omega_S} \mathbf{N}_S^T \rho_S \mathbf{N}_S \, \mathrm{d}V, \qquad & \mathbf{K}_S &= \int_{\Omega_S} (\tilde{\boldsymbol{\nabla}}\mathbf{N}_S)^T \mathbf{D}_S \tilde{\boldsymbol{\nabla}}\mathbf{N}_S \, \mathrm{d}V, \\ \mathbf{f}_{l,S} &= \int_{\Omega_S} \mathbf{N}_S^T \mathbf{b}_S \, \mathrm{d}V, & \mathbf{f}_{b,S} &= \int_{\partial\Omega_S} \mathbf{N}_S^T \mathbf{t}_S \, \mathrm{d}S. \end{aligned} \tag{3}$$

where $\mathbf{M}_S$ is the mass matrix, $\mathbf{K}_S$ is the stiffness matrix, $\mathbf{a}_S$ is the nodal displacement vector, $\mathbf{f}_{l,S}$ is the body load vector, $\mathbf{f}_{b,S}$ is the boundary load vector, $\mathbf{N}_S$ contains the FE shape functions, $\mathbf{D}_S$ is the constitutive stress-strain matrix and $\mathbf{t}_S$ is the surface traction vector. Normally, a term $\mathbf{C}_S\dot{\mathbf{a}}_s$, where $\mathbf{C}_S$ is the damping matrix, is added to the left-hand side of Eq. (2) to account for viscous forces present in the structure.

2.1.2 Acoustic fluid domain

In addition to the assumption of small displacements, the governing equations of the acoustic fluid are derived supposing the fluid to be irrotational. The motion of an acoustic fluid can be described using different primary variables, such as the fluid displacement or a fluid displacement potential. In the FE formulation presented here, the acoustic pressure is used as primary variable. A detailed description of the FE formulation of an acoustic fluid, and the structure-acoustic coupling, can be found in [8], for example. The motion of the fluid in the acoustic fluid domain Ω_F is governed by the equation of motion and the continuity equation

$$\rho_0 \frac{\partial^2 \mathbf{u}_F}{\partial t^2} + R \frac{\partial \mathbf{u}_F}{\partial t} + \boldsymbol{\nabla} p_F = 0, \tag{4}$$

$$\frac{\partial p_F}{\partial t} + \rho_0 c_0^2 \boldsymbol{\nabla} \cdot \frac{\partial \mathbf{u}_F}{\partial t} = 0, \tag{5}$$

where p_F is the acoustic pressure, ρ_0 is the static density, R is the flow resistivity, c_0 is the speed of sound and $\boldsymbol{\nabla}$ is the gradient operator. By differentiating Eq. (5) with respect to time and inserting it in Eq. (4), the wave equation in the acoustic fluid domain is obtained as

$$\frac{1}{c_0^2} \frac{\partial^2 p_F}{\partial t^2} + \frac{R}{\rho_0 c_0^2} \frac{\partial p_F}{\partial t} - \boldsymbol{\nabla}^2 p_F = 0. \tag{6}$$

An FE discretisation and use of Galerkin's method results in an FE formulation in the acoustic fluid domain, given as

$$\mathbf{M}_F \ddot{\mathbf{p}}_F + \mathbf{C}_F \dot{\mathbf{p}}_F + \mathbf{K}_F \mathbf{p}_F = \mathbf{f}_{b,F}, \tag{7}$$

$$\begin{aligned} \mathbf{M}_F &= \frac{1}{c_0^2} \int_{\Omega_F} \mathbf{N}_F^T \mathbf{N}_F \, \mathrm{d}V, & \mathbf{C}_F &= \frac{R}{\rho_0 c_0^2} \int_{\Omega_F} \mathbf{N}_F^T \mathbf{N}_F \, \mathrm{d}V, \\ \mathbf{K}_F &= \int_{\Omega_F} (\boldsymbol{\nabla} \mathbf{N}_F)^T \boldsymbol{\nabla} \mathbf{N}_F \, \mathrm{d}V, & \mathbf{f}_{b,F} &= \int_{\partial \Omega_F} \mathbf{N}_F^T \mathbf{n}_F^T \boldsymbol{\nabla} p_F \, \mathrm{d}S, \end{aligned} \tag{8}$$

where $\mathbf{p}_F$ is the nodal pressure vector, $\mathbf{f}_{b,F}$ is the boundary load vector and $\mathbf{n}_F^T$ is the boundary normal vector, pointing outwards from the acoustic fluid domain.

2.1.3 Coupling of domains

At interfaces connecting a structural domain to an acoustic fluid domain, denoted $\partial \Omega_{SF}$, there will naturally be a continuity both in terms of displacements and pressures. By imposing conditions of continuity as boundary conditions at the interface, the two systems of equations describing the separate domains are coupled into a single system, including the interaction of the domains. The continuity in displacements and pressures at $\partial \Omega_{SF}$ can be expressed as

$$\mathbf{u}_S \mathbf{n}_F = \mathbf{u}_F \mathbf{n}_F, \tag{9}$$

$$\boldsymbol{\sigma}_S|_{n_F} = -p_F, \tag{10}$$

where $\boldsymbol{\sigma}_S|_{n_F}$ is the stress normal to $\partial\Omega_{SF}$. By introducing the spatial coupling matrix

$$\mathbf{H}_{SF} = \int_{\partial\Omega_{SF}} \mathbf{N}_S^T \mathbf{n}_F \mathbf{N}_F \, \mathrm{d}S, \tag{11}$$

the boundary load vectors at $\partial\Omega_{SF}$ can be rewritten as

$$\mathbf{f}_{b,S} = \mathbf{H}_{SF}\mathbf{p}_F, \tag{12}$$

$$\mathbf{f}_{b,F} = -\rho_0 \mathbf{H}_{SF}^T \ddot{\mathbf{a}}_S - R\mathbf{H}_{SF}^T \dot{\mathbf{a}}_S. \tag{13}$$

Using Eq. (12) and Eq. (13) in combination with Eq. (2) and Eq. (7), results in the structure-acoustic system of equations

$$\begin{aligned} &\begin{bmatrix} \mathbf{M}_S & \mathbf{0} \\ \rho_0 \mathbf{H}_{SF}^T & \mathbf{M}_F \end{bmatrix} \begin{bmatrix} \ddot{\mathbf{a}}_S \\ \ddot{\mathbf{p}}_F \end{bmatrix} + \begin{bmatrix} \mathbf{C}_S & \mathbf{0} \\ R\mathbf{H}_{SF}^T & \mathbf{C}_F \end{bmatrix} \begin{bmatrix} \dot{\mathbf{a}}_S \\ \dot{\mathbf{p}}_F \end{bmatrix} \\ &\quad + \begin{bmatrix} \mathbf{K}_S & -\mathbf{H}_{SF} \\ \mathbf{0} & \mathbf{K}_F \end{bmatrix} \begin{bmatrix} \mathbf{a}_S \\ \mathbf{p}_F \end{bmatrix} = \begin{bmatrix} \mathbf{f}_{l,S} \\ \mathbf{0} \end{bmatrix} + \begin{bmatrix} \mathbf{f}_{b,S} \\ \mathbf{f}_{b,F} \end{bmatrix}, \end{aligned} \tag{14}$$

where $\mathbf{f}_{b,S}$ and $\mathbf{f}_{b,F}$ contain contributions from the parts of the domain boundaries $\partial\Omega_S$ and $\partial\Omega_F$, respectively, separated from the interface boundary $\partial\Omega_{SF}$.

2.2 Porous material models

The use of different types of mineral wool in façades and interior walls of lightweight buildings is common in order to improve both thermal and acoustic insulation. The interaction between air and fibres of the wool affects the propagation of pressure waves in the air, the porous structure forcing the waves to travel a longer distance and a dampening effect occurring due to friction at the surface of the fibres. Moreover, the pressure waves in the air interact with any potential motion of the fibres. Different approaches for modelling porous materials have been proposed in the literature, some being based on empirical studies, suggesting prediction formulae of acoustic properties based on parameter fitting to experimental data. Others are analytical and based on certain assumptions regarding the geometry and behaviour of the structural frame and the interaction with the air. This section presents three porous material models, two of them empirical and one analytical, as well as brief literature reviews concerning other models within the two categories. The three models presented here consider the porous materials as equivalent acoustic fluids. They can, therefore, be analysed with the numerical methods employed for acoustic fluids and are integrated in a structure-acoustic model in a straightforward manner.

In Eq. (4) and (5), two material parameters describing an acoustic fluid were introduced, namely the speed of sound c_0 and the static density ρ_0. A common, alternative, way of describing an acoustic fluid is by its static density together with the bulk modulus K, related to the speed of sound according to

$$K = \rho_0 c_0^2. \tag{15}$$

Another pair of material parameters that are frequently employed to describe an acoustic fluid are the characteristic impedance Z together with the propagation constant k. The two latter alternatives of material parameters are related according to

$$Z = \sqrt{\rho_0 K}, \tag{16}$$

$$k = \omega \sqrt{\frac{\rho_0}{K}}, \tag{17}$$

where ω is the angular frequency.

2.2.1 Empirical models

Delany-Bazley

Empirical relationships relating the real and imaginary parts of the characteristic impedance and the propagation constant to the quotient (f/R), where f is frequency, were developed in [9]. Measurements of the characteristic impedance, propagation constant and flow resistivity were carried out for a range of mineral wools, the following power law relations being obtained by fitting the coefficients to experimental data:

$$Z = \rho_0 c_0 \left(1 + 9.08 \left(\frac{f}{R} \right)^{-0.75} - i\, 11.9 \left(\frac{f}{R} \right)^{-0.73} \right), \tag{18}$$

$$k = \frac{\omega}{c_0} \left(10.3 \left(\frac{f}{R} \right)^{-0.59} + i \left[1 + 10.8 \left(\frac{f}{R} \right)^{-0.70} \right] \right), \tag{19}$$

where data in the range $0.01 \leq f/R \leq 1.0$ (Nm^{-4}) were used. It is advised not to extrapolate the power law relations outside this range.

Miki

The real part of the characteristic impedance calculated according to Eq. (18) becomes negative at low frequencies. To avoid this unphysical phenomena, new power law relations were developed in [10], making use of the experimental data utilised in [9] and imposing constraints for the real part of the characteristic impedance to be positive, resulting in

$$Z = \rho_0 c_0 \left(1 + 5.50 \left(\frac{f}{R} \right)^{-0.632} - i\, 8.43 \left(\frac{f}{R} \right)^{-0.632} \right), \tag{20}$$

$$k = \frac{\omega}{c_0} \left(7.81 \left(\frac{f}{R} \right)^{-0.618} + i \left[1 + 11.41 \left(\frac{f}{R} \right)^{-0.618} \right] \right). \tag{21}$$

The developed empirical formulae are physically realisable at lower frequencies compared to the formulae by Delany & Bazley. Unphysical properties will, however, occur also in this case, the real part of the density becoming negative at low frequencies. As the power law relations were fitted to the experimental data in [9], no conclusions can be made regarding the validity of the model outside the range $0.01 \leq f/R \leq 1.0$ (Nm^{-4}).

Other empirical models

In addition to the formulae by Delany & Bazley and Miki, a number of empirical relations for Z and k have been suggested in the literature. The same procedure as in [9] was applied to measurement data for foam materials in [11]. In [12], measurements were performed for a wide range of glass and rock wools, concluding that prediction formulae involving logarithmic terms resulted in better correlation to the measurement data in comparison to power law relations developed in the same manner as in [9]. In [13] and [14], porous material models combining the empirical formulae by Delany & Bazley with analytical microstructure models, assuming parallel fibres, were presented, resulting in physically meaningful predictions at low frequencies.

2.2.2 Analytical models

Already in 1868, a theory for sound propagation in cylindrical tubes, including both viscous and thermal effects, was presented in [15], a simplified model later being presented in [16]. Porous materials generally have complex geometries, making it practically impossible to analyse the exact microstructure. This is why most porous material models are phenomenological, an approach being valid in case the wave lengths are much larger than the characteristic dimensions of the microstructure. Several analytical models for porous materials, involving different assumptions regarding the geometry and behaviour of the structural frame as well as the interaction between the frame and the acoustic fluid, have been proposed.

Equivalent acoustic fluid model – rigid structural frame

Phenomenological equivalent acoustic fluid models assuming the structural frame to be rigid have been presented in [16, 17]. These models involve two properties of the structural frame, namely the porosity ϕ and the structure factor K_S, also known as the tortuosity. ϕ is the ratio of fluid volume to total volume while K_S is defined as $\rho_e = K_S\rho_0$, relating the density of the acoustic fluid in the pores to an effective density ρ_e of the equivalent acoustic fluid. With a rigid structural frame, the equation of motion and the continuity equation, given in Eq. (4-5), become

$$K_S\rho_0\frac{\partial^2 u_F}{\partial t^2} + R\frac{\partial u_F}{\partial t} + \boldsymbol{\nabla} p_F = 0, \tag{22}$$

$$\phi\frac{\partial p_F}{\partial t} + \rho_0 c_0^2 \boldsymbol{\nabla}\cdot\frac{\partial u_F}{\partial t} = 0. \tag{23}$$

By differentiating Eq. (23) with respect to time and inserting Eq. (22), the wave equation for the equivalent acoustic fluid is obtained as

$$\frac{K_S\phi}{c_0^2}\frac{\partial^2 p_F}{\partial t^2} + \frac{R\phi}{\rho_0 c_0^2}\frac{\partial p_F}{\partial t} - \boldsymbol{\nabla}^2 p_F = 0, \tag{24}$$

which is the wave equation for an acoustic fluid as given in Eq. (6) with coefficients modified by the properties of the structural frame. In Eq. (6), R accounts for the dissipation of energy in an acoustic fluid domain in a smeared approach while it is a property of the structural frame in Eq. (24).

Other analytical models

Most of the porous material models available in the literature assume the structural frame to be rigid, a thorough review of such models developed before and after 1980 being found in [18] and [19], respectively. A model assuming the structural frame to be limp is presented in [20]. In [21], two models with rigid and limp frame, respectively, were compared to measurements, studying the high and low frequency limits of the resulting effective densities. Biot's theory [22] includes the flexibility of the structural frame at the cost of introducing displacement degrees of freedom, the porous material no longer being modelled as an equivalent acoustic fluid. The theory combines an elastic continuum formulation for the structural frame and sound propagation in a rigid structural frame by considering a coupling of the stress-strain relationships and the inertial and viscous forces.

3 Numerical studies

In the numerical studies presented here, the effect of modelling the air and insulation inside cavities of TVE buildings on the vibration transmission was investigated. First, a comparative study was carried out for the three porous material models introduced in Section 2.2, a section of a wooden double-plate wall panel being employed as test model. Furthermore, a section of a TVE-based building was analysed, comparing the vibrations induced in the structure by a load acting on a floor structure for models including acoustic media in different ways.

3.1 Comparative study – porous material models

The empirical porous material models by Delany & Bazley and Miki as well as the equivalent acoustic fluid model with rigid structural frame were compared for a FE model of a section in a wooden double-plate wall panel, shown in Figure 3. The wall panel consisted of a $2500 \times 645 \times 116$ mm^3 wood frame covered with gypsum plates on both sides, creating a low-stiffness model with a cavity between the plates. The cavity was modelled in five different ways: (1) with no acoustic media, (2) filled with air and (3-5) filled with insulation, employing the three different porous material models. The properties used for the porous material are presented in Table 1, their values falling within realistic ranges for mineral wool materials. Measured values of the material parameters can be found in, for example, [12, 23–26]. A relatively low value for the flow resistivity is selected in order for the empirical models to be physically valid in a major part of the frequency range of interest. For the selected flow resistivity, the models by Delany & Bazley and Miki are feasible for analysis above 70 Hz and 40 Hz respectively. Below those frequencies, unphysical values of the bulk modulus and density are obtained. Steady-state analyses were performed up to 200 Hz, locking the displacements at the four corners of the panel. The wall panel was excited by a harmonic unit point load in the middle of one of the gypsum plates, the source plate, and the accelerations were evaluated at the opposite side of the other plate, the receiver plate. The acceleration amplitudes were evaluated in terms of an RMS value of the magnitude in all nodes of the receiver plate's outer surface, given by

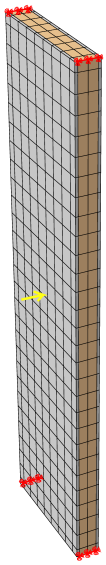

Figure 3: FE model of a section in a wood-framed wall panel, employed for comparing different porous material models. The yellow arrow shows the applied load.

σ	ϕ	α
6000	0.96	1.1

Table 1: The porous material properties employed in the comparative study. Flow resistivity in N/m^{-4}s.

$$a_{\text{RMS}}(f) = \sqrt{\frac{1}{n}\sum_{i=1}^{n} a_i^2(f)}, \tag{25}$$

where a_i is the magnitude of the complex acceleration in node i and n is the number of nodes in the outer surface of the receiver plate. An RMS value was calculated for each excitation frequency in the steady-state analysis.

In Figure 4, the acceleration amplitudes for the different models of the wall cavity, in the frequency range 20-200 Hz, are shown. For frequencies below the first resonance frequency, located at 30 Hz, the acoustic media have a negligible influence on the acceleration amplitudes, whereas for frequencies in the range 30-90 Hz, the effect of including air in the cavity is small. Including a porous material, however, lowers the acceleration amplitudes due to its viscous effects. Above 90 Hz, it is evident that a large part of the energy is transmitted through the acoustic medium, since its inclusion increases the acceleration amplitudes significantly. Generally, using the porous material models results in lower acceleration amplitudes compared to the model with only air in the cavity. In their valid frequency ranges, the different methods for modelling the porous material yield very similar results. Hence, it is sufficient to include one of the three models in the subsequent analyses and the model with rigid structural frame was selected due to the unphysical behaviour of the empirical models at lower frequencies.

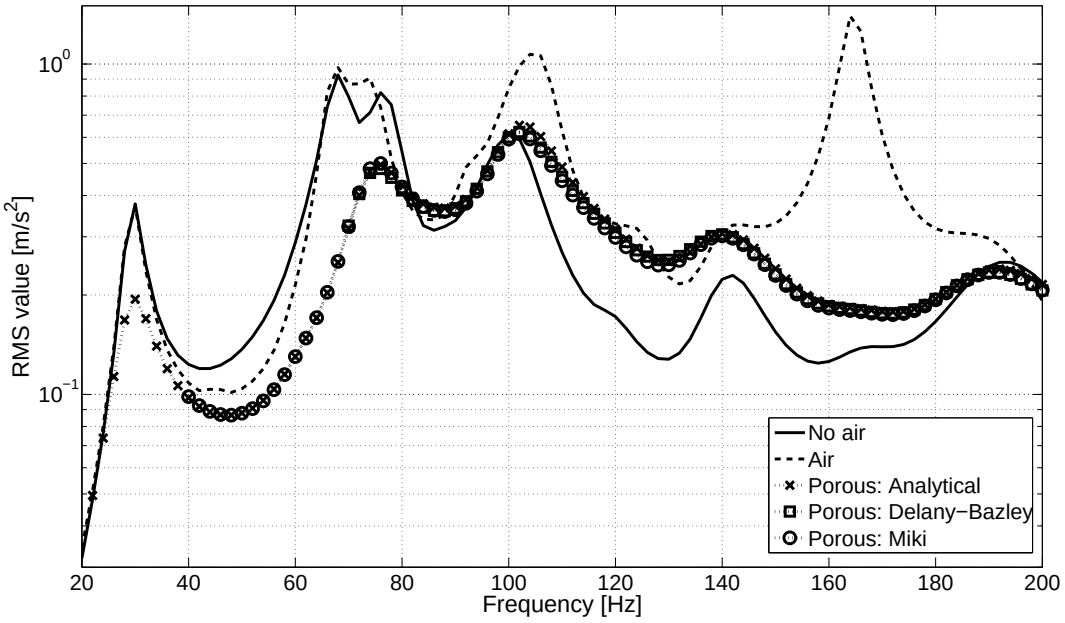

Figure 4: RMS values of the acceleration amplitudes evaluated at the receiver plate of the wall panel model, employed for comparing different porous material models.

3.2 Acoustic media in cavities of TVE buildings

A section of a TVE-based building was analysed in order to investigate the effect of modelling air and insulation, as acoustic media, inside cavities on the vibrations caused by a harmonic point load acting on a floor structure. Specifically, the response of the floor and the transmission to the underlying ceiling and surrounding walls were investigated for a model containing two stacked TVEs, Figure 5 showing a quarter of these. Each TVE was $8961 \times 3894 \times 3418$ mm^3 large (the long side walls being apartment separating and the short side walls being façades) and modelled according to the drawings in Figure 2. Moreover, the walls of the neighbouring TVEs were included at the apartment separating walls, meaning that the cavities in those walls were included in the model. No structural connection to the walls of the neighbouring TVEs was, however, included.

The materials of the structure are listed in Figure 2; the particle board, plaster board and plywood being modelled as isotropic materials with properties according to Table 2, whereas the wood beams were modelled as orthotropic materials with properties according to Table 3. A type of elastomer often used in TVE buildings is Sylodyn, a mixed cellular polyurethane dampening material developed by Getzner Werkstoffe GmbH. The blocks modelled in this study were $100\times95\times25$ mm^3 large, of type Sylodyn NE, and placed between the two stacked TVEs with a centre-to-centre distance from one another of 600 mm along the walls. Frequency-dependent viscoelastic material properties for the elastomers were determined in [27] by performing laboratory testing and FE simulations to match experimental data. The porous material properties used for modelling the insulation were selected according to Table 4. The analytical porous

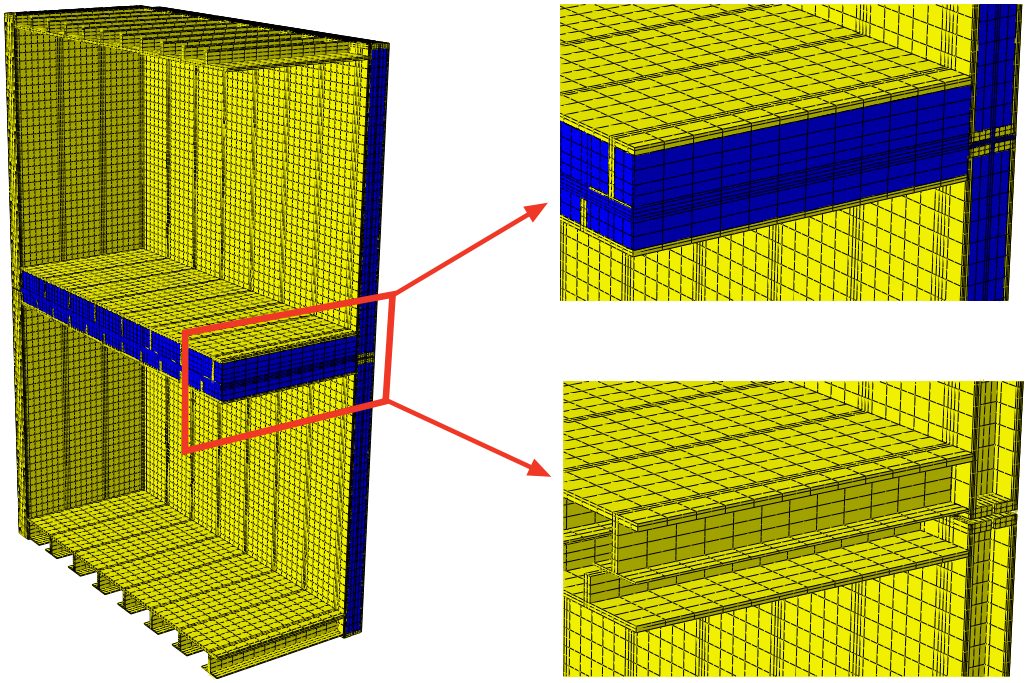

Figure 5: A quarter of the model of two TVEs, the acoustic media being shown in blue. The junction between floor, ceiling and apartment separating walls is shown to the right, with and without acoustic media inside the cavities.

material model assuming a rigid structural frame was employed to model the insulation in the analyses. In contrast to the comparative study in Section 3.1, a higher flow resistivity was used here, the selected value falling within the mid-range of values for mineral wools found in the literature.

The model was created in the commercial FE software *Abaqus* [28]. The structural parts were meshed with 20-node solid hexahedral elements, employing quadratic interpolation and reduced integration. For the elastomer blocks, elements with a hybrid formulation were used in order to avoid locking. The air and the insulation, in turn, were meshed with 20-node acoustic hexahedral elements, employing quadratic interpolation. The mesh sizes for both the structural and acoustic parts were decided based on the wavelengths expected to occur at the highest frequency of interest, namely 200 Hz.

Due to the complexity when assessing damping, a global damping ratio of 5.77 %, calculated using the measurement data in [29], was assigned to all materials as opposed to considering individual damping for each material. The damping matrix was constructed by means of the Rayleigh method, see e.g. [30], selecting the constants for the mass- and stiffness proportionality to be 17.37 and $9.77 \cdot 10^{-5}$, respectively.

In the analyses, the surfaces of the two TVEs, where elastomer blocks would be placed if further storeys were included, were modelled as clamped. Moreover, the walls of the neighbouring modules were clamped at the vertical edges. A vertical unit point load, acting on the middle of the floor in the upper TVE, was applied and steady-state analyses performed for frequencies up to 200 Hz.

Material	E	ν	ρ
Particle board	3000	0.3	767
Plaster board	2000	0.2	692.3
Plywood	12400	0.3	710

Table 2: Material parameters used for the isotropic materials. Modulus of elasticity in MPa and density in kg/m^3.

E_1	E_2	E_3	G_{12}	G_{13}	G_{23}	ν_{12}	ν_{13}	ν_{23}	ρ
8500	350	350	700	700	50	0.2	0.2	0.3	432

Table 3: Material parameters used for the wood beams. Stiffness parameters in MPa and density in kg/m^3.

σ	ϕ	α
40000	0.96	1.1

Table 4: Porous material properties used in the numerical studies. Flow resistivity in N/m^{-4}s.

3.2.1 Vibrations in the floor and underlying ceiling

First, the vibrations in the floor of the upper TVE and the underlying ceiling were investigated for different ways of modelling air and insulation inside the cavity between the floor and the ceiling. A model without acoustic media was compared to models with air alone and air together with insulation in the cavity, the insulation being placed according to the drawings in Figure 2. All analyses were performed applying two different boundary conditions, $p = 0$ and $\nabla p = 0$, at the interfaces of the acoustic media bordering to surrounding cavities in order to investigate their effect on the vibrations transmitted over the cavity. These interfaces are illustrated in Figure 6, showing the full TVEs. At all boundaries of the acoustic media in contact with structural components, structure-acoustic coupling was considered.

The acceleration amplitudes obtained in the analyses of the different models were extracted from half of the nodes (due to the symmetry) at the floor surface and the ceiling surface, respectively, and RMS values of the complex acceleration magnitudes were calculated according to Eq. (25).

In Figure 7, the RMS values of the acceleration amplitudes at the floor are shown. Including air alone in the cavity had a small effect on the levels of vibration in the floor, the RMS values being changed by just over 1 % in average. An exception is found at 30 Hz, where the inclusion of air lowers the vibration amplitudes. Considering both air and insulation in the cavity led to a dampening effect, lowering the levels of vibration by approximately 15 % while the frequency response function is similar in shape to that obtained when including no acoustic media in the cavity. Moreover, it can be observed that the choice of boundary conditions for the acoustic media has a negligible influence.

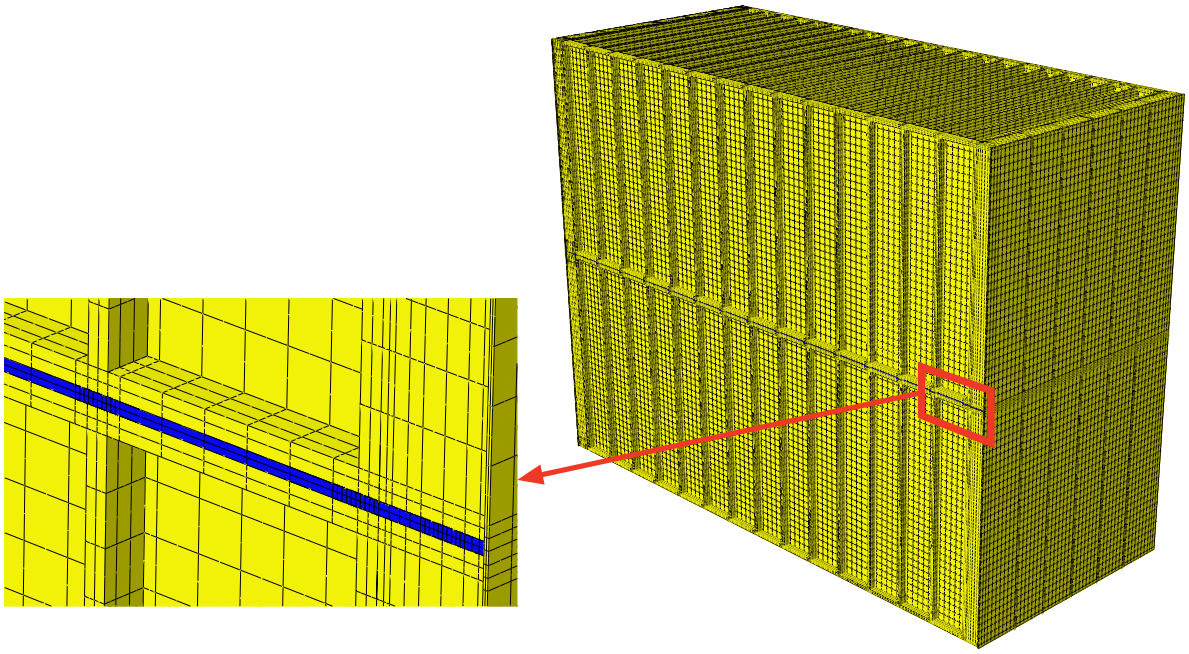

Figure 6: The model of the two TVEs; the acoustic media in contact with the surrounding cavities, where different boundary conditions were applied, being shown to the left. The acoustic media is shown in blue.

In Figure 8, the RMS values of the acceleration amplitudes at the ceiling are shown. It can be observed that including air alone resulted in higher acceleration amplitudes, especially at lower frequencies. For low frequencies, the modelling of both air and insulation resulted in acceleration amplitudes in-between the case with air alone and the case with no acoustic media in the floor-ceiling cavity. At higher frequencies, the acceleration amplitudes obtained for the case with air and insulation are similar to those obtained for the case with no acoustic media, deviating with less than a factor of 2. At some frequencies, the dampening effect of the insulation resulted in reduced vibration amplitudes when including both air and insulation, as compared to having no acoustic media. When air alone was considered, the levels of vibration were influenced by the choice of boundary conditions for the acoustic media, the effect, however, being relatively small when both air and insulation were included in the model.

3.2.2 Vibrations in the surrounding walls

Next, the vibrations in the walls of the lower TVE were investigated for different ways of modelling the air and insulation in the cavity between the floor and the ceiling as well as the cavities in the apartment separating walls. Models including acoustic media either in the floor-ceiling cavity alone or in both the floor-ceiling cavity and the wall cavities were compared to a model with no acoustic media. In the models including acoustic media, it was included as air alone or air together with insulation. The insulation in the walls was placed according to the drawings in Figure 2, i.e. between the beams of each wall, having a small air gap between the walls of two neighbouring TVEs. Moreover, models having the floor-ceiling cavity and the wall cavities separated were created by introducing a separating wall in the junction between

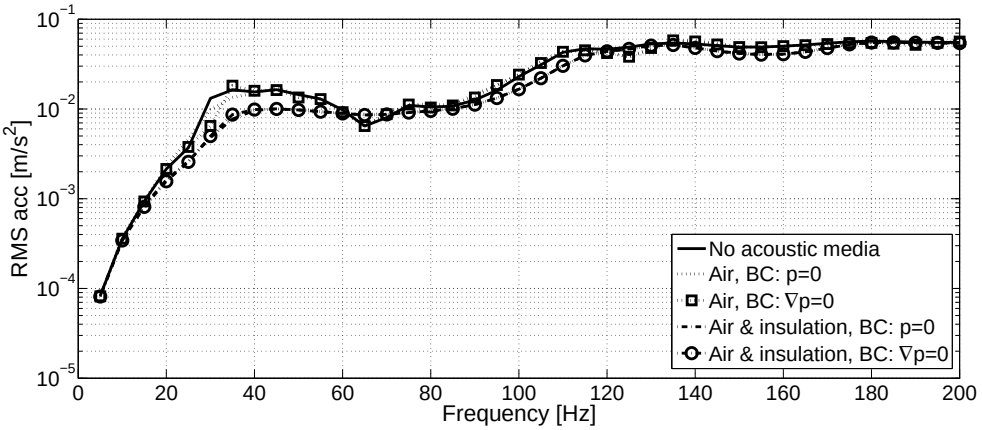

Figure 7: RMS values of the acceleration amplitudes evaluated at the floor for the different models of the acoustic media inside the floor-ceiling cavity.

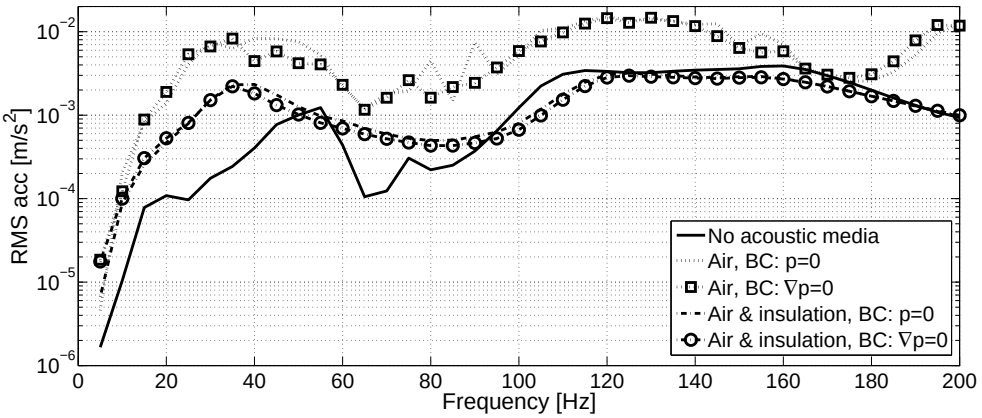

Figure 8: RMS values of the acceleration amplitudes evaluated at the ceiling for the different models of the acoustic media inside the floor-ceiling cavity.

the cavities, the junction being shown in Figure 5. These models were compared to the models with connected cavities in order to investigate if the acoustic pressure waves travelling between the cavities affect the vibration amplitudes in the walls.

At the boundaries to the acoustic media in surrounding cavities, only $\nabla p = 0$ was applied as it was observed in the evaluation of the ceiling vibrations that the boundary conditions have a negligible effect on the vibration transmission. The acceleration amplitudes obtained in the analyses of the different models were extracted in all nodes at the surface of an apartment separating wall of the lower TVE. RMS values of the complex acceleration magnitudes were calculated according to Eq. (25).

In Figure 9, the RMS values of the acceleration amplitudes at the wall of the lower TVE are shown, including results for the models where air alone is used as acoustic media in the cavities. In Figure 10, the RMS values are shown for the models where the acoustic media is comprised both of air and insulation. The frequency range is divided into two parts, including frequencies in the ranges 0-100 Hz and 100-200 Hz, respectively. Observe that different scales

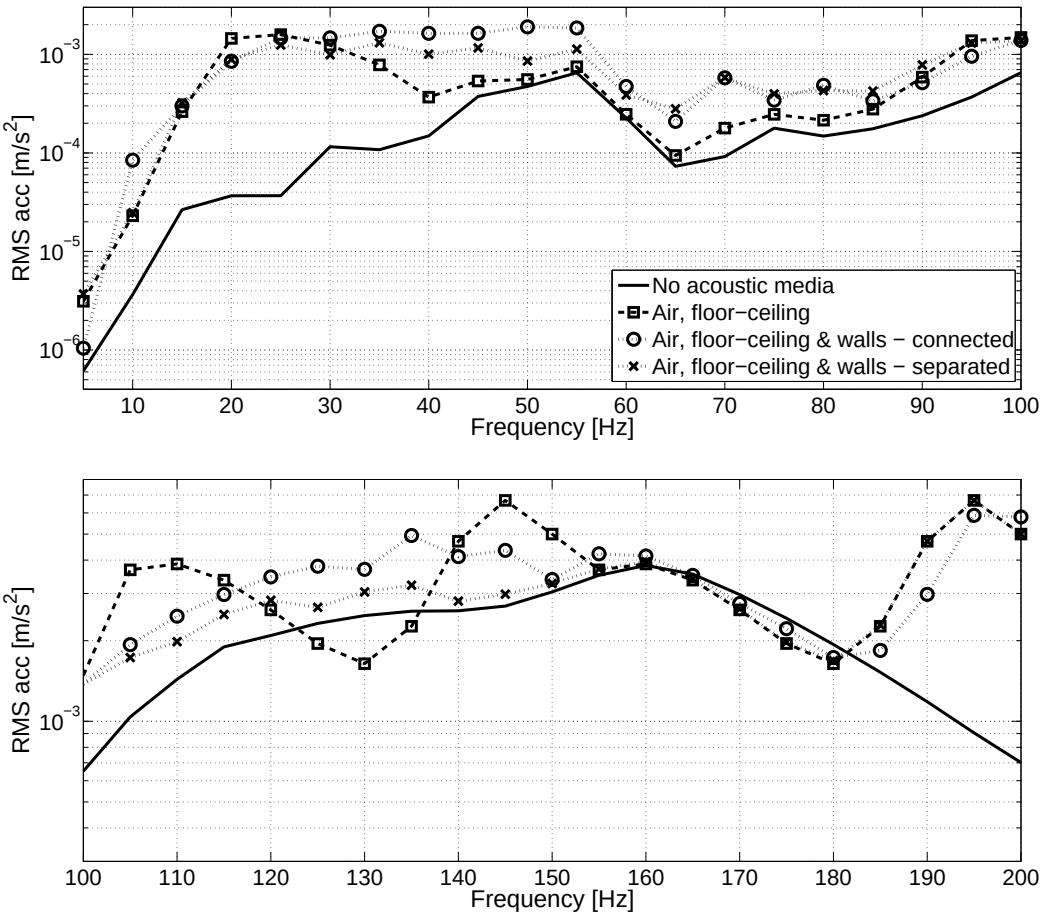

Figure 9: RMS values of the acceleration amplitudes, evaluated at the apartment separating wall of the lower TVE, for the different models including air alone as acoustic media. Note that the two plots employ different scales at the y-axis.

are employed for the y-axes in the two frequency ranges.

It can be observed in Figure 9 that including acoustic media in terms of air alone in the cavities has a large effect on the vibration transmission from the floor to the walls of the TVE below. The system becomes more resonant when air is included and the acceleration amplitudes at the wall panel are generally higher, except at some frequencies between resonance peaks, where the amplitudes are reduced compared to the model with no acoustic media. At most frequencies, the acceleration amplitudes are higher when the floor-ceiling cavity is connected to the wall cavities compared to having the cavities being separated. At low and high frequencies (below 15 Hz and above 155 Hz), the model with air in all cavities, having the cavities separated, results in acceleration amplitudes very similar to the model with air only in the floor-ceiling cavity. Hence, if the cavities are separated, the air in the wall panels has a negligible effect at those frequencies.

In Figure 10, it can be observed that considering both air and insulation as acoustic media in the cavities results in smoother spectrums compared to including air alone. For most frequencies, with the exception being frequencies below 40 Hz, the acceleration amplitudes are

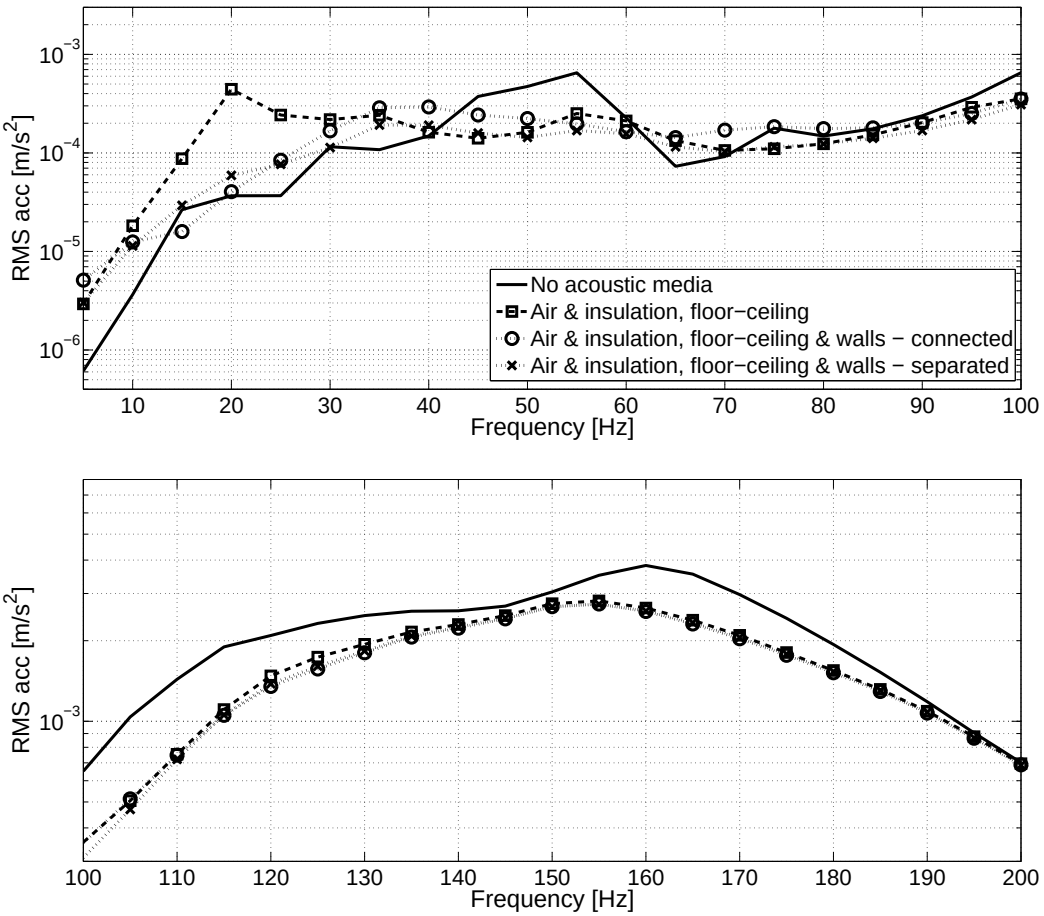

Figure 10: RMS values of the acceleration amplitudes, evaluated at the apartment separating wall of the lower TVE, for the different models including both air and insulation as acoustic media. Note that the two plots employ different scales at the y-axis.

decreased when including air and insulation in the cavities compared to having no acoustic media. A resonance frequency is observed at 20 Hz for the model with acoustic media only in the floor-ceiling cavity, which is not present for any of the other models. Hence, a resonance occurs due to the inclusion of air and insulation in the floor-ceiling cavity which is cancelled when considering the acoustic media also in the wall cavities. In general, the acceleration amplitudes when considering both air and insulation, as compared to including air alone in the cavities, are closer to the case with no acoustic media. Above 60 Hz, the inclusion of air and insulation as acoustic media results in acceleration amplitudes deviating with a factor of less than 2 compared to having no acoustic media. Above 100 Hz, all three models with air and insulation in the cavities result in very similar acceleration amplitudes. This shows that at higher frequencies, the effect of including acoustic media in the wall cavities, on the vibration transmission to the wall panels, is small in case both air and insulation are considered.

4 Conclusions

The main conclusion from the numerical studies is that acoustic media in the cavities of wooden lightweight buildings affect the vibration transmission. It was observed that the vibrations transmitted from a load acting on a floor structure affected the acceleration amplitudes in both the underlying ceiling, structurally separated from the floor, and the walls of the storey below. The effect is especially distinct when air alone is considered as acoustic media. Generally, including air alone results in a more resonant system with higher acceleration amplitudes while including both air and insulation introduces a dampening effect, especially at higher frequencies. The dampening effect of the insulation results in decreased acceleration amplitudes at higher frequencies as compared to having no acoustic media included. In reality, the cavities normally contain insulation, the modelling of air alone, thus, leading to an overestimation of the vibrations transmitted by the acoustic media.

The levels of vibration in the floor were only marginally affected by the inclusion of air alone as acoustic media in the floor-ceiling cavity. When considering both air and insulation as acoustic media, the shape of the frequency response function did not change to any appreciable extent but a dampening effect was observed. This could be accounted for by increasing the damping of the structure, thereby avoiding the inclusion of acoustic media in the model.

In the analyses of the vibrations in the floor and in the ceiling, it was concluded that the choice of boundary conditions for the acoustic media bordering to surrounding cavities had a small effect in terms of vibration transmission from the floor to the ceiling below. This implies that the acoustic media in surrounding cavities has a weak influence on the vibrations transmitted locally over the floor-ceiling cavity.

In the analyses of the vibrations in the walls of the lower TVE, it was observed that including air and insulation in the wall cavities had no effect on the transmission to the wall panels above 100 Hz. If the vibrations transmitted from the floor to surrounding walls is studied for frequencies over 100 Hz, it is, hence, sufficient to include the air and insulation only in the floor-ceiling cavity. This result indicates that the effect of including acoustic media in cavities is decreasing with the distance from the load. It should be investigated further how far from the load the acoustic media has to be considered.

It can be preferable to use different models for different frequency ranges. At higher frequencies, less acoustic media has to be included in the model while a finer mesh is required for resolving the shorter wavelengths. At lower frequencies, more acoustic media have to be included whilst a coarser mesh can be adopted.

The porous material models investigated in this paper are only a few of many available in the literature. Especially, no models assuming limp or elastic structural frame have been evaluated here. As it was concluded that acoustic media inside cavities of multi-storey wood buildings have to be considered when performing vibration analyses, the material model for the insulation should be validated.

Acknowledgements

The financial support for this work provided by the Silent Spaces project, a part of the EU program Interreg IV A, is gratefully acknowledged.

References

[1] Andersen L., Kirkegaard P.H., Dickow K.A., Kiel N., Persson K. Influence of wall surface and air modelling in finite-element analysis of sound transmission between rooms in lightweight buildings. Proceedings of the Internoise 2012/ASME NCAD meeting, New York.

[2] Domadiya P.G., Dickow K.A., Andersen L., Sorokin S.V. Mitigation of flanking noise in double-plate panel structures by periodic stiffening – Finite element analysis in the low-frequency range", Proceedings of COMPDYN 2011, Corfu, Greece.

[3] Dickow K.A., Gandalal P.D., Andersen L., Kirkegaard P.H. Transmission of sound through double-plate panel structures – a numerical study of coupling parameters in lightweight panel structures. Proceedings of COMPDYN 2011, Corfu, Greece.

[4] Ljunggren F., Ågren A.. Potential solutions to improved sound performance of volume based lightweight multi-storey timber buildings. Appl Acoust, 2011;72:231–240.

[5] Ottosen N., Petersson H. Introduction to the finite element method. Pearson Education Ltd., Harlow, United Kingdom, 1992.

[6] Bathe K.J. Finite element procedures. Prentice Hall, New York, 1996.

[7] Holzapfel G.A. Nonlinear solid mechanics: a continuum approach for engineering. John Wiley & Sons Ltd., Chichester, United Kingdom, 2000.

[8] Sandberg G. Finite element modelling of fluid-structure interaction, PhD thesis, Division of Structural Mechanics, Lund University, Sweden, 1986.

[9] Delany M.E., Bazley E.N. Acoustical properties of fibrous absorbent materials. Appl Acoust, 1970;3(2):105–116.

[10] Miki Y. Acoustical properties of porous materials-Modifications of Delany-Bazley models. J Acoust Soc Jpn, 1990;11(1):19–24.

[11] Dunn I.P., Davern W.A. Calculation of acoustic impedance of multi-layer absorbers. Appl Acoust, 1986;19(5):321–334.

[12] Komatsu T. Improvement of the Delany-Bazley and Miki models for fibrous sound-absorbing materials. Acoust Sci Technol, 2008;29(2):121–129.

[13] Mechel F.P. Ausweitung der absorberformel von delany and bazley zu tiefen frequenzen. Acustica, 1976;35(3):210–213.

[14] Kirby R., Cummings A. Prediction of the bulk acoustic properties of fibrous materials at low frequencies. Appl Acoust, 1999;56(2):101–125.

[15] Kirchhoff G. On the influence of heat conduction in a gas on sound propagation. Ann Phys Chem, 1868;134:177–193.

[16] Zwikker C., Kosten C.W. Sound absorbing materials. Elsevier, Amsterdam, 1949.

[17] Morse P.M, Ingard K.U. Theoretical acoustics. Princeton University Press, New Jersey, 1968.

[18] Attenborough K. Acoustical characteristics of porous materials. Phys Rep, 1982;82(3):179–227.

[19] Allard J.F., Atalla N. Propagation of sound in porous media – modelling sound absorbing materials 2nd ed. John Wiley & Sons Ltd., Chichester, United Kingdom, 2009.

[20] Göransson P. Acoustic finite element formulation of a flexible porous material – a correction for inertial effects. J Sound Vib, 1995;185(4):559–580.

[21] Panneton R. Comments on the limp frame equivalent fluid model for porous media. J Acoust Soc Am, 2007;122(6):217-222.

[22] Biot M.A. Theory of propagation of elastic waves in a fluid-saturated porous solid. I. Low-frequency range. J Acoust Soc Am, 1956;28(2):168–178.

[23] Schiavi A., Guglielmone C., Miglietta P. Effect and importance of static-load on air-flow resistivity determination and its consequences on dynamic stiffness. Appl Acoust, 2011;72(9):705–710.

[24] Olny X., Panneton R. Acoustical determination of the parameters governing thermal dissipation in porous media. J Acoust Soc Am, 2008;123(2):814–824.

[25] Sagartzazu X., Hervella-Nieto L., Pagalday J.M. Review in sound absorbing materials. Arch Comput Methods Eng, 2008;15(3):311–342.

[26] Kino N., Takayasu U. Experimental determination of the micro-and macrostructural parameters influencing the acoustical performance of fibrous media. Appl Acoust, 2007;68(11):1439–1458.

[27] Negreira J. Vibrations in lightweight buildings – Perception and prediction. Licentiate dissertation, Division of Engineering Acoustics, Lund University, Sweden, 2013.

[28] Dassault Systèmes, Abaqus 6.12 documentation, 2012.

[29] AkuLite. Mätrapport 10052. Brunnby Park, Upplands Väsby, Sweden, 2012.

[30] Chopra A.K. Dynamics of structures. Prentice Hall, New Jersey, 2007.

Paper B

Reduction methods for the dynamic analysis of substructure models of lightweight building structures

O. Flodén, K. Persson, G. Sandberg

Lund University
Department of Construction Sciences
P.O. Box 118, SE-22100 Lund, Sweden

Submitted for publication

Reduction methods for the dynamic analysis of substructure models of lightweight building structures

Ola Flodén, Kent Persson, Göran Sandberg
Lund University, Department of Construction Sciences, P.O. Box 118, SE-22100 Lund, Sweden

Abstract

In the present study, different model order reduction methods were compared in terms of their effects on the dynamic characteristics of individual building components. A wide variety of methods were employed in two numerical examples, both being models of wooden floor structures, in order to draw conclusions regarding their relative efficiency when applied to models of such structures. It was observed that a comparison of the methods requires the reduced models to be exposed to realistic boundary conditions, free-free eigenvalue analyses being insufficient for evaluating the accuracy of the reduced models when employed in an assembly of substructures.

Keywords: Model order reduction; Finite element modeling; Substructure modeling; Vibration analysis; Lightweight building structures

1 Introduction

Lightweight buildings are often constructed using prefabricated planar or volume elements, often with use of low-stiffness panels mounted on high-stiffness beams. Accurately assessing the dynamic behaviour of these elements when rather high vibration frequencies are involved requires use of finite element (FE) models representing the geometry in considerable detail. Assembling the individual elements of multi-storey lightweight buildings within the framework of global FE models of entire buildings results in very large models, the number of degrees of freedom (dofs) of which easily exceeds the limits of computer capacity, at least for computations to be performed within reasonable lengths of time. The question arises then of how such FE models can be reduced in size while at the same time being able to represent the dynamic characteristics of the building or buildings in question with sufficient accuracy. The method of dividing a large model into components and creating a global model through coupling models of reduced size of each component is referred to as substructuring. In the present study,

low-frequency vibrations in multi-storey lightweight buildings are modelled by adopting a sub-structuring approach.

In recent decades, a number of methods for model order reduction of dynamic problems have been developed within the area of structural mechanics, mode-based methods being the methods most frequently used. Fairly recently, methods originating from control theory, designated here as modern reduction methods, have been employed within structural mechanics. In contrast to mode-based methods which have an explicit physical interpretation, the modern reduction methods are developed from a purely mathematical point of view. Some mode-based methods are implemented in commercial FE software which enables them to be applied to large-scale problems directly. In order to apply other methods to models created in commercial FE software, the system matrices involved need to be exported from the software and be reduced in another environment.

A number of comparative studies have been published in which the performance of different reduction methods has been evaluated, in connection with mechanical engineering problems. In [1] and [2], modern reduction methods were compared with mode-based methods. In [1], a rack consisting of steel beams was used as a numerical example, the reduction methods involved being compared by studying the structural response within the time domain and the Frobenius norm of the transfer function matrix for different load cases. It was concluded that the modern reduction methods produce excellent reduction results and are more effective than mode-based methods are. In [2], a crankshaft of a piston served as a numerical example, the Frobenius norm of the transfer function matrix being used to compare the reduction methods in question. It was concluded that substantial benefits can be achieved by use of the modern reduction methods. In [3], a wide range of methods was compared by studying the eigenfrequencies and eigenmodes of an elastic rod. The modern reduction methods were found to perform better for mechanical problems than several of the classic methods. In [4], however, in which a clamped beam structure served as a numerical example, it was concluded that mode-based methods are better suited for the analysis of multibody systems than modern reduction methods are. The eigenfrequencies and eigenmodes were analysed with different boundary conditions applied at the interface of the reduced models. It was concluded that mode-based methods are less dependent than the modern reduction methods are on variations in the boundary conditions, something which would clearly be an important advantage in multibody dynamics.

In the comparative studies just referred to, conclusions were drawn on the basis of numerical examples involving relatively simple structures. Lightweight floor and wall structures, however, generally have a much more complex geometry, making it difficult to extrapolate the conclusions in question. Also, in the comparative studies referred to, different types of analyses were used for evaluating the performance of the reduction methods employed, this providing diverse information that can be evaluated in a variety of ways. By applying analyses of multiple types to a given numerical example it should be possible to obtain a broader understanding of the behaviour of different reduction methods than a single type of analysis would provide. Moreover, analysing the reduced models with realistic boundary conditions is necessary since the boundary conditions employed can have a strong influence on the performance of different reduction methods, as demonstrated in [4].

The objective of the analyses carried out in the present investigation was to evaluate the performance of a rather wide range of model order reduction methods by comparing their accuracy and computational cost when applied to detailed FE models of floor and wall structures.

The conclusions will be of value in the process of constructing efficient substructure models for vibration analysis of multi-storey lightweight buildings. The reduced models employed are in this paper evaluated in terms of eigenfrequencies and eigenmodes in a free-free state, as well as in terms of vibration transmission behaviour when the structures in question are exposed to realistic boundary conditions, obtained by connecting them with other building components. New insight is offered regarding both the efficiency of the reduction methods when employed in the analysis of complex structures and the effect of applying realistic boundary conditions to the reduced models.

Commercial FE software of different kinds represent convenient tools for both pre- and post-processing, such as in the coupling of substructures and in the visualisation of results. Since some reduction methods reported on in the literature are incompatible with such software, methods of this sort are either excluded from the analyses here or are used in a modified fashion. A broad range of model order reduction methods presented in the literature will be discussed and the theories behind them taken up. The performance of the reduction methods, applied to lightweight building structures, was evaluated for frequencies of less than 100 Hz by studying two numerical examples. The first example is a model of moderate size of a wooden floor structure, a model created in the commercial FE software Abaqus, from which the system matrices were exported to Matlab, in which various of the reduction methods described in Section 2 were employed. The second example is a large and detailed model of an experimental wooden floor structure, analysed with use of model order reduction methods implemented in Abaqus as well as by use of an alternative approach employing structural elements. Although the conclusions presented in this paper are based in principle on the results of the two numerical examples, many wooden floor and wall structures have geometries and materials similar to those of the structures studied in the two examples. Accordingly, the main conclusions arrived at would appear to be applicable to a wide variety of wooden floor and wall structures similar in topology to these two floors.

2 Model order reduction

An FE formulation of a structural dynamics problem results in a linear equation of motion of the following form [5]:

$$\mathbf{M}\ddot{\mathbf{u}} + \mathbf{C}\dot{\mathbf{u}} + \mathbf{K}\mathbf{u} = \mathbf{f}, \tag{1}$$

where $\mathbf{M, C, K} \in \mathbb{R}^{n\times n}$ are the mass, damping and stiffness matrices respectively, $\mathbf{f} = \mathbf{f}(t) \in \mathbb{R}^{n\times 1}$ is the load vector and $\mathbf{u} = \mathbf{u}(t) \in \mathbb{R}^{n\times 1}$ is the state vector which is sought. A dot denotes differentiation with respect to time, t. The objective of model reduction here is to find a system of m dofs in which $m << n$, one which preserves the dynamic characteristics of the full model. The general approach is to approximate the state vector by use of the transformation $\mathbf{u} = \mathbf{T}\mathbf{u}_R$, where $\mathbf{T} \in \mathbb{R}^{n\times m}$ is a transformation matrix and $\mathbf{u}_R \in \mathbb{R}^{m\times 1}$ is a reduced state vector. Applying the transformation in question to Eq. (1) results in

$$\mathbf{M}_R\ddot{\mathbf{u}}_R + \mathbf{C}_R\dot{\mathbf{u}}_R + \mathbf{K}_R\mathbf{u}_R = \mathbf{f}_R, \tag{2}$$

$$\mathbf{M}_R = \mathbf{T}^T\mathbf{M}\mathbf{T}, \quad \mathbf{C}_R = \mathbf{T}^T\mathbf{C}\mathbf{T}, \quad \mathbf{K}_R = \mathbf{T}^T\mathbf{K}\mathbf{T}, \quad \mathbf{f}_R = \mathbf{T}^T\mathbf{f}, \tag{3}$$

where $\mathbf{M}_R, \mathbf{K}_R, \mathbf{C}_R \in \mathbb{R}^{m\times m}$ are the reduced mass, damping and stiffness matrices, respectively, and $\mathbf{f}_R \in \mathbb{R}^{m\times 1}$ is the reduced load vector. In recent decades, many different methods for model order reduction, involving procedures of varying types for establishing the transformation matrix and the reduced state vector involved, have been proposed in the literature. The dofs in the reduced state vector can be divided into two categories: physical dofs and generalised coordinates. Physical dofs are the dofs of the full system that are retained in the reduction process, whereas the generalised coordinates represent the amplitudes of various Ritz basis vectors [6] that describe the deflection shapes that are allowed in the reduced system. The reduction methods can be categorised according to the type of dofs generated in the reduction process, where *condensation methods* involve only physical dofs, *generalised coordinate methods* are based solely on generalised coordinates, and *hybrid reduction methods* employ a combination of dofs of both types. A number of important methods within each category are listed below.

- Condensation methods
  - Guyan reduction [7]
  - Dynamic reduction [8]
  - Improved reduction system (IRS) [9, 10]
  - System equivalent expansion reduction process (SEREP) [11]
- Generalised coordinate methods
  - Modal truncation [5, 12]
  - Component mode synthesis by Craig–Chang [12, 13]
  - Krylov subspace methods [14, 15]
  - Balanced truncation [16, 17]
- Hybrid methods
  - Component mode synthesis by Craig–Bampton [12, 18]
  - Component mode synthesis by MacNeal [19]
  - Component mode synthesis by Rubin [20]

The methods just referred to, except for the Krylov subspace methods and balanced truncation, which have their origin in control theory and are considered to be modern reduction methods, were developed specifically for structural mechanics. Modal truncation and component mode synthesis by Craig–Chang, Craig–Bampton, Rubin or MacNeal are all mode-based methods, which means that structural eigenmodes of some sort are employed as Ritz basis vectors. In commercial FE software, generalised coordinates are treated as internal dofs and the coupling of substructures is usually realised at the physical dofs by use of Lagrange multipliers [5]. Consequently, if the global model involved is to be analysed and post-processed in commercial FE software, any methods for model order reduction based solely on generalised coordinates are excluded. However, such methods can be combined with condensation methods to obtain hybrid versions of the methods. Component mode synthesis by Craig-Bampton, for example, is modal truncation combined with Guyan reduction. Moreover, variants of component mode synthesis in which Krylov subspace methods instead of modal truncation are combined with Guyan reduction have been described in [21, 22]. Model order reduction methods that result in

reduced models in which the physical dofs at the interfaces are preserved are often referred to as structure-preserving methods.

In the present study, five of the above-listed reduction methods are investigated: Guyan reduction, dynamic reduction, IRS and component mode synthesis, the latter both in the mode-based Craig–Bampton form and in the Krylov subspace version. Out of the mode-based component mode synthesis methods, the Craig–Bampton version, the most commonly employed method among structural engineers, is selected. The Krylov subspace version is included in the studies to investigate the potential improvement in efficiency offered by the increasingly popular methods from control theory when employed for the type of problems studied here. Moreover, modified versions of the component mode synthesis methods are investigated using IRS instead of Guyan reduction as the condensation method, these being referred to as improved component mode synthesis methods [21]. In addition, a set of alternative methods termed generalised methods [23], obtained by deriving the above mentioned methods in a slightly different manner, are investigated.

In the derivations of the reduction methods presented below, the case considered is an undamped one. Since the damping ratio of the structures analysed in the study is relatively low, it has a negligible effect on the eigenfrequencies and the eigenmodes. Also, the damping matrix employed provides only a rough approximation of all the damping phenomena occurring in the structures as a whole. Accordingly, as an alternative to its being reduced in the same way as the mass and stiffness matrices, the damping matrix can be constructed in the reduced system directly.

2.1 Original methods

As mentioned above, the model order reduction methods can be derived in a slightly different manner than in their original versions, this resulting in methods referred to as generalised methods, as presented in Section 2.2. Below, the original versions of the methods investigated here are presented.

Guyan reduction

In the condensation methods, the dofs are separated into masters (m) and slaves (s), the slave dofs being condensed in the reduction process, resulting in a reduced state vector containing only the master dofs. Partitioning the state vector in terms of the master and slave categories enables the system matrices in Eq. (1) to be partitioned into sub-blocks as follows:

$$\begin{bmatrix} \mathbf{M}_{mm} & \mathbf{M}_{ms} \\ \mathbf{M}_{sm} & \mathbf{M}_{ss} \end{bmatrix} \begin{bmatrix} \ddot{\mathbf{u}}_m \\ \ddot{\mathbf{u}}_s \end{bmatrix} + \begin{bmatrix} \mathbf{K}_{mm} & \mathbf{K}_{ms} \\ \mathbf{K}_{sm} & \mathbf{K}_{ss} \end{bmatrix} \begin{bmatrix} \mathbf{u}_m \\ \mathbf{u}_s \end{bmatrix} = \begin{bmatrix} \mathbf{f}_m \\ \mathbf{f}_s \end{bmatrix}. \tag{4}$$

Solving the equation in the second row in Eq. (4) for $\mathbf{u}_s$ results in

$$\mathbf{u}_s = -\mathbf{K}_{ss}^{-1} \left(\mathbf{M}_{sm} \ddot{\mathbf{u}}_m + \mathbf{M}_{ss} \ddot{\mathbf{u}}_s + \mathbf{K}_{sm} \mathbf{u}_m \right), \tag{5}$$

where it has been assumed that there are no loads acting on the slave dofs, so that $\mathbf{f}_s = \mathbf{0}$. Neglecting the inertia terms in Eq. (5) results in the transformation of the state vector for Guyan reduction

$$\begin{bmatrix} \mathbf{u}_m \\ \mathbf{u}_s \end{bmatrix} = \begin{bmatrix} \mathbf{I} \\ -\mathbf{K}_{ss}^{-1} \mathbf{K}_{sm} \end{bmatrix} \mathbf{u}_m = \mathbf{T}_{\text{Guyan}} \mathbf{u}_m, \tag{6}$$

where the transformation matrix $\mathbf{T}_{\text{Guyan}}$ can be used in Eq. (3) to obtain the reduced system matrices and the reduced load vector. Guyan reduction is often referred to as static condensation, since models reduced with Guyan reduction do not result in any errors in static analysis. Due to its static nature, Guyan reduction can be expected to only produce acceptable results for frequencies close to the lowest eigenfrequencies of the system. At higher frequencies, the neglected inertia terms have a stronger influence, resulting in errors of larger size. The performance of this method is highly dependent upon the approach for selecting master dofs. In the numerical examples studied here, only the dofs needed to connect the substructures to the surroundings serve as masters, although additional dofs can be employed as master dofs as well, various methods for selecting such dofs having been proposed [24, 25].

Dynamic reduction

If a harmonic time-dependent load, $\mathbf{f} = \hat{\mathbf{f}} exp(i\omega t)$, is assumed, this results in a harmonic response, $\mathbf{u} = \hat{\mathbf{u}} exp(i\omega t)$, where $i = \sqrt{-1}$ is the imaginary unit, ω is the angular frequency and $\hat{\mathbf{f}}$ and $\hat{\mathbf{u}}$ are the complex load and displacement amplitudes, respectively. Introducing this assumption into Eq. (4) results in the equation of motion applying to the frequency domain

$$\begin{bmatrix} \mathbf{D}_{mm}(\omega) & \mathbf{D}_{ms}(\omega) \\ \mathbf{D}_{sm}(\omega) & \mathbf{D}_{ss}(\omega) \end{bmatrix} \begin{bmatrix} \hat{\mathbf{u}}_m \\ \hat{\mathbf{u}}_s \end{bmatrix} = \begin{bmatrix} \hat{\mathbf{f}}_m \\ \hat{\mathbf{f}}_s \end{bmatrix}, \tag{7}$$

$$\mathbf{D}(\omega) = -\omega^2 \mathbf{M} + \mathbf{K}. \tag{8}$$

Solving the equation in the lower row in Eq. (7) for $\hat{\mathbf{u}}_s$, assuming $\hat{\mathbf{f}}_s = \mathbf{0}$, results in

$$\hat{\mathbf{u}}_s = -\mathbf{D}_{ss}^{-1}(\omega)\, \mathbf{D}_{sm}(\omega)\, \hat{\mathbf{u}}_m, \tag{9}$$

and, consequently, the transformation of the state vector for dynamic reduction is given by

$$\begin{bmatrix} \hat{\mathbf{u}}_m \\ \hat{\mathbf{u}}_s \end{bmatrix} = \begin{bmatrix} \mathbf{I} \\ -\mathbf{D}_{ss}^{-1}(\omega)\, \mathbf{D}_{sm}(\omega) \end{bmatrix} \hat{\mathbf{u}}_m = \mathbf{T}_{\text{Dynamic}} \hat{\mathbf{u}}_m, \tag{10}$$

where the transformation matrix $\mathbf{T}_{\text{Dynamic}}$ requires a selection of ω in order to be established. The special case of dynamic reduction in which $\omega = 0$ results in the transformation of Guyan reduction shown in Eq (6). For harmonic load cases in which the excitation frequency has the same value as ω, dynamic reduction provides exact results. This suggests dynamic reduction to be an effective scheme for analysing a structure subjected to load cases having narrow frequency content. For steady-state analyses, fully accurate reduced models can be obtained by reducing the system matrices at each discrete frequency, yet this is a costly procedure that requires the availability of large memory resources for storing the resulting matrices.

Improved reduction system (IRS)

The term *improved* in the name improved reduction system refers to a perturbation of the transformation taking place in Guyan reduction, Eq. (6). The previously neglected inertia terms are then included as pseudo-static forces. The occurrence of free undamped vibrations of a system reduced by means of a Guyan reduction results in the following expression for the acceleration of the master dofs:

$$\ddot{\mathbf{u}}_m = -\mathbf{M}_{\text{Guyan}}^{-1} \mathbf{K}_{\text{Guyan}} \mathbf{u}_m, \tag{11}$$

where $\mathbf{M}_{\text{Guyan}}$ and $\mathbf{K}_{\text{Guyan}}$ are the reduced stiffness- and mass matrices obtained by employing Guyan reduction. Differentiating Eq. (6) and making use of the relationship expressed in Eq. (11) results in the following expression for acceleration of the slave dofs:

$$\ddot{\mathbf{u}}_s = -\mathbf{K}_{ss}^{-1}\mathbf{K}_{sm}\ddot{\mathbf{u}}_m = \mathbf{K}_{ss}^{-1}\mathbf{K}_{sm}\mathbf{M}_{\text{Guyan}}^{-1}\mathbf{K}_{\text{Guyan}}\mathbf{u}_m. \tag{12}$$

Inserting Eq. (11) and Eq. (12) into Eq. (5) results in the approximation of the slave dofs

$$\mathbf{u}_s = \mathbf{K}_{ss}^{-1}\left(\mathbf{M}_{sm}\mathbf{M}_{\text{Guyan}}^{-1}\mathbf{K}_{\text{Guyan}} - \mathbf{M}_{ss}\mathbf{K}_{ss}^{-1}\mathbf{K}_{sm}\mathbf{M}_{\text{Guyan}}^{-1}\mathbf{K}_{\text{Guyan}} - \mathbf{K}_{sm}\right)\mathbf{u}_m. \tag{13}$$

This rather complicated expression can be written in more compact form so as to obtain the transformation matrix for IRS

$$\mathbf{T}_{\text{IRS}} = \mathbf{T}_{\text{Guyan}} + \mathbf{S}\mathbf{M}\mathbf{T}_{\text{Guyan}}\mathbf{M}_{\text{Guyan}}^{-1}\mathbf{K}_{\text{Guyan}}, \tag{14}$$

$$\mathbf{S} = \begin{bmatrix} \mathbf{0} & \mathbf{0} \\ \mathbf{0} & \mathbf{K}_{ss}^{-1} \end{bmatrix}. \tag{15}$$

In the IRS transformation, the reduced system matrices that Guyan reduction provides are utilised so as to produce updated reduced matrices. As a further extension of this, the updated matrices can be used to create an iterative scheme where the transformation for the ith iteration is given by

$$\mathbf{T}_{\text{IRS},i} = \mathbf{T}_{\text{Guyan}} + \mathbf{S}\mathbf{M}\mathbf{T}_{\text{IRS},i-1}\mathbf{M}_{\text{IRS},i-1}^{-1}\mathbf{K}_{\text{IRS},i-1}, \tag{16}$$

and the iterations are started by calculating $\mathbf{T}_{\text{IRS},1}$ according to Eq. (14). $\mathbf{K}_{\text{IRS},i-1}$ and $\mathbf{M}_{\text{IRS},i-1}$ are the reduced stiffness- and mass matrices of iteration $i-1$, obtained by using $\mathbf{T}_{\text{IRS},i-1}$ in Eq. (3). The iterative scheme converges to form the transformation matrix of SEREP [11], creating a reduced system that reproduces exactly the lowest eigenfrequencies and eigenmodes of the full system. The rate of convergence depends upon the selection of master dofs. In contrast to Guyan reduction, however, IRS does not reproduce the static behaviour of the full system exactly.

Component mode synthesis by Craig–Bampton (CMS)

Use of component mode synthesis by Craig–Bampton, here denoted CMS, compensates for the neglected inertia terms in Guyan reduction through its including a set of generalised coordinates $\boldsymbol{\xi}$. These generalised coordinates represent the amplitudes of a set of eigenmodes for the slave structure, calculated with the master dofs being fixed. Setting $\mathbf{u}_m = \mathbf{0}$ and $\mathbf{f}_s = \mathbf{0}$ in Eq. (4) and assuming a harmonic solution results in the following eigenvalue problem:

$$\mathbf{K}_{ss}\Phi = \lambda\mathbf{M}_{ss}\Phi, \tag{17}$$

which can be solved for the eigenvalues $\lambda = \omega^2$ and the eigenmodes Φ. A number of eigenmodes obtained from Eq. (17), referred to as retained eigenmodes, are selected as additional basis vectors to the approximation of the slave dofs in Eq. (6), resulting in

$$\mathbf{u}_s = -\mathbf{K}_{ss}^{-1}\mathbf{K}_{sm}\mathbf{u}_m + \sum \Phi_i\xi_i = \boldsymbol{\Psi}\mathbf{u}_m + \boldsymbol{\Phi}\boldsymbol{\xi}. \tag{18}$$

This gives the following transformation of the state vector for CMS:

$$\begin{bmatrix} \mathbf{u}_m \\ \mathbf{u}_s \end{bmatrix} = \begin{bmatrix} \mathbf{I} & \mathbf{0} \\ \mathbf{\Psi} & \mathbf{\Phi} \end{bmatrix} \begin{bmatrix} \mathbf{u}_m \\ \boldsymbol{\xi} \end{bmatrix} = \mathbf{T}_{\text{CMS}} \begin{bmatrix} \mathbf{u}_m \\ \boldsymbol{\xi} \end{bmatrix}, \tag{19}$$

which defines the transformation matrix $\mathbf{T}_{\text{CMS}}$. As for Guyan reduction, the accuracy of CMS depends upon the selection of master dofs, this affecting both the static modes and the eigenmodes of the slave structure. Also, the accuracy depends upon the selection of retained eigenmodes, certain eigenmodes having a larger influence than others on the solution of a specific problem. To obtain a reduced model with as great an accuracy for general load distributions as possible, however, all the eigenmodes up to some given limit that is chosen should be included.

Krylov subspace component mode synthesis (KCMS)

The Krylov subspace is defined as

$$K_q\left(\mathbf{A}, \mathbf{b}\right) = span\left\{\mathbf{b}, \mathbf{A}\mathbf{b}, ..., \mathbf{A}^{q-1}\mathbf{b}\right\}, \tag{20}$$

where $\mathbf{A} \in \mathbb{R}^{n \times n}$, $\mathbf{b} \in \mathbb{R}^{n \times 1}$ is called the starting vector and q is a positive integer. $\mathbf{b}$ can also be a block of vectors, in which case each Krylov projection generates a new block of vectors. Since methods originating from control theory are ones developed for systems of an input-output form, the equation of motion is rewritten here as a system of this sort of the following form:

$$\mathbf{M}\ddot{\mathbf{u}} + \mathbf{K}\mathbf{u} = \mathbf{B}\mathbf{x}, \tag{21}$$

$$\mathbf{y} = \mathbf{N}^T\mathbf{u}, \tag{22}$$

where $\mathbf{x} = \mathbf{x}\left(t\right) \in \mathbb{R}^{x \times 1}$ is the input vector, $\mathbf{y} = \mathbf{y}\left(t\right) \in \mathbb{R}^{y \times 1}$ the output vector, $\mathbf{B} \in \mathbb{R}^{n \times x}$ a matrix describing the spatial load distributions and $\mathbf{N} \in \mathbb{R}^{n \times y}$ a matrix relating the state vector to the output vector. A Laplace transformation of the input-output system yields the transfer function $\mathbf{G}(s)$:

$$\mathbf{G}\left(s\right) = \mathbf{N}^T\left(s^2\mathbf{M} + \mathbf{K}\right)^{-1}\mathbf{B}. \tag{23}$$

Krylov subspace methods, which have their origin in the area of control theory, are based on so-called *moment matching*. The moments involved are defined as the coefficients of a Taylor series expansion of $\mathbf{G}(s)$ around $s = 0$. It can be shown that the first q moments of the full system and of a reduced system match if the reduced basis is selected as the Krylov subspace generated by $\mathbf{A} = \mathbf{K}^{-1}\mathbf{M}$ and $\mathbf{b} = \mathbf{K}^{-1}\mathbf{B}$ [15]. In the present study it is required that the reduction methods employed are structure-preserving, i.e. retains the physical dofs at the interfaces. Accordingly, the approach of using Krylov subspace vectors in a component mode synthesis manner, as described in [21, 22], here denoted KCMS, is adopted. Inserting $\mathbf{u}_m = 0$ and $\mathbf{f}_s = \mathbf{B}_s\mathbf{x}_s$ into Eq. (4) results in the following equation of motion for the slave structure:

$$\mathbf{M}_{ss}\ddot{\mathbf{u}}_s + \mathbf{K}_{ss}\mathbf{u}_s = \mathbf{B}_s\mathbf{x}_s. \tag{24}$$

A Krylov subspace is generated for the slave structure by selecting $\mathbf{A} = \mathbf{K}_{ss}^{-1}\mathbf{M}_{ss}$ and $\mathbf{b} = \mathbf{K}_{ss}^{-1}\mathbf{B}_s$:

$$K_q\left(\mathbf{K}_{ss}^{-1}\mathbf{M}_{ss},\mathbf{K}_{ss}^{-1}\mathbf{B}_s\right)=span\left\{\underbrace{\mathbf{K}_{ss}^{-1}\mathbf{B}_s}_{V_{\mathrm{k}}^1},\underbrace{\left(\mathbf{K}_{ss}^{-1}\mathbf{M}_{ss}\right)\mathbf{K}_{ss}^{-1}\mathbf{B}_s}_{V_{\mathrm{k}}^2},...,\underbrace{\left(\mathbf{K}_{ss}^{-1}\mathbf{M}_{ss}\right)^{q-1}\mathbf{K}_{ss}^{-1}\mathbf{B}_s}_{V_{\mathrm{k}}^q}\right\}, \quad (25)$$

and the approximation of the slave dofs in KCMS is given by

$$\mathbf{u}_s=-\mathbf{K}_{ss}^{-1}\mathbf{K}_{sm}\mathbf{u}_m+\sum V_{\mathrm{k}}^i\xi_i=\mathbf{\Psi}\mathbf{u}_m+\mathbf{V}_{\mathrm{k}}\boldsymbol{\xi}, \quad (26)$$

one which is similar to that of component mode synthesis by Craig–Bampton shown in Eq. (18), but with the eigenmodes of the slave structure exchanged for the Krylov subspace vectors as defined in Eq. (25). This results in the transformation of the state vector for KCMS

$$\begin{bmatrix}\mathbf{u}_m\\ \mathbf{u}_s\end{bmatrix}=\begin{bmatrix}\mathbf{I} & \mathbf{0}\\ \mathbf{\Psi} & \mathbf{V}_{\mathrm{k}}\end{bmatrix}\begin{bmatrix}\mathbf{u}_m\\ \boldsymbol{\xi}\end{bmatrix}=\mathbf{T}_{\mathrm{KCMS}}\begin{bmatrix}\mathbf{u}_m\\ \boldsymbol{\xi}\end{bmatrix}, \quad (27)$$

defining the transformation matrix $\mathbf{T}_{\mathrm{KCMS}}$. In order to avoid numerical issues, the Krylov subspace is generated by using the Arnoldi algorithm with modified Gram-Schmidt orthogonalization [14], which creates a set of linearly independent vectors. Calculating the starting vector $\mathbf{b}$ requires that $\mathbf{B}_s$, which describes the spatial load distribution on the slave structure, be selected. In the present study, a substructuring approach for the modelling of multi-storey buildings is adopted. Smaller parts of such buildings are considered as being substructures of these, most of these substructures having no loads that act upon the slave structure. Accordingly, a fictitious load needs to be selected, in the present study a random distribution being used for this.

In contrast to CMS, which includes eigenmodes of the full model as Ritz basis vectors, no eigenvalue extraction is required for creating reduced models by means of the KCMS method. Consequently, it is less costly to create the reduced models employing KCMS and in application where the computation time of this process is of importance, this gives KCMS an advantage over CMS.

Improved component mode synthesis

The two component mode synthesis methods described above are obtained by complementing Guyan reduction by a set of Ritz basis vectors for the slave structure, these being either eigenmodes or Krylov subspace vectors. IRS can be seen as representing an improvement as compared to Guyan reduction, an improvement that can also be applied to the component mode synthesis methods employed here. The transformation matrices of the improved component mode synthesis methods, improved CMS and improved KCMS (ICMS and IKCMS, respectively), can be obtained by simply replacing the basis vectors of Guyan reduction by the basis vectors of IRS:

$$\mathbf{T}_{\mathrm{ICMS}}=\begin{bmatrix}\mathbf{T}_{\mathrm{IRS}} & \hat{\mathbf{\Phi}}\end{bmatrix};\quad \hat{\mathbf{\Phi}}=\begin{bmatrix}\mathbf{0}\\ \mathbf{\Phi}\end{bmatrix}, \quad (28)$$

$$\mathbf{T}_{\mathrm{IKCMS}}=\begin{bmatrix}\mathbf{T}_{\mathrm{IRS}} & \hat{\mathbf{V}}_{\mathrm{k}}\end{bmatrix};\quad \hat{\mathbf{V}}_{\mathrm{k}}=\begin{bmatrix}\mathbf{0}\\ \mathbf{V}_{\mathrm{k}}\end{bmatrix}, \quad (29)$$

where $\mathbf{T}_{\text{IRS}}$ can be given either by the original form of IRS, Eq. (14), or its iterated version, Eq. (16). The use of IRS instead of Guyan reduction can be expected to improve the dynamic behaviour of the reduced models, at the expense of introducing errors in static analyses.

2.2 Generalised methods

The generalised versions of the reduction methods (denoted here by a "g-" in the method names) are obtained by re-formulating the equation of motion. Instead of using the block-partitioning of the system matrices in Eq. (4), the following partitioning is employed:

$$\begin{bmatrix}\mathbf{M}_m & \mathbf{M}_s\end{bmatrix}\begin{bmatrix}\ddot{\mathbf{u}}_m \\ \ddot{\mathbf{u}}_s\end{bmatrix} + \begin{bmatrix}\mathbf{K}_m & \mathbf{K}_s\end{bmatrix}\begin{bmatrix}\mathbf{u}_m \\ \mathbf{u}_s\end{bmatrix} = \begin{bmatrix}\mathbf{f}_m \\ \mathbf{f}_s\end{bmatrix}, \tag{30}$$

with the non-square submatrices $\mathbf{K}_m, \mathbf{M}_m \in \mathbb{R}^{n\times m}$ and $\mathbf{K}_s, \mathbf{M}_s \in \mathbb{R}^{n\times s}$. A drawback of the generalised versions of the methods, in comparison to the original versions, is the increased computational resources needed to construct the reduced models, since this requires the generalised inverses of matrices that are very large.

Generalised Guyan reduction

In the same manner as in Eq. (5) and Eq. (6), the inertia terms in Eq. (30) are neglected when solving for the slave dofs, resulting in the following transformation of the state vector for generalised Guyan (g-Guyan) reduction:

$$\begin{bmatrix}\mathbf{u}_m \\ \mathbf{u}_s\end{bmatrix} = \begin{bmatrix}\mathbf{I} \\ -\mathbf{K}_s^{+}\mathbf{K}_m\end{bmatrix}\mathbf{u}_m = \mathbf{T}_{\text{g-Guyan}}\mathbf{u}_m, \tag{31}$$

where $\mathbf{K}_s^{+} = \left(\mathbf{K}_s^T\mathbf{K}_s\right)^{-1}\mathbf{K}_s^T$ is the generalised left-inverse of $\mathbf{K}_s$ and $\mathbf{T}_{\text{g-Guyan}}$ is the transformation matrix. Note that in the approximation of the slave dofs it is assumed that there are no loads that act on either the master dofs or the slave dofs, $\mathbf{f}_m = \mathbf{0}$ and $\mathbf{f}_s = \mathbf{0}$, respectively, in contrast to the original Guyan reduction, in which only $\mathbf{f}_s = \mathbf{0}$ needs to be assumed.

Generalised dynamic reduction

Through use of an approach corresponding to the derivation of g-Guyan reduction, the transformation matrix of generalised dynamic (g-dynamic) reduction, $\mathbf{T}_{\text{g-Dynamic}}$, can be defined as

$$\begin{bmatrix}\hat{\mathbf{u}}_m \\ \hat{\mathbf{u}}_s\end{bmatrix} = \begin{bmatrix}\mathbf{I} \\ -\mathbf{D}_s^{+}(\omega)\,\mathbf{D}_m(\omega)\end{bmatrix}\hat{\mathbf{u}}_m = \mathbf{T}_{\text{g-Dynamic}}\hat{\mathbf{u}}_m, \tag{32}$$

where $\mathbf{D}_s(\omega) = -\omega^2\mathbf{M}_s + \mathbf{K}_s$ and $\mathbf{D}_m(\omega) = -\omega^2\mathbf{M}_m + \mathbf{K}_m$.

Generalised improved reduction system (g-IRS)

The transformation matrix of generalised IRS is obtained by including the inertia terms found in Eq. (30) as pseudo-static forces, using approximations corresponding to those employed in Eq. (11) and Eq. (12), resulting in

$$\mathbf{T}_{\text{g-IRS}} = \mathbf{T}_{\text{g-Guyan}} + \hat{\mathbf{S}}\mathbf{M}\mathbf{T}_{\text{g-Guyan}}\mathbf{M}_{\text{g-Guyan}}^{-1}\mathbf{K}_{\text{g-Guyan}}, \tag{33}$$

$$\hat{\mathbf{S}} = \begin{bmatrix}\mathbf{0} \\ \mathbf{K}_s^{+}\end{bmatrix}, \tag{34}$$

where $\mathbf{M}_{\text{Guyan}}$ and $\mathbf{K}_{\text{Guyan}}$ are the reduced stiffness- and mass matrices obtained by employing g-Guyan reduction. g-IRS can also be extended to produce an iterative scheme in the same manner as in the original IRS, where the transformation matrix for the ith iteration is given by

$$\mathbf{T}_{\text{g-IRS},i+1} = \mathbf{T}_{\text{g-Guyan}} + \hat{\mathbf{S}}\mathbf{M}\mathbf{T}_{\text{g-IRS},i}\mathbf{M}_{\text{g-IRS},i}^{-1}\mathbf{K}_{\text{g-IRS},i}, \tag{35}$$

and the iterations are started by calculating $\mathbf{T}_{\text{g-IRS},1}$ according to Eq. (33).

Generalised component mode synthesis

The generalised versions of Guyan reduction and IRS can be used to obtain the transformation matrices for the generalised versions of CMS, KCMS, ICMS and IKCMS (g-CMS, g-KCMS, g-ICMS and g-IKCMS, respectively)

$$\mathbf{T}_{\text{g-CMS}} = \begin{bmatrix} \mathbf{T}_{\text{g-Guyan}} & \hat{\mathbf{\Phi}} \end{bmatrix}, \tag{36}$$

$$\mathbf{T}_{\text{g-KCMS}} = \begin{bmatrix} \mathbf{T}_{\text{g-Guyan}} & \hat{\mathbf{V}}_{\text{k}} \end{bmatrix}, \tag{37}$$

$$\mathbf{T}_{\text{g-ICMS}} = \begin{bmatrix} \mathbf{T}_{\text{g-IRS}} & \hat{\mathbf{\Phi}} \end{bmatrix}, \tag{38}$$

$$\mathbf{T}_{\text{g-IKCMS}} = \begin{bmatrix} \mathbf{T}_{\text{g-IRS}} & \hat{\mathbf{V}}_{\text{k}} \end{bmatrix}, \tag{39}$$

where $\hat{\mathbf{\Phi}}$ and $\hat{\mathbf{V}}_{\text{k}}$ are defined in Eq. (28) and Eq. (29), respectively.

2.3 Summary of methods

Table 1 summarises the methods for model order reduction which are presented above and investigated in the numerical examples.

3 Numerical examples

This section considers two numerical examples in which different model order reduction methods are applied to FE models of wooden floor structures. In the first example, a model of moderate size created in Abaqus is studied. The system matrices were exported to Matlab, where the reduction methods described in Section 2 were employed, the reduced models that resulted being analysed. The second example concerns a large and detailed model that was both created and analysed in Abaqus, using reduction methods implemented in the software together with an alternative approach involving use of structural elements. In both examples, two types of analyses were performed: eigenvalue analysis and steady-state analysis. The eigenvalue analysis was performed in a free-free state, i.e. without any displacements of the physical dofs being prescribed. The rigid body eigenmodes that occur in a free-free state are disregarded in the results that are presented. A steady-state analysis was performed to investigate the vibration transmission found in the reduced floor models when realistic boundary conditions were involved, these being accomplished by connecting the reduced models to the top of a pair of wall panel models. The displacement spectrum for one of the wall panels was analysed when a unit load was applied to the other panel.

Condensation methods	
Method name	**Abbrevation**
Guyan reduction	–
Dynamic reduction	–
Improved reduction system	IRS
Generalised Guyan reduction	g-Guyan reduction
Generalised dynamic reduction	g-dynamic reduction
Generalised IRS	g-IRS
Hybrid methods	
Method name	**Abbrevation**
Component mode synthesis by Craig–Bampton	CMS
Improved CMS	ICMS
Krylov subspace component mode synthesis	KCMS
Improved KCMS	IKCMS
Generalised CMS	g-CMS
Generalised ICMS	g-ICMS
Generalised KCMS	g-KCMS
Generalised IKCMS	g-IKCMS

Table 1: The model order reduction methods presented in Section 2 and investigated in Section 3.

3.1 Error quantities

Both the eigenfrequencies and the eigenmodes of the reduced models were studied in the eigenvalue analysis carried out. The eigenfrequencies were compared with those of the full (non-reduced) model in terms of the normalised relative frequency difference (NRFD) and the eigenmodes with those of the full model in terms of the modal assurance criterion (MAC). To obtain a measure for the displacement spectrum of the whole receiver wall panel in the steady-state analysis, a root mean square (RMS) value for the displacement magnitudes in all the nodes of the panel was calculated for each of the frequency steps.

Normalised relative frequency difference (NRFD)

The NRFD of the ith eigenfrequency is defined as

$$\text{NRFD} = \frac{\left| f_i^{red} - f_i^{full} \right|}{f_i^{full}} \cdot 100, \tag{40}$$

where f_i^{full} is the eigenfrequency of the full model and f_i^{red} is the eigenfrequency of the reduced model. This quotient is multiplied by 100 to obtain the NRFD value as a percentage.

Modal assurance criterion (MAC)

The MAC value for the jth eigenmode of the reduced model, Φ_j^{red}, as compared with the ith eigenmode of the full model, Φ_i^{full}, is defined as

$$\text{MAC} = \frac{\left|(\Phi_j^{red})^T(\Phi_i^{full})\right|^2}{(\Phi_j^{red})^T(\Phi_j^{red})(\Phi_i^{full})^T(\Phi_i^{full})}. \tag{41}$$

The eigenmodes of a reduced model often appear in shifted order as compared with the full model. Accordingly, each of the eigenmodes of a reduced model is compared with each of eigenmodes of the full model, within the frequency range which is specified.

Root mean square (RMS)

For any given excitation frequency f in the steady-state analysis, the RMS value is defined here as

$$U_{RMS}(f) = \sqrt{\frac{1}{n_{dof}} \sum_{i=1}^{n_{dof}} U_i(f)^2}, \tag{42}$$

where $U_i(f)$ is the magnitude of the complex amplitude for the ith displacement dof and n_{dof} is the number of displacement dofs of the receiver wall panel. A normalised error of the RMS value for a reduced model, U_{RMS}^{red}, as compared with the RMS value for the full model, U_{RMS}^{full}, can be calculated as

$$U_{RMS}^{\text{error}}(f) = \frac{\left|U_{RMS}^{red}(f) - U_{RMS}^{full}(f)\right|}{U_{RMS}^{full}(f)} \cdot 100. \tag{43}$$

Calculating the error for each excitation frequency enables an error spectrum to be obtained. Since the error spectra typically fluctuate to a marked degree, the result plots used for comparing the different reduction methods make use of averaged error spectra. The errors are averaged by sweeping a 20 Hz wide window over the frequency range and calculating the mean value of the spectrum inside the window for each frequency. Accordingly, the frequency range of the plots is one of 10-90 Hz.

3.2 Numerical example 1: A moderate-sized floor structure

In the first numerical example, a model of a 2445×4090 mm^2 large floor structure was studied. The structure consisted primarily of five load-bearing wooden beams, using a centre-to-centre distance of the successive beams from one another of 600 mm, supporting a particle board surface. At the two shorter sides of the floor, wooden beams were placed perpendicular to the five beams just referred to, creating a box-like structure. Each of these wood beams had a cross-section of 45×220 mm^2 and was modelled using an orthotropic material model possessing the properties shown in Table 2. The particle board had a thickness of 22 mm and was modelled using an isotropic material model having the properties shown in Table 3. The structure was meshed using 20-node brick elements with quadratic interpolation, resulting in 30,807 dofs.

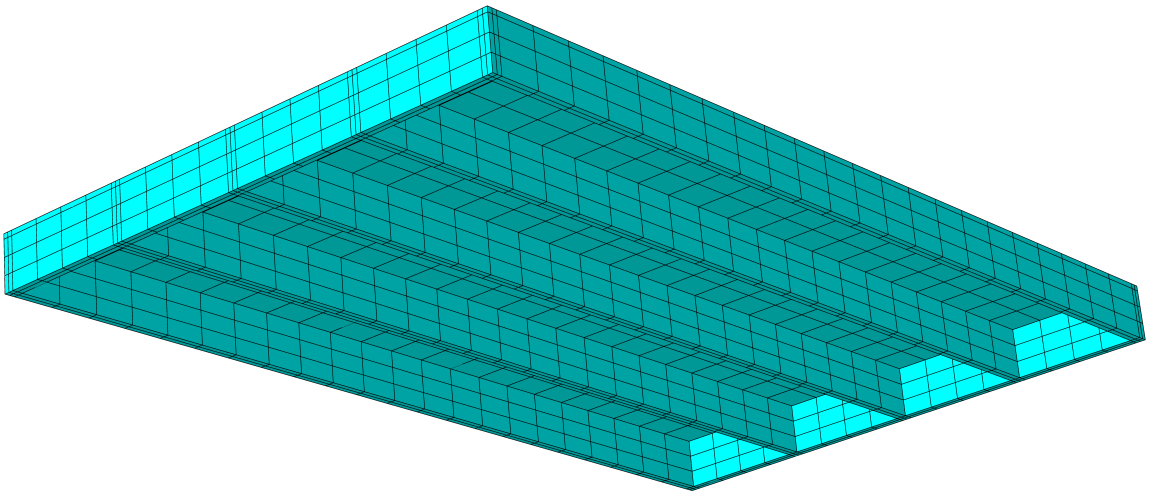

Figure 1: The mesh of the floor structure in numerical example 1.

E_1	E_2	E_3	G_{12}	G_{13}	G_{23}	ν_{12}	ν_{13}	ν_{23}	ρ
8500	350	350	700	700	50	0.2	0.2	0.3	432

Table 2: The material parameters used for the wooden beams [26], the stiffness parameters being given in terms of MPa and the density in kg/m^3.

E	ν	ρ
3000	0.3	767

Table 3: The material parameters used for the particle board [26], the modulus of elasticity being given in terms of MPa and the density in kg/m^3.

The mesh, viewed from below, is shown in Figure 1. The structural components shared mesh nodes at the intersections, the connections thus being modelled as fully interactive.

All the dofs along the centre line on the underside of the outermost beams were selected as master dofs, resulting in there being 576 master dofs altogether, this representing the minimum number of dofs in the reduced models. Reduced models of the full floor-structure model were created by employing the 14 methods for model order reduction listed in Table 1. The dynamic reduction involved a frequency shift of 53.1 Hz, this being the eigenfrequency of the full model closest to 50 Hz, located at the centre of the frequency range. IRS and the improved CMS methods were employed in their iterated versions, using three iterations. A total of 50 generalised coordinates were made use of in the hybrid reduction methods employed. Accordingly, 50 eigenmodes were included in the mode-based methods and 50 Krylov vectors in the Krylov-based methods, resulting in reduced models having 626 dofs.

The reduced models established by employing all of the reduction methods listed in Table 1 resulted in very similar computation times, the condensation methods resulting in marginally shorter times compared to the component mode synthesis methods. The similarity can be explained by the size of the reduced models being similar and the band width of the matrices being very large for all methods. The computation time for the eigenvalue analysis of each of the reduced models was approximately $3\ \%$ of the computation time for the full model.

3.2.1 Eigenvalue analysis

The NRFD values for the original methods are shown in Figure 2, 19 eigenfrequencies being included there, this being the number of eigenfrequencies of less than 100 Hz contained in the full model. The red, yellow and green dashed lines in the figure represent the error levels 10 %, 1 % and 0.1 %, respectively. Guyan reduction provides an acceptable accuracy only for the first eigenfrequency of the full model, whereas dynamic reduction yields high NRFD values for each of the eigenfrequencies. CMS and KCMS provide relatively good and very similar results, the improved variants of both methods increasing the performance appreciably due to the high degree of accuracy of iterated IRS, quite to be expected since the eigenfrequencies iterated IRS provides converge in such a way as to reproduce the eigenfrequencies of the full model exactly.

The NRFD values for the generalised methods are shown in Figure 3. As is evident there, the generalised versions of Guyan reduction and dynamic reduction improve the accuracy as compared with the original versions. The accuracy of IRS decreases for the lower frequencies when its generalised version is employed and, consequently, the accuracy of ICMS and IKCMS decreases as well. The results obtained when employing CMS and KCMS are slightly improved, however, when use is made of the generalised versions of the two.

In Figure 4, the MAC values for the seven original methods and for the generalised versions of Guyan reduction, dynamic reduction, CMS and KCMS are shown. A plot comparing the full model with itself is included in order to demonstrate the orthogonality properties of the eigenmodes. Since the eigenmodes are non-orthogonal in the dot product, the off-diagonal terms are not generally zero in value, although this is the case in the example given here (within the discretization of the MAC plots, the off-diagonal terms being less than 0.1). In agreement with the NRFD results, the MAC values for the original versions of the Guyan reduction and the dynamic reduction correlate poorly with the full model, whereas the generalised versions show a relatively high degree of accuracy. All of the other original reduction methods, except for CMS, show a high degree of correlation with the full model for each of the eigenmodes.

3.2.2 Steady-state analysis

The setup for the steady-state analysis is shown in Figure 5. The floor models were connected to the top of two wall panels, the one a source panel and the other a receiver panel, supporting each end of the load-bearing beams. The wall panels were modelled as shells provided with beam stiffeners at successive spacings from one another of 600 mm each, representing a 2500 mm high wood-framed wall having a plaster board surface. The floor models were tied to the displacement dofs of the wall panels by use of Lagrange multipliers, the bottom edge of the wall panels being fixed. A unit point load in all three directions, shown by the yellow arrows in the figure, was applied to the source panel. The displacements of the receiver wall panel were evaluated in accordance with Eq. (42) for excitation frequencies of up to 100 Hz.

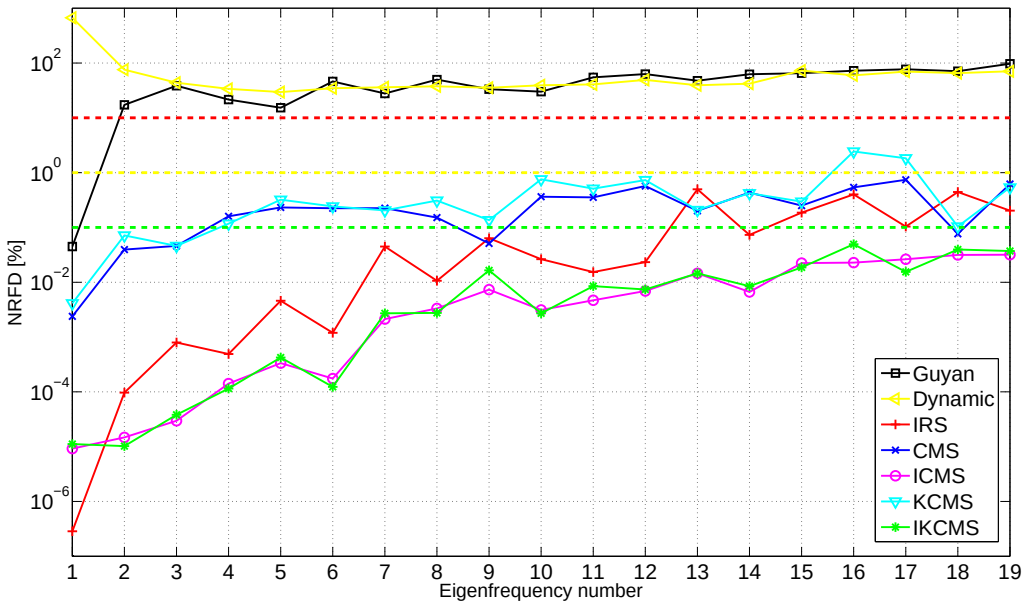

Figure 2: NRFD values for the original model order reduction methods applied to numerical example 1.

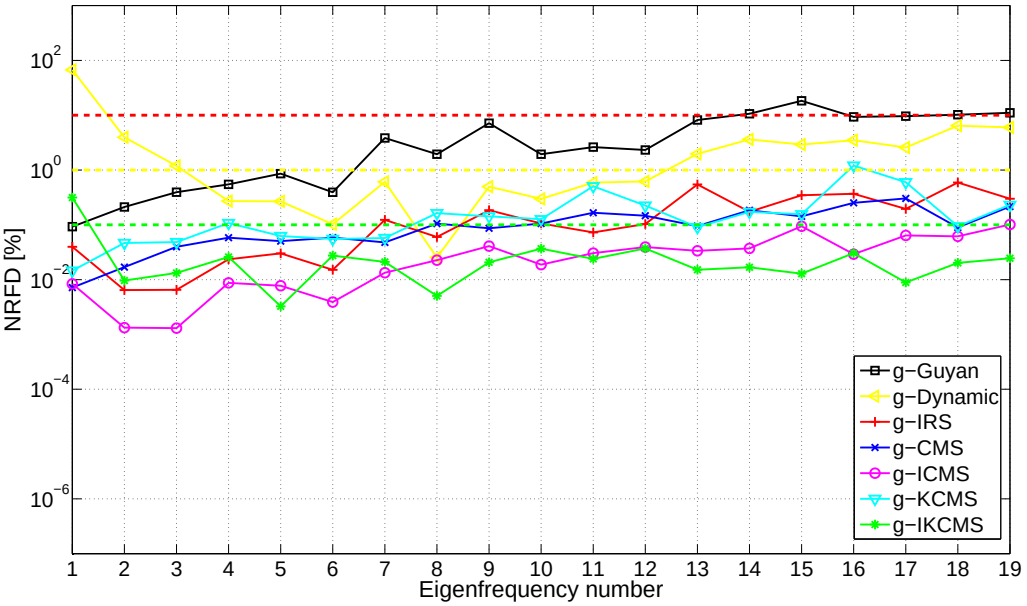

Figure 3: NRFD values for the generalised model order reduction methods applied to numerical example 1.

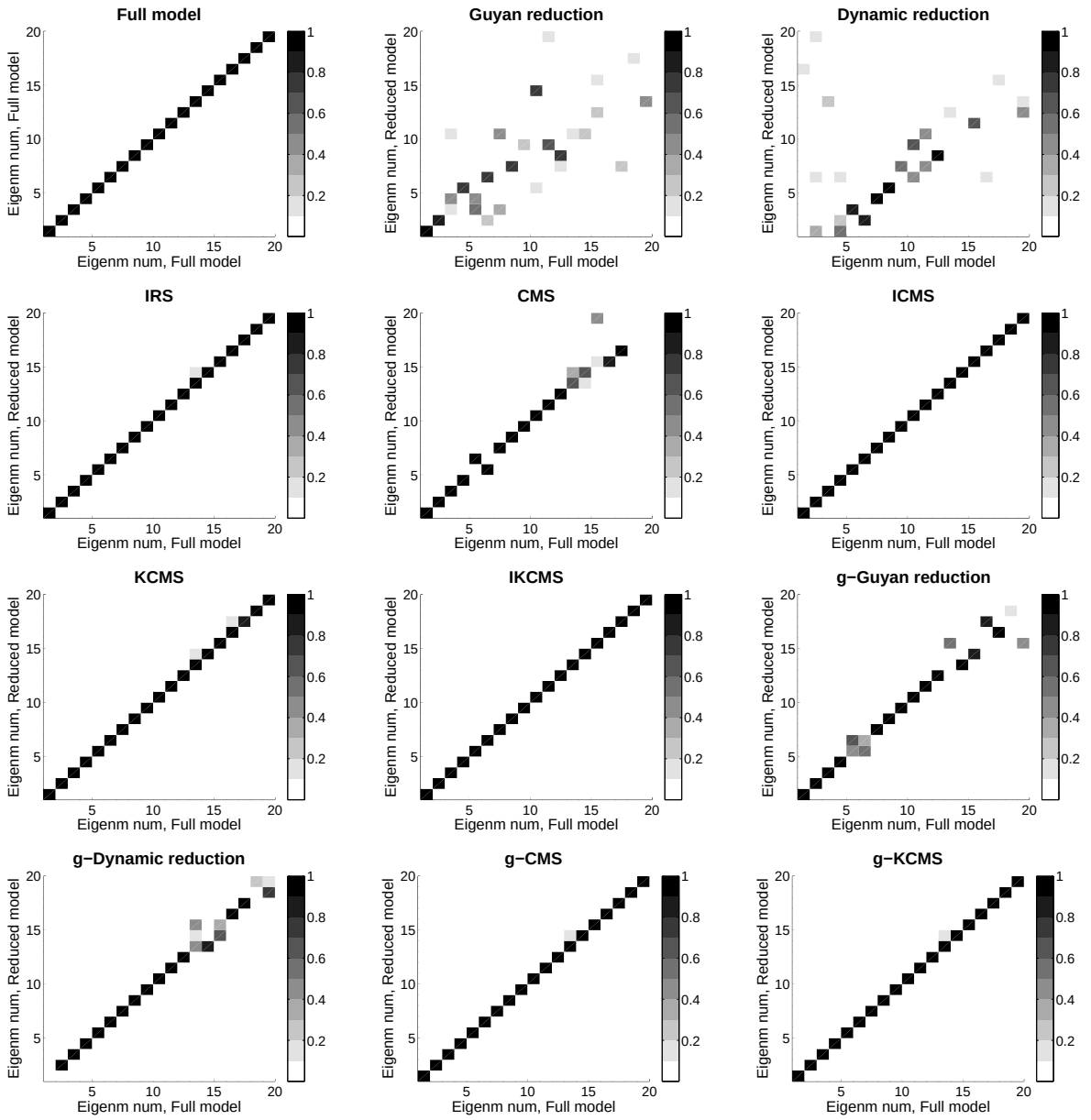

Figure 4: MAC values for the different model order reduction methods applied to numerical example 1.

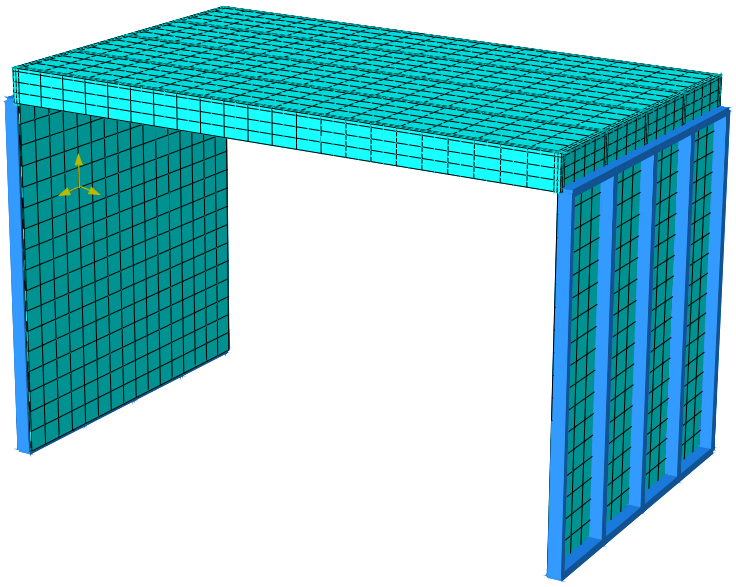

Figure 5: The setup for the steady-state analysis in numerical example 1.

The averaged error of the RMS values obtained using the original methods and the generalised methods is shown in Figure 6 and Figure 7, respectively. The dashed black line in both figures indicates the 10 % error level. In studying Figure 6, one can note that the frequency shift in dynamic reduction strongly affect the performance. Whereas Guyan reduction (corresponding to a 0 Hz shift) generates lower errors when the frequencies involved are lower, dynamic reduction results in the degree of errors being lowest at around 50 Hz, close to the frequency shift selected. CMS and KCMS can be seen to behave very similarly at the higher frequencies, whereas at the lower frequencies the latter is more accurate. In contrast to the results of the eigenvalue analysis, ICMS and IKCMS lower the level of performance for most frequencies as compared with conventional CMS and KCMS. In Figure 7, one can note that the accuracy of Guyan reduction and of dynamic reduction is appreciably greater with use of the generalised versions of these. The accuracy of KCMS decreases markedly at lower frequencies and increases at the higher frequencies when the generalised version of it is employed. As can be seen by comparing the results in Figure 6 and Figure 7, there is, generally speaking, a lesser degree of spread among the results for the different reduction methods when their generalised versions are employed.

In Table 4, the maximum and the mean errors for the frequency range as a whole (without averaging) are shown for both the original and the generalised methods. As is evident, using the generalised versions only has a strong positive effect in the case of Guyan reduction and of dynamic reduction. For most of the hybrid methods, use of the generalised versions leads to a reduction in performance. Of all the reduction methods, it is KCMS that provides the most accurate results in terms both of average and of maximum error levels.

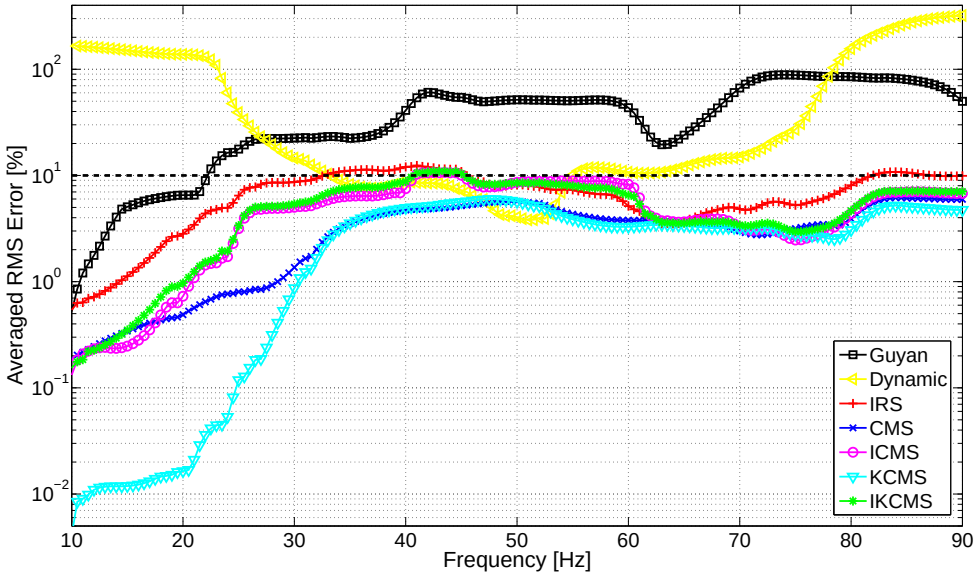

Figure 6: Averaged errors of the RMS values for numerical example 1, as determined with use of the original model order reduction methods.

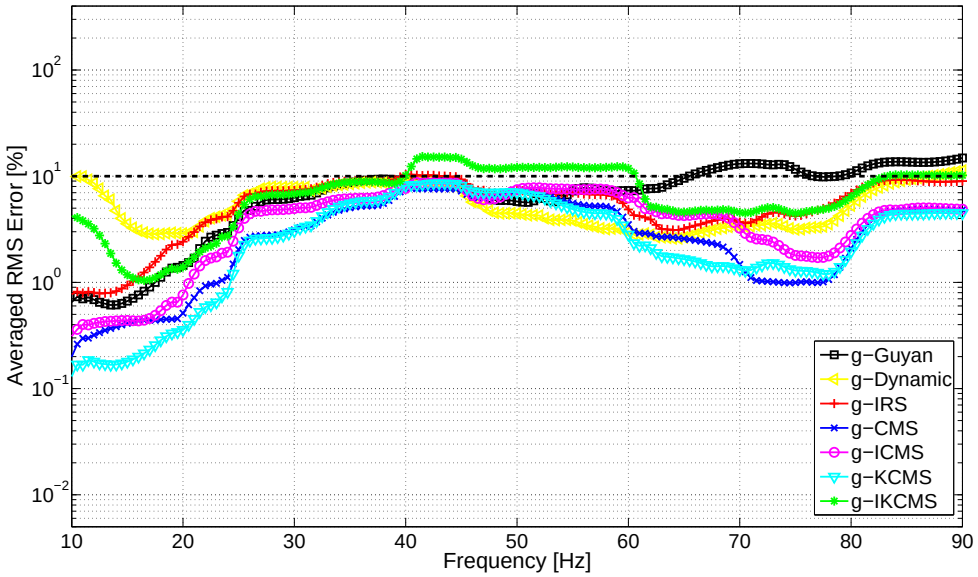

Figure 7: Averaged errors of the RMS values for numerical example 1, as determined with use of the generalised model order reduction methods.

Model	Mean error [%]	Maximum error [%]
Guyan reduction	37.7	276
g-Guyan reduction	8.26	35.0
Dynamic reduction	106	1120
g-dynamic reduction	7.49	54.6
IRS	6.52	39.4
g-IRS	5.70	37.5
CMS	3.26	20.9
g-CMS	3.35	27.0
ICMS	4.81	63.4
g-ICMS	4.18	33.9
KCMS	2.92	20.2
g-KCMS	3.21	27.8
IKCMS	4.96	42.6
g-IKCMS	7.67	98.1

Table 4: Average and maximum error levels of the RMS values obtained for the reduction methods applied to numerical example 1.

3.3 Numerical example 2: A large two-span floor structure

In the second numerical example, a model of an experimental floor structure that was compared with measurements in [26] was studied. The 3645×9045 mm^2 large floor structure consists of seven load-bearing wooden beams, at a centre-to-centre distance of the successive beams from one another of 600 mm, supporting a particle board surface, secondary spaced boarding being attached to the underside of the beams. In the FE model, the wooden beams were placed perpendicular to the load-bearing beams at the two short sides of the floor, creating a box-like structure, in contrast to the experimental structure in which the ends of the beams were free. Each of the wooden beams had a cross-section of 45×220 mm^2 and was modelled using an orthotropic material model having the properties shown in Table 2. The secondary spaced boarding had a cross-section of 28×70 mm^2 and was modelled as having the same material properties as the wooden beams. The particle board had a thickness of 22 mm and was modelled using an isotropic material model possessing the properties shown in Table 3. The structure was meshed using 20-node brick elements with quadratic interpolation, resulting in 632,820 dofs. The mesh, as viewed from below, is shown in Figure 8. The structural components shared mesh nodes at the intersections, the connections thus being modelled as fully interactive.

For reasons of efficiency, it is desirable to connect the floor structure to other structures at discrete points so as to minimise the number of physical dofs retained in the reduced models. Discrete point connections require that rotational dofs fulfil conditions of compatibility. To create rotational coupling in the case of the solid elements, 173 additional nodes, indicated by the yellow crosses in Figure 8, having both displacement dofs and rotational dofs, were created.

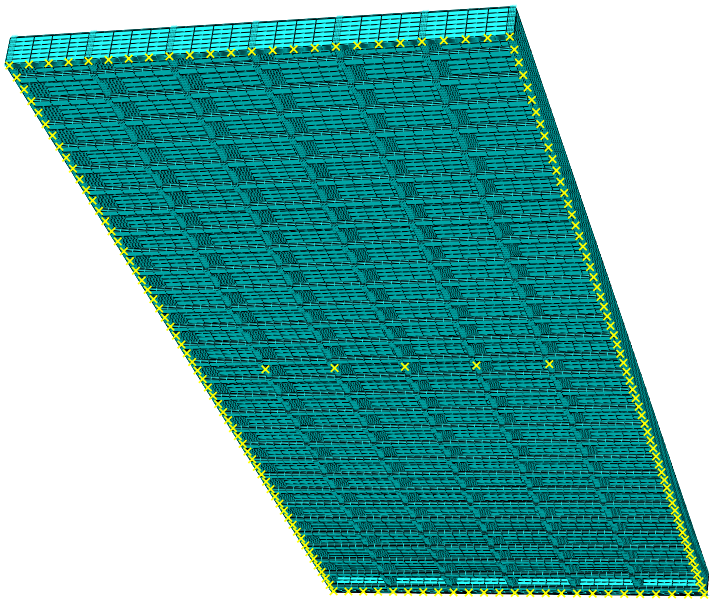

Figure 8: The mesh of the floor structure model in numerical example 2.

These nodes were connected to the neighbouring mesh nodes under conditions of rigid beam constraints, the rotational dofs thus being connected to the rotations of the structure as a whole. The experimental structure has both a mid-span support and end supports. To provide for a modelling of all of the supports, the model has additional nodes possessing rotational dofs both along the underside of the outermost beams and at the middle of the load-bearing beams. The dofs at the 173 additional nodes served as master dofs in the model order reduction, resulting in 1038 master dofs. The model was reduced by use of the two model order reduction methods implemented in Abaqus: Guyan reduction and CMS. The number of eigenmodes retained in the CMS reduction was varied so as to study the convergence of errors.

When employing the model order reduction methods, computationally effective models are obtained by reducing the size of the large system matrices obtained by use of detailed FE models. As an alternative, smaller systems can be constructed directly by use of structural finite elements, beam or shell elements, for example, assumptions being made regarding the kinematic relations and the equilibrium equations involved. These assumptions can turn out to have no more than a negligible effect in static analysis if one or two dimensions of the structure are significantly smaller than the other or others. In dynamic analysis, however, the constraints implied by beam and shell theory can have a strong effect on the structural behaviour in the case of higher frequencies. A structural FE model of the floor structure was created by modelling the panels and the wooden beams in terms of Reissner-Mindlin shell elements, and the secondary spaced boarding in terms of Timoshenko beam elements. The two theories involved allow for shear deformation of the normal to the shell plane and of the beam axis, respectively. Further discussion of the beam and the shell theory can be found in e.g. [5, 27]. The structural-element model was meshed with 720 beam elements and 3,312 shell elements, resulting in 24,762 dofs.

Table 5 shows the size (number of dofs) of the reduced models as well as the computation times obtained for a Lanczos eigenvalue analysis of the 55 first eigenmodes and a steady-state

Model	**Size** (number of dofs)	**Time [s]** (eigenvalue anal.)	**Time [s]** (steady-state anal.)
Full model	632820	590	220000
Structural elements	24762	7.6	1200
Guyan reduction	1038	3.1	410
CMS, 10 re*	1048	3.2	410
CMS, 20 re*	1058	3.2	410
CMS, 50 re*	1088	3.7	420
CMS, 100 re*	1138	5.5	440
CMS, 200 re*	1238	5.7	480
CMS, 500 re*	1538	8.5	620
CMS, 1000 re*	2038	15	970

Table 5: The size and computation times, both for eigenvalue analyses and steady-state analyses, of the reduced models analysed in connection with numerical example 2, the analyses running on one core of an Intel Xeon W3530 CPU of 2.80 GHz, having 10 GB of RAM memory available. *retained eigenmodes

analysis involving 200 steps. The analyses were carried out employing Abaqus/Standard. It can be observed that the computation times are affected by increasing the number of eigenmodes retained in the CMS reduction, the retaining of 1000 eigenmodes (a duplication of the number of dofs compared to Guyan reduction) resulting in the computation times being increased significantly. The number of eigenmodes retained is, of course, a trade-off between accuracy and computational cost, the gain in accuracy being illustrated in the analysis results presented below. It is, however, not possible to estimate the number of eigenmodes required for obtaining a certain accuracy without analysing the full model. Moreover, it can be observed that the computation times for both types of analyses of the structural elements model is similar to those for a model reduced with CMS where 500-1000 eigenmodes are retained, in spite of the former model being over 10 times larger. This is a consequence of the transformation of the system matrices involved in model order reduction, destroying the narrow bandwidth of matrices constructed with the FE method.

3.3.1 Eigenvalue analysis

Figure 9 shows the NRFD values for the reduced models, including CMS when 10, 100 and 1000 eigenmodes are retained. The red, yellow and green dashed lines in the figure show the error levels of 10 %, 1 % and 0.1 %, respectively. The results included 55 eigenfrequencies, which is the number of eigenfrequencies of the full model up to 100 Hz. Guyan reduction assesses only the lowest eigenfrequencies of the full model with an acceptable level of accuracy. Use of CMS in which 10 eigenmodes are retained improves the accuracy obtained for the first 20 eigenmodes, but is inaccurate for the remaining eigenmodes. When 100 eigenmodes are retained, relatively accurate results can be obtained for all of the eigenfrequencies, the retaining of

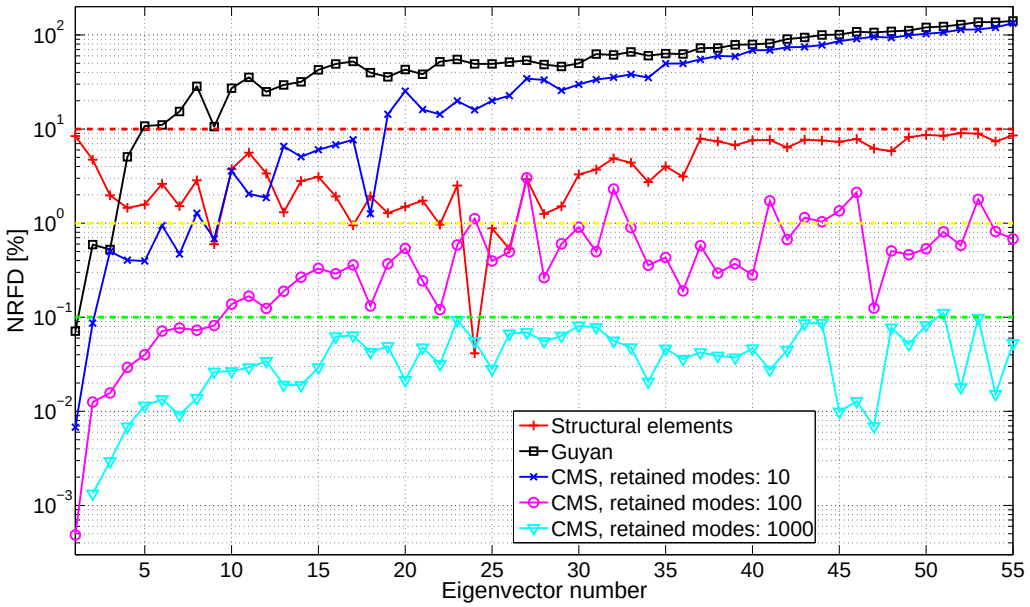

Figure 9: NRFD values for the different reduction methods applied to numerical example 2.

1000 eigenmodes resulting in very small errors. Use of structural elements results in relatively large errors, although the errors are less frequency-dependent than when any of the model order reduction methods are employed.

Figure 4 shows the MAC values obtained with use of the reduced models, including CMS when 10, 50, 100, 500 and 1000 eigenmodes are retained, as well as the full model being compared with itself. For practical reasons, only the master dofs of the reduced models were used for evaluating the eigenmodes. In comparing the plots, it could be noted that the MAC values of the higher eigenmodes were improved with use of CMS when the number of eigenmodes retained was increasing. Whereas Guyan reduction (no eigenmodes retained) only succeeds in modelling a few of the eigenmodes in the full model accurately, the MAC plot for CMS when 1000 eigenmodes are retained is identical to the MAC plot for the full model. The structural element model only models a few of the eigenmodes of the full model with a high degree of accuracy. The correlation there with results of the full model is better for the higher frequencies, however, than is the case of Guyan reduction or CMS when only a few eigenmodes are retained.

3.3.2 Steady-state analysis

The transmission of vibrations was studied using the same approach as in the first numerical example, shown in Figure 5, where the floor models were connected to the top of two wall panels, the one a source panel and the other a receiver panel, supporting each end of the load-bearing beams. The floor models were, in the second numerical example, connected to a third wall panel located at the centre of the floor models through the nodes in the middle of the load-bearing beams. Both the displacement dofs and rotational dofs of the wall panels were linked to the floor models by use of Lagrange multipliers, except in the case of the mid-span wall panel,

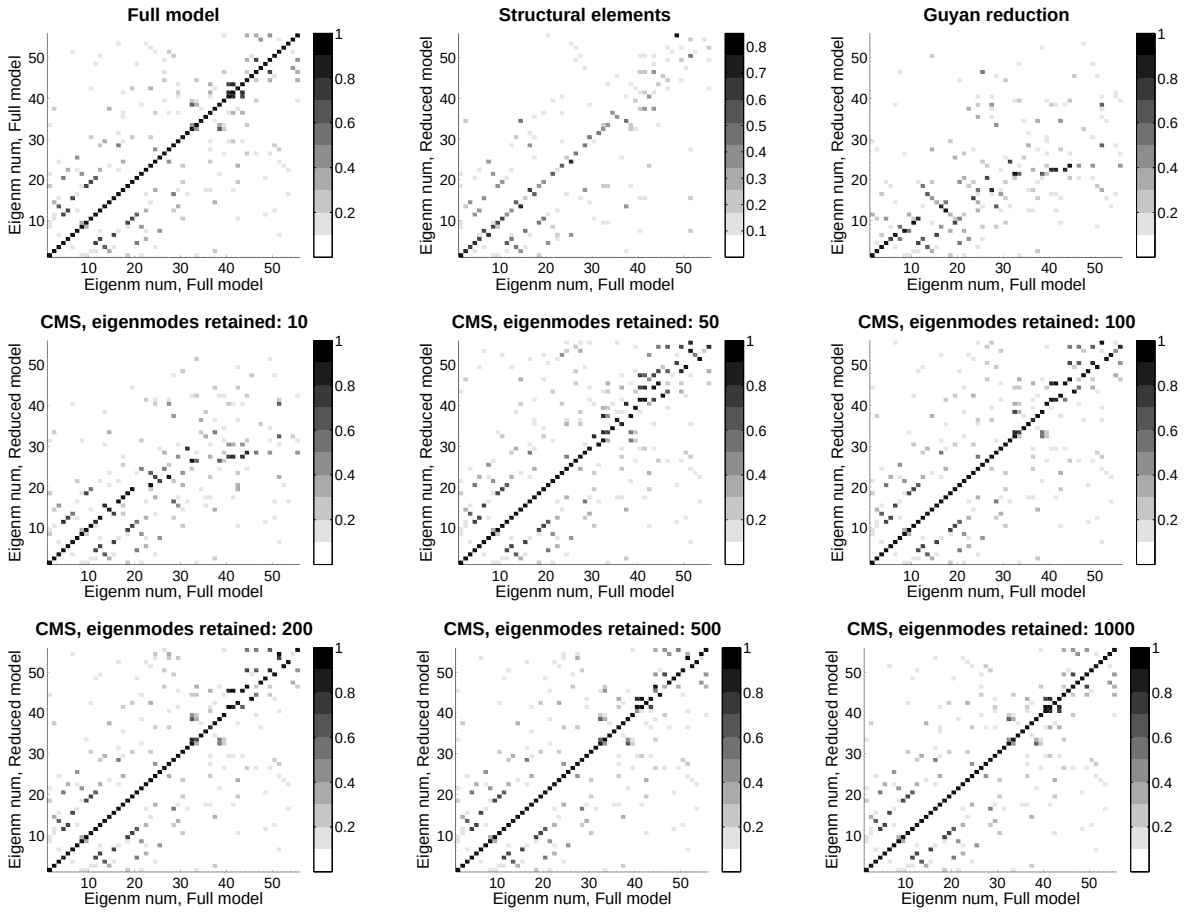

Figure 10: MAC values for the reduction methods employed in connection with numerical example 2.

at which only the displacement dofs were connected. A unit point load in all three directions was applied to the source panel, the displacements at the receiver panel being evaluated for excitation frequencies of up to 100 Hz by use of Eq. (42).

The averaged error of the RMS values for the reduced models, including CMS when 10, 100 and 1000 eigenmodes are retained, is shown in Figure 11. The dashed black line indicates the 10 % error level. Guyan reduction was found to produce large errors for most of the frequencies. Use of CMS in which 10 eigenmodes were retained was found to produce large errors as well, whereas CMS in which 100 eigenmodes were retained was found to be relatively accurate for most of the frequencies. A reduced model in which close to 1000 eigenmodes were retained was needed, however, to obtain satisfactory results for higher frequencies. As in the eigenvalue analysis, the structural element model was found to produce relatively large errors, but with a lesser frequency dependence than for the other methods.

The maximum and the mean error values obtained for the frequency range as a whole (without averaging) are shown in Table 6. As can be seen, the levels of error converge when the number of retained eigenmodes employed in the CMS reduction is increased. When as many as 50 eigenmodes are included, there is a large reduction in the error as compared with Guyan reduction, in spite of the CMS model being only 5 % larger. The convergence is slower when

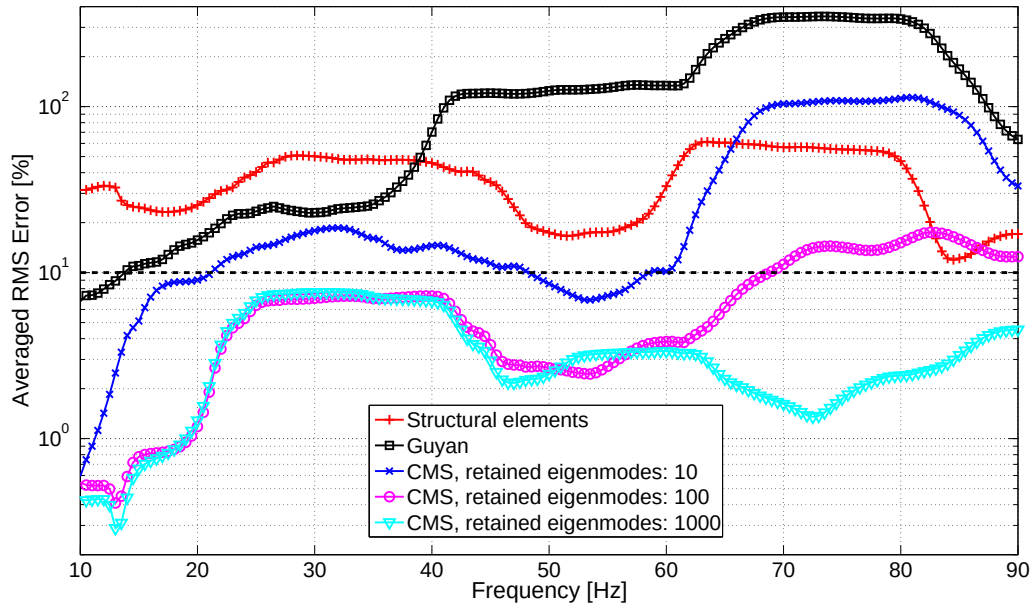

Figure 11: Averaged errors of RMS values obtained for the model order reduction methods used in connection with numerical example 2.

a greater number of eigenmodes are retained, but as shown in Figure 11, at higher frequencies a greater number of eigenmodes are required in order to obtain accurate results. It could also be observed that including a greater number of retained eigenmodes can result in an increase in the maximum error. Consequently, for a given frequency, increasing the number of retained eigenmodes does not necessarily result in a decrease in the level of error involved.

4 Conclusions

The objective of the analyses carried out in the present investigation was to evaluate the performance of a wide range of methods for model order reduction by comparing their accuracy and computational cost when applied to detailed FE models of floor and wall structures. In the first numerical example, it was evident that an eigenvalue analysis of the structure in a free-free state is insufficient for analysing the performance of the different reduction methods. A sensitivity of certain of the reduction methods to boundary conditions was demonstrated, differing observations being made regarding the accuracy of the methods in question in the two analyses: the eigenvalue analysis and the steady-state analysis. This shows the need for the reduced models to be analysed with use of realistic boundary conditions, such as in the case of the steady-state analyses that were considered here.

As was expected, Guyan reduction delivered acceptable results only at frequencies close to the lowest eigenfrequencies of the system, due to the method's static nature. Dynamic reduction was only found to be accurate close to the frequency shift selected and provided inaccurate

Model	Mean error [%]	Maximum error [%]
Structural elements	34.9	61.4
Guyan reduction	113	349
CMS, 10 retained eigenmodes	33.1	114
CMS, 20 retained eigenmodes	11.5	38.4
CMS, 50 retained eigenmodes	7.75	16.3
CMS, 100 retained eigenmodes	6.88	21.4
CMS, 500 retained eigenmodes	3.86	8.92
CMS, 1000 retained eigenmodes	3.38	7.61

Table 6: Average and maximum errors of the RMS values obtained in connection with numerical example 2.

results at frequencies differing to any appreciable extent from this. Iterated improved reduction system (IRS) provided considerably better results than the other condensation methods.

In both numerical examples, component mode synthesis by Craig-Bampton (CMS) proved to be an effective method. The Krylov subspace component mode synthesis (KCMS) method used in the present study was found to be a good alternative as compared with CMS, the two methods offering comparable accuracy. Using IRS to create the improved variants of CMS and KCMS (ICMS and IKCMS, respectively) enabled the accuracy in terms of eigenfrequencies and eigenmodes to be improved appreciably, although at the same time the errors in the steady-state analysis were found to increase, indicating the improved variants to possibly be more sensitive to the boundary conditions introduced in the analysis.

The performance of Guyan reduction and of dynamic reduction was found to clearly be improved by use of the generalised versions of these methods. For the remaining methods, the accuracy was only marginally affected by use of the generalised versions and, for most of the methods, it was decreased at lower frequencies.

The alternative approach of using structural finite elements was found to result in relatively large errors, the computation time, however, being significantly shorter considering the size of the model. The structural element model can, however, be optimised further regarding such matters as the selection of structural element types and the connections involved.

Acknowledgements

The financial support for this work provided by the Silent Spaces project, a part of the EU program Interreg IV A, is gratefully acknowledged.

References

[1] Fehr J., Eberhard P. Simulation process of flexible multibody systems with non-modal model order reduction techniques. Multibody Syst Dyn, 2011;25(3):313-334.

[2] Nowakowski C., Kürschner P., Eberhard P., Benner P. Model reduction of an elastic crankshaft for elastic multibody simulations. J Appl Math and Mech, 2013;93(4):198-216.

[3] Koutsovasilis P., Beitelschmidt M. Comparison of model reduction techniques for large mechanical systems. Multibody Syst Dyn, 2008;20(2):111-128.

[4] Witteveen W. On the modal and non-modal model reduction of metallic structures with variable boundary conditions. World J Mech, 2012;2(6):311-324.

[5] Bathe K.J. Finite element procedures. Prentice Hall, New York, 1996.

[6] Arnold R.R., Citerley R.L. Application of Ritz vectors for dynamic analysis of large structures. Comput Struct, 1985;21(5):901-907.

[7] Guyan R.J. Reduction of stiffness and mass matrices. AIAA J, 1965;3:380.

[8] Leung A.Y.T. An accurate method of dynamic condensation in structural analysis, Int J Numer Methods Eng, 1978;12:1705–1715.

[9] O'Callahan J. A procedure for an improved reduced system (IRS) model. Proc 7th Int Modal Anal Conf, 1989;17–21.

[10] Friswell M.I., Garvey S.D., Penny J.E.T. Model reduction using dynamic and iterated IRS techniques. J Sound Vib, 1995;186:311–323.

[11] O'Callahan J., Avitabile P., Riemer R. System equivalent reduction expansion process (SEREP). Proc 7th Int Modal Anal Conf, 1989;29–37.

[12] Craig R.R. Structural dynamics – An introduction to computer methods. John Wiley & sons Inc., New York, 1981.

[13] Craig R.R., Chang C.J. A review of substructure coupling methods for dynamic analysis. Adv Eng Sci, 1976;2:393-408.

[14] Lohmann B., Salimbahrami B. Introduction to Krylov subspace methods in model order reduction. Methods Appl Autom, 2003;1-13.

[15] Salimbahrami B., Lohmann B. Order reduction of large scale second-order systems using Krylov subspace methods. Linear Algebra Appl, 2006;415(2):385-405.

[16] Benner P. Numerical linear algebra for model reduction in control and simulation. GAMM Mitt, 2006;29(2):275-296.

[17] Reis T., Stykel T. Balanced truncation model reduction of second-order systems. Math Comput Model Dyn Syst, 2008;14(5):391-406.

[18] Craig R.R., Bampton M. Coupling of substructures in dynamic analysis. AIAA J, 1968;6:1313–1319.

[19] MacNeal R.H. A hybrid method of component mode synthesis. Comput Struct, 1971;1(4):581-601.

[20] Rubin S. Improved component-mode representation for structural dynamic analysis. AIAA J, 1975;13:995-1006.

[21] Koutsovasilis P., Beitelschmidt M. Model order reduction of finite element models: improved component mode synthesis. Math Comput Model Dyn Syst, 2010;16(1):57–73.

[22] Häggblad B., Eriksson L. Model reduction methods for dynamic analyses of large structures. Comput Struct, 1993;47(4):735–749.

[23] Koutsovasilis P. Improved component mode synthesis and variants. Multibody Syst Dyn, 2013;29(4):343–359.

[24] Bouhaddi N., Fillod R. A method for selecting master dof in dynamic substructuring using the Guyan condensation method. Comput Struct, 1992;45(5):941-946.

[25] Shah V., Raymund M. Analytical selection of masters for the reduced eigenvalue problem. Int J Numer Methods Eng, 1982;18(1):89–98.

[26] Flodén O., Ejenstam J., Vibration analyses of a wooden floor-wall structure – Experimental and finite element studies. Masters dissertation, Division of Structural Mechanics, Lund University, Sweden, 2011.

[27] Zienkiewicz O.C., Taylor R.L. The finite element method – Fifth edition, Volume 2. MacGraw-Hill, London, 1994.

Paper C

Coupling elements for substructure modelling of lightweight multi-storey buildings

O. Flodén, K. Persson, G. Sandberg

Lund University
Department of Construction Sciences
P.O. Box 118, SE-22100 Lund, Sweden

Accepted for the proceedings of *IMAC XXXII*, Orlando, USA, February 2014

Coupling elements for substructure modelling of lightweight multi-storey buildings

Ola Flodén, Kent Persson, Göran Sandberg
Lund University, Department of Construction Sciences, P.O. Box 118, SE-22100 Lund, Sweden

Abstract

Accurately modelling the dynamic behaviour of multi-storey buildings in wood requires the geometry involved to be represented in great detail, resulting in systems having many millions of degrees of freedom. Consequently, there is a need for model order reduction and the methodology of substructure modelling is employed here to create reduced models for analysis of low-frequency vibrations. The full finite element model of a building is divided into substructures which are reduced in size before being assembled to form the global model. The efficiency of the reduced models is strongly dependent on the number of degrees of freedom at the interface surfaces of the substructures, why it may be necessary to perform interface reduction of some sort. Multi-storey buildings in wood are often constructed with elastomer layers separating the structural components, these offering a natural choice of dividing the buildings into substructures. In this paper, the methodology of introducing a condensation node is adopted for employing interface reduction at the interfaces between the elastomer layers and the structural components in wood. Different methods of coupling the condensation node to the interface surfaces were compared in a test model consisting of a floor-ceiling structure in wood, where the floor and the ceiling are separated by elastomer blocks. It was concluded that a rigid coupling is the most appropriate choice for the interface surfaces of the elastomer blocks, while a distributed coupling provides the most accurate results for the interface surfaces of the floor and the ceiling.

Keywords: Multi-storey buildings; Vibrations; Finite element method; Substructure modelling; Interface reduction

1 Introduction

In 1994, a century-old ban on the construction of wooden buildings more than two storeys in height in Sweden was lifted, leading to the reintroduction of such buildings. The use of wood as a construction material in fact has many advantages. The lightweight properties of wood, for example, lower the material transportation costs involved and reduce the size of the foundations

needed [1]. In addition, the energy consumption which occurs during the construction and the lifecycle of wooden buildings is lower than that of concrete buildings of comparable size [2]. At the same time, however, it is more difficult to build lightweight structures of wood in such a way that noise and disturbing vibrations in the different storeys and rooms is avoided, especially at low frequencies. The vibrations can be caused by, for example, footsteps, airborne sound, vibrating machines and external sources such as railway and road traffic.

To produce buildings of high performance regarding vibrations and structure-borne sound, it is desirable to have tools for predicting the effects of structural modifications prior to construction. Testing prototypes and performing experiments is both time-consuming and expensive. The long-term aim is therefore to develop prediction tools making use of finite element (FE) models that are valid for general load-cases. Accurately assessing the dynamic behaviour of lightweight multi-storey buildings requires use of FE models representing the geometry in considerable detail, resulting in very large models, the number of degrees of freedom (dofs) of which easily exceeds the limits of computer capacity. The question arises then of how such FE models can be reduced in size while at the same time being able to represent the dynamic characteristics of the building or buildings in question with sufficient accuracy. In the study, multi-storey buildings in wood are modelled by adopting a substructuring approach, in which the FE model of the full geometry is divided into substructures, these being reduced in size by employing some model order reduction method and coupled to form a reduced global model.

The methodology of substructuring originates from the component mode synthesis (CMS) by Craig and Bampton, presented in [3]. It is a suitable methodology for constructing reduced order models of structures which are divided into components in a natural way, such as engines and turbines, when the flexibility of each component has to be accounted for. A set of interface nodes, required for coupling of the substructures, are identified for the FE model of each substructure. The dofs at the interface nodes are retained when employing model order reduction, the other dofs being eliminated. Model order reduction is a Ritz procedure [4], selecting a number of basis vectors to approximate the deflection of the full model. Usually, the reduced models include deflection patterns caused by static loads acting on each interface dof, resulting in exact responses for static load cases. The dynamics of the eliminated dofs are approximated by including a set of additional Ritz basis vectors, in CMS by Craig and Bampton selected to be the eigenmodes of the substructure having the interface dofs constrained. Other model order reduction methods, offering alternative methods for selecting the Ritz basis vectors have been proposed and the efficiency of different reduction methods has been evaluated for various types of structures in [5–9]. In general, the reduced system matrices have large bandwidths, making substructures with more than a few thousand dofs infeasible to analyse. It can therefore be necessary to restrict the number of interface dofs of each substructure, which can be rather large in case the substructure is in contact with the surroundings at surfaces with dense node distribution.

In a methodology commonly adopted for interface reduction, an additional node, referred to as a condensation node, is introduced to act as the interface to other substructures. The condensation node has both translational and rotational dofs, resulting in six dofs in a three-dimensional analysis, and is coupled to the nodes of the interface surface by some constraints. The coupling between a condensation node and the interface surface can be realised in different ways, a rigid body constraint for the interface surface being the most common option. Alternatively, the forces and moments acting on the condensation node can be distributed to the nodes

of the interface surface by certain weight factors, resulting in the motion of the condensation node being a weighted average of the motion of the interface dofs. The two different types of coupling will be referred to here as rigid coupling and distributed coupling. These types of couplings are investigated in [10] and their respective advantages and drawbacks discussed. Rigid coupling will introduce additional stiffness in the model while distributed coupling is likely to underestimate the stiffness since it allows for sliding and penetration of the contact surfaces.

It should be noted that interface reduction is independent of the model order reduction of a substructure. The interface reduction will on the other hand affect the efficiency of the model order reduction since the Ritz basis vectors generated by a certain model order reduction method will be affected by the constraints imposed in the interface reduction. A number of studies have been presented in which the methodology of a condensation node is employed, for example, using rigid coupling in [11–13], distributed coupling in [14–16] and a combination of both types of couplings in [17]. There is, however, a lack of publications comparing the efficiency of different types of couplings for interface reduction. Moreover, the efficiency of different couplings are likely to vary to a great extent for different problems.

1.1 Timber Volume Elements

The lightweight properties of wood simplify the use of prefabrication in the construction process compared to conventional concrete buildings. A type of prefabricated multi-storey building in wood, increasing in popularity in Sweden, is timber volume element (TVE) buildings. A TVE is a prefabricated module consisting of floor-, roof- and wall elements completed with electrical installations, flooring, cabinets, wardrobes, finishing etc. Each TVE typically constitutes a small apartment, one room or part of a larger room. The TVEs are transported to the construction site where they are stacked to form a complete building. In Figure 1, the conceptual layout of a TVE building is illustrated, and in Figure 2, drawings of junctions between a floor-ceiling structure and an apartment separating wall (to the left) and a façade wall (to the right) are shown. An advantage regarding vibrations and acoustic performance is that a floor is structurally separated from the ceiling of the storey below; the upper volume contains the floor whereas the lower volume comprises the ceiling. In between volumes, elastomer blocks are placed on the flanks to reduce the vibration transmission through the junctions. The elastomers are frequency dependent visco-elastic materials, the properties of such a material being determined in [18]. The major structural connection between adjacent volumes is by means of the elastomers, the only additional connection being through a few tie plates used to fixate the TVEs.

1.2 Objective

The studies presented in the paper provide important input to a project aiming at enabling the modelling of an assembly of TVEs. A FE model of a single TVE, meshed to behave accurately up to 200 Hz, contains millions of dofs. Hence, model order reduction is required to analyse a complete assembly of modules, even when powerful computational resources available. The TVE buildings, consisting of stacked volume elements coupled by small elastomer blocks, is suitable for substructure modelling, considering each module as a substructure. Since the material properties of the elastomers are frequency-dependent, the blocks cannot be included in conventional substructures, which are described by constant, frequency-independent, system

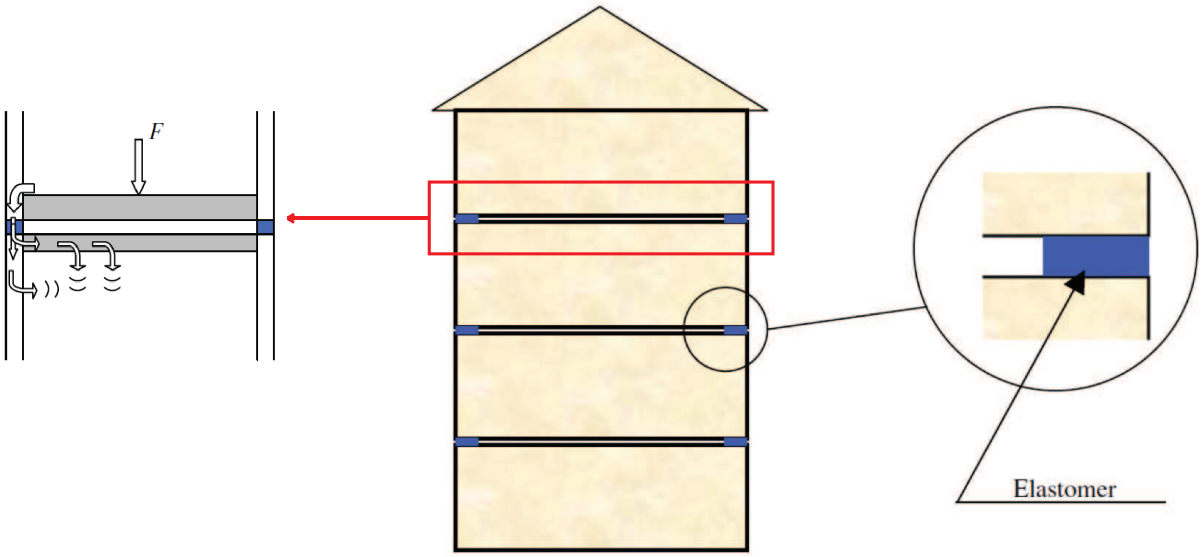

Figure 1: Sketch of a TVE building [19]. The path of structural vibrations between storeys is illustrated in the figure to the left and an elastomer block is illustrated in the figure to the right.

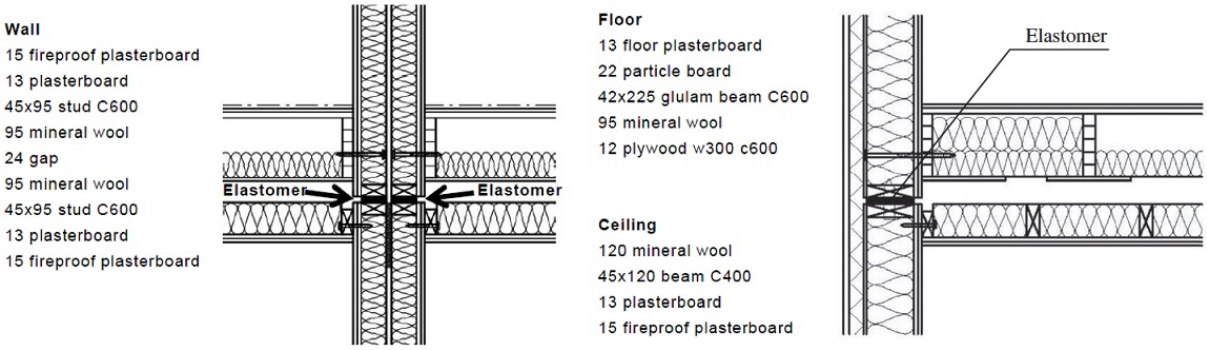

Figure 2: Drawings of the TVE building system, showing sections of a floor-ceiling structure and junctions with an apartment separating wall (left) and a façade wall (right).

matrices. Consequently, elastomer blocks will act as coupling elements, connecting the TVEs in the assembly of substructures.

Although a TVE is in contact with elastomer blocks only at small part of its surface, there is still a need for interface reduction since the TVEs can be connected to more than a hundred elastomer blocks, resulting in the total number of interface nodes being large. The methodology of using a condensation node is therefore employed to obtain efficient coupling of the substructures. Condensation nodes will be created both for the interface surfaces of the elastomer blocks and the TVEs. The displacement field of the elastomer blocks is not of interest, why the models of the elastomers can be modelled as some sort of coupling elements, describing the transfer function between the condensation nodes on each side of the blocks. Such an approach is described in Section 3. Section 4 presents a test model which was used for investigating how different methods for interface reduction affect the vibrations transmitted from a floor structure

to the ceiling below, having a geometry of the type found in TVE buildings. The models were created and analysed in the commercial FE software *Abaqus*.

2 Governing theory

When a model has been divided into substructures, two main issues have to be considered: selecting a reduced basis for each substructure and defining efficient coupling of the substructures. This section describes the general theory of model order reduction and, in specific, the method of CMS by Craig and Bampton, commonly employed in substructure modelling. Moreover, a mathematical description is presented for the constraints involved in the interface reduction methods employed in the studies presented in this paper.

2.1 Model order reduction

Assuming linear deformations, the dynamics of each substructure can be described by a FE system of equations of the following form [20]:

$$\mathbf{M}\ddot{\mathbf{u}} + \mathbf{C}\dot{\mathbf{u}} + \mathbf{K}\mathbf{u} = \mathbf{f}, \tag{1}$$

where $\mathbf{M, C, K} \in \mathbb{R}^{n\times n}$ are the mass, damping and stiffness matrices respectively, $\mathbf{f} = \mathbf{f}(t) \in \mathbb{R}^{n\times 1}$ is the load vector and $\mathbf{u} = \mathbf{u}(t) \in \mathbb{R}^{n\times 1}$ is the state vector. A dot denotes differentiation with respect to time, t. The objective of model reduction is to find a system of m dofs in which $m << n$, one which preserves the dynamic characteristics of the full model. The general approach is to approximate the state vector by use of the transformation $\mathbf{u} = \mathbf{T}\mathbf{u}_R$, where $\mathbf{T} \in \mathbb{R}^{n\times m}$ is a transformation matrix and $\mathbf{u}_R \in \mathbb{R}^{m\times 1}$ is a reduced state vector. Applying the transformation in question to Eq. (1) results in

$$\mathbf{M}_R\ddot{\mathbf{u}}_R + \mathbf{C}_R\dot{\mathbf{u}}_R + \mathbf{K}_R\mathbf{u}_R = \mathbf{f}_R, \tag{2}$$

$$\mathbf{M}_R = \mathbf{T}^T\mathbf{M}\mathbf{T}, \quad \mathbf{K}_R = \mathbf{T}^T\mathbf{K}\mathbf{T}, \quad \mathbf{C}_R = \mathbf{T}^T\mathbf{C}\mathbf{T}, \quad \mathbf{f}_R = \mathbf{T}^T\mathbf{f}, \tag{3}$$

where $\mathbf{M}_R, \mathbf{K}_R, \mathbf{C}_R \in \mathbb{R}^{m\times m}$ are the reduced mass, damping and stiffness matrices respectively and $\mathbf{F}_R \in \mathbb{R}^{m\times 1}$ is the reduced load vector. The dofs in the reduced state vector can be divided into two categories: physical dofs and generalised coordinates. Physical dofs are the dofs of the full system that are retained in the reduction process, whereas the generalised coordinates represent the amplitudes of various Ritz basis vectors that describe deflection shapes of the full model that are allowed in the reduced model.

In recent decades, many different model order reduction methods, involving procedures of varying types for establishing the transformation matrix and the reduced state vector involved, have been proposed in the literature. Guyan (static) reduction [21], Improved reduction system (IRS) [22] and CMS by Craig and Bampton [3] and by Craig and Chang [23] are examples of methods with physical interpretation, specifically developed for problems in structural dynamics, while methods based on Krylov subspace iterations [24] and balanced truncation [25], originating from control theory, can be employed for structural dynamics as well.

2.1.1 Component Mode Synthesis by Craig and Bampton

The first step in obtaining a system reduced according to CMS by Craig and Bampton is to perform a static reduction, retaining only the interface dofs. In the derivations below, the interface dofs are referred to as master dofs (m) and the remaining dofs referred to as slave dofs (s). Partitioning the state vector in terms of the master and slave categories enables the system matrices in Eq. (1) to be partitioned into sub-blocks as follows:

$$\begin{bmatrix} \mathbf{M}_{mm} & \mathbf{M}_{ms} \\ \mathbf{M}_{sm} & \mathbf{M}_{ss} \end{bmatrix} \begin{bmatrix} \ddot{\mathbf{u}}_m \\ \ddot{\mathbf{u}}_s \end{bmatrix} + \begin{bmatrix} \mathbf{K}_{mm} & \mathbf{K}_{ms} \\ \mathbf{K}_{sm} & \mathbf{K}_{ss} \end{bmatrix} \begin{bmatrix} \mathbf{u}_m \\ \mathbf{u}_s \end{bmatrix} = \begin{bmatrix} \mathbf{f}_m \\ \mathbf{f}_s \end{bmatrix}. \tag{4}$$

Solving the equation in the second row in Eq. (4) for $\mathbf{u}_s$ results in

$$\mathbf{u}_s = -\mathbf{K}_{ss}^{-1} \left(\mathbf{M}_{sm} \ddot{\mathbf{u}}_m + \mathbf{M}_{ss} \ddot{\mathbf{u}}_s + \mathbf{K}_{sm} \mathbf{u}_m \right), \tag{5}$$

where it has been assumed that there are no loads acting on the slave dofs, so that $\mathbf{f}_s = \mathbf{0}$. The inertia terms in Eq. (5) are neglected, resulting in the following transformation of the state vector for Guyan reduction:

$$\begin{bmatrix} \mathbf{u}_m \\ \mathbf{u}_s \end{bmatrix} = \begin{bmatrix} \mathbf{I} \\ -\mathbf{K}_{ss}^{-1} \mathbf{K}_{sm} \end{bmatrix} \mathbf{u}_m = \mathbf{T}_{\text{Guyan}} \mathbf{u}_m. \tag{6}$$

The inertia terms neglected in the condensation are compensates for by including a set of generalised coordinates $\boldsymbol{\xi}$. These generalised coordinates represent the amplitudes of a set of eigenmodes for the slave structure, calculated with the master dofs being fixed. Setting $\mathbf{u}_m = \mathbf{0}$ and $\mathbf{f}_s = \mathbf{0}$ in Eq. (4) and assuming a harmonic solution results in the following eigenvalue problem:

$$\mathbf{K}_{ss} \Phi = \lambda \mathbf{M}_{ss} \Phi, \tag{7}$$

which can be solved for the eigenmodes Φ and the eigenvalues λ. A number of eigenmodes obtained from Eq. (7), referred to as retained eigenmodes, are selected as additional basis vectors to the approximation of the slave dofs in Eq. (6), resulting in

$$\mathbf{u}_s = -\mathbf{K}_{ss}^{-1} \mathbf{K}_{sm} \mathbf{u}_m + \sum \Phi_i \xi_i = \boldsymbol{\Psi} \mathbf{u}_m + \boldsymbol{\Phi} \boldsymbol{\xi}, \tag{8}$$

which gives the transformation of the state vector for CMS by Craig and Bampton:

$$\begin{bmatrix} \mathbf{u}_m \\ \mathbf{u}_s \end{bmatrix} = \begin{bmatrix} \mathbf{I} & \mathbf{0} \\ \boldsymbol{\Psi} & \boldsymbol{\Phi} \end{bmatrix} \begin{bmatrix} \mathbf{u}_m \\ \boldsymbol{\xi} \end{bmatrix} = \mathbf{T}_{\text{CMS}} \begin{bmatrix} \mathbf{u}_m \\ \boldsymbol{\xi} \end{bmatrix}. \tag{9}$$

The accuracy of the reduced model depends upon the selection of retained eigenmodes, certain eigenmodes having a larger influence than others on the solution of a specific problem. To obtain a reduced model with as great an accuracy for general load distributions as possible, however, all the eigenmodes up to some chosen limit should be included, all eigenmodes below twice the highest frequency of interest being a rule of thumb. Substructures described by systems of the form in Eq. (9) can be coupled at the interface dofs, $\mathbf{u}_m$, either by a direct assembling procedure or by use of Lagrange multipliers [20].

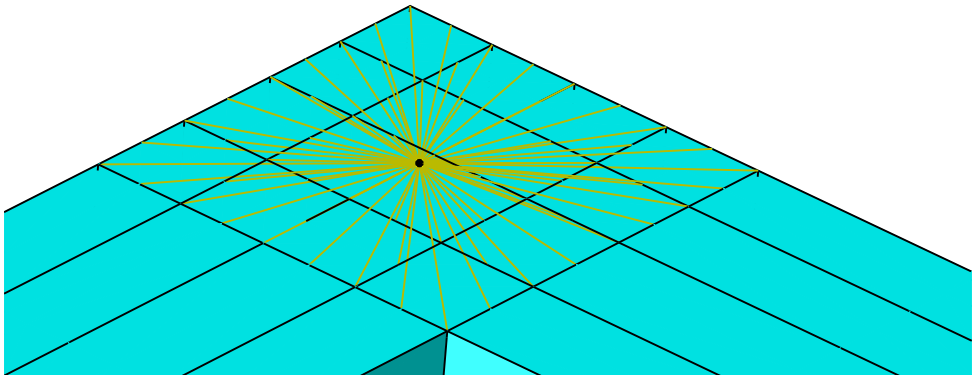

Figure 3: Illustration of a condensation node (black dot) coupled to the nodes of an interface surface, the constraints being illustrated by the yellow lines.

2.2 Interface reduction

Without the use of interface reduction, the vector $\mathbf{u}_m$ in Eq. (4) will contain all dofs of the interface surfaces for a certain substructure, making the model order reduction inefficient in case the number of interface nodes is large. The efficiency can be improved by coupling the dofs of each interface surface to a condensation node, as illustrated in Figure 3, resulting in $\mathbf{u}_m$ containing only the dofs of the condensation nodes. In the simplest approach, a rigid coupling between an interface surface and its condensation node is assumed, such that the displacements $\mathbf{u}_i$ in node i of the interface surface is described by

$$\mathbf{u}_i = \mathbf{u}_c + \boldsymbol{\Theta}_c \times \mathbf{r}_{ci}, \tag{10}$$

assuming small deformations. $\mathbf{u}_c$ and $\boldsymbol{\Theta}_c$ are the displacements and rotations of the condensation node respectively and $\mathbf{r}_{ci}$ is the vector from the condensation node to node i of the interface surface. In case two connecting substructures have very different stiffness properties, a rigid coupling is likely to provide acceptable results for the softer surface. If the additional stiffness introduced by the rigid coupling, however, results in large errors, a distributed coupling can be a more suitable alternative. In a distributed coupling, the forces and moments acting on the condensation node are distributed over the nodes of the interface surface according to

$$\mathbf{f}_i = \hat{\omega}_i \left(\mathbf{f}_c + \left(\mathbf{T}^{-1} \left(\mathbf{m}_c + \mathbf{r}_c \times \mathbf{f}_c \right) \right) \times \mathbf{r}_i \right), \tag{11}$$

$$\mathbf{T} = \sum_i \hat{\omega}_i \left(\left(\mathbf{r}_i \cdot \mathbf{r}_i \right) \mathbf{I} - \left(\mathbf{r}_i \mathbf{r}_i \right) \right), \tag{12}$$

$$\mathbf{r}_i = \mathbf{x}_i - \bar{\mathbf{x}}, \qquad \mathbf{r}_c = \mathbf{x}_c - \bar{\mathbf{x}}, \tag{13}$$

$$\bar{\mathbf{x}} = \sum_i \hat{\omega}_i \mathbf{x}_i, \qquad \hat{\omega}_i = \frac{\omega_i}{\sum_i \omega_i}, \tag{14}$$

where $\mathbf{f}_i$ is the force acting on node i of the interface surface, $\mathbf{f}_c$ and $\mathbf{m}_c$ are the force and moment acting on the condensation node, $\mathbf{x}_i$ and $\mathbf{x}_c$ are the coordinates of node i and the condensation

node respectively and ω_i is the weight factor for node i. The method of distributing the forces and moments leads to the motion of the condensation node being a weighted average of the displacements in the interface surface nodes,

$$\mathbf{u}_c = \sum_i \hat{\omega}_i \mathbf{u}_i, \tag{15}$$

$$\mathbf{\Theta}_c = \sum_i \hat{\omega}_i \frac{\mathbf{r}_{ci}}{|\mathbf{r}_{ci}|^2} \times \mathbf{u}_i. \tag{16}$$

The weight factors are arbitrary, meaning that an infinite number of distributed coupling methods can be defined. Four methods for determining the weight factors, all implemented in *Abaqus*, are presented below. The most straightforward method is uniform weighting, distributing equal load to all nodes of the interface surface. The three remaining methods employ decreasing weight at farther distance from the condensation node, using polynomials of different degrees.

Uniform weighting

$$\omega_i = 1. \tag{17}$$

Linearly decreasing weighting

$$\omega_i = 1 - \left| \frac{\mathbf{r}_{ci}}{\mathbf{r}_{c0}} \right|, \tag{18}$$

where $\mathbf{r}_{c0}$ is the vector from the condensation node to the furthest node at the interface surface.

Quadratically decreasing weighting

$$\omega_i = 1 - \left| \frac{\mathbf{r}_{ci}}{\mathbf{r}_{c0}} \right|^2. \tag{19}$$

Cubically decreasing weighting

$$\omega_i = 1 - 3\left| \frac{\mathbf{r}_{ci}}{\mathbf{r}_{c0}} \right|^2 + 2\left| \frac{\mathbf{r}_{ci}}{\mathbf{r}_{c0}} \right|^3. \tag{20}$$

3 Elastomer blocks as coupling elements

The elastomer layers were, in the numerical studies presented here, modelled as blocks of Sylodyn®, a closed-cell polyurethane material manufactured by Getzner Werkstoffe G.m.b.H. A Sylodyn elastomer block of size $100 \times 95 \times 25$ mm^3, used in real TVE buildings, was studied, the FE mesh being shown in Figure 4. In [18], frequency-dependent viscoelastic material parameters were evaluated for a type of Sylodyn, these parameters being employed here.

Having frequency-dependent substructures is possible in steady-state analyses but results in inefficient models since different system matrices are required for each frequency step in the analyses. It is therefore preferable to exclude the elastomer blocks from the substructures

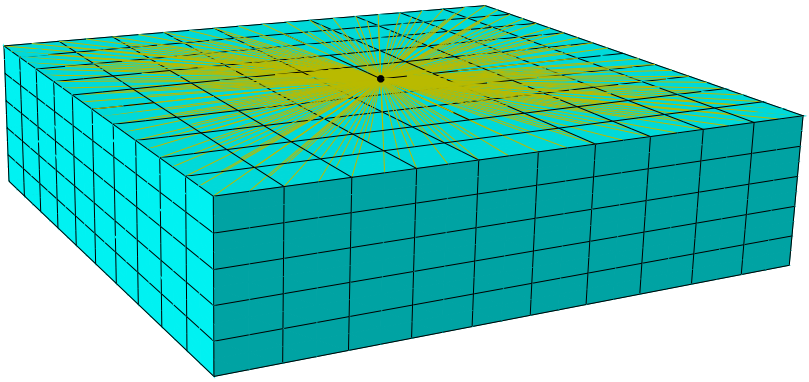

Figure 4: The FE mesh for the model of an elastomer block. The black dot illustrates a condensation node and the yellow lines the constraints between the condensation node and the interface surface.

because of their frequency-dependent material properties. This results in the substructures being described by constant, frequency-independent, system matrices.

In substructure models of TVE buildings, the elastomer blocks can be regarded as coupling elements connecting the substructures of TVE modules. The interface surfaces are the top and bottom surfaces of the elastomer blocks, these being reduced by introducing condensation nodes as illustrated in Figure 4, resulting in a total of twelve interface dofs per elastomer block. The elastomers are in general much softer than the wood components they are connected to. Consequently, the interface surfaces of the elastomer blocks are exposed to relatively small strains compared to the rest of the blocks, implying rigid coupling to be a good approximation in the interface reduction.

The displacement field in the elastomer blocks are in general not of interest, why the full model of a block may be replaced by some sort of simplified coupling element connecting the condensation nodes on each side. It is assumed here that the elastomer block can be represented by six frequency-dependent spring-damper systems connecting each of the six dofs, three translations and three rotations, of the two condensation nodes. The motion of a parallel spring-damper system connecting two nodes with displacements u_1 and u_2 is described by

$$k \begin{bmatrix} 1 & -1 \\ -1 & 1 \end{bmatrix} \begin{bmatrix} u_1 \\ u_2 \end{bmatrix} + c \begin{bmatrix} 1 & -1 \\ -1 & 1 \end{bmatrix} \begin{bmatrix} \dot{u}_1 \\ \dot{u}_2 \end{bmatrix} = \begin{bmatrix} f_1 \\ f_2 \end{bmatrix}, \tag{21}$$

where k is the stiffness coefficient, c the damping coefficient and f_1 and f_2 the forces acting on the two nodes. By assuming $u_1 = 0$ and a harmonic load and response for the system,

$$f_2 = F_2 exp(i\omega t), \quad u_2 = U_2 exp(i\omega t) \tag{22}$$

where F_2 and U_2 are the complex force and load amplitudes and ω the angular frequency, Eq. (21) is reduced to

$$k(\omega)U_2 + i\omega c(\omega)U_2 = F_2, \tag{23}$$

where the frequency dependence of $k(\omega)$ and $c(w)$ is introduced. Applying a unit load, $F_2 = 1$, results in

$$k(\omega) + i\omega c(\omega) = \frac{1}{U_2}, \tag{24}$$

which is used to identify $k(\omega)$ and $c(w)$ as

$$k(\omega) = \text{Re}\left(\frac{1}{U_2}\right), \quad c(\omega) = \frac{1}{\omega}\text{Im}\left(\frac{1}{U_2}\right). \tag{25}$$

The two condensation nodes of the elastomer block shown in Figure 4 have the translational dofs $u^1_{1,2,3}$ and $u^2_{1,2,3}$ respectively and the rotational dofs $\Theta^1_{1,2,3}$ and $\Theta^2_{1,2,3}$ respectively, where the superscripts denote the condensation node and the subscripts denotes the direction of the dof. The forces acting on the two condensation nodes are denoted $f^1_{1,2,3}$ and $f^2_{1,2,3}$ and the momentums denoted $m^1_{1,2,3}$ and $m^1_{1,2,3}$. Replacing the elastomer block with six frequency-dependent spring-damper systems of the form in Eq. (21) results in the following equation system describing the block:

$$\mathbf{K}\mathbf{u} + \mathbf{C}\dot{\mathbf{u}} = \mathbf{f}, \tag{26}$$

$$\mathbf{K}(\omega) = \begin{bmatrix} \mathbf{K}^u_1(\omega) & \mathbf{0} & \cdots & & \cdots & \mathbf{0} \\ \mathbf{0} & \mathbf{K}^u_2(\omega) & & & & \\ \vdots & & \mathbf{K}^u_3(\omega) & & & \\ & & & \mathbf{K}^\Theta_1(\omega) & & \vdots \\ \vdots & & & & \mathbf{K}^\Theta_2(\omega) & \mathbf{0} \\ \mathbf{0} & \cdots & & \cdots & \mathbf{0} & \mathbf{K}^\Theta_3(\omega) \end{bmatrix},$$

$$\mathbf{C}(\omega) = \begin{bmatrix} \mathbf{C}^u_1(\omega) & \mathbf{0} & \cdots & & \cdots & \mathbf{0} \\ \mathbf{0} & \mathbf{C}^u_2(\omega) & & & & \\ \vdots & & \mathbf{C}^u_3(\omega) & & & \\ & & & \mathbf{C}^\Theta_1(\omega) & & \vdots \\ \vdots & & & & \mathbf{C}^\Theta_2(\omega) & \mathbf{0} \\ \mathbf{0} & \cdots & & \cdots & \mathbf{0} & \mathbf{C}^\Theta_3(\omega) \end{bmatrix},$$

$$\mathbf{u}^T = \begin{bmatrix} u^1_1 & u^2_1 & u^1_2 & u^2_2 & u^1_3 & u^2_3 & \Theta^1_1 & \Theta^2_1 & \Theta^1_2 & \Theta^2_2 & \Theta^1_3 & \Theta^2_3 \end{bmatrix},$$

$$\mathbf{f}^T = \begin{bmatrix} f^1_1 & f^2_1 & f^1_2 & f^2_2 & f^1_3 & f^2_3 & m^1_1 & m^2_1 & m^1_2 & m^2_2 & m^1_3 & m^2_3 \end{bmatrix},$$

where $\mathbf{K}^{u,\Theta}_{1,2,3}, \mathbf{C}^{u,\Theta}_{1,2,3} \in \mathbb{R}^{2\times 2}$ are the stiffness and damping matrices as defined in Eq. (21) for each of the six spring-damper systems. Eq. (25) can be used to identify all the matrices $\mathbf{K}^{u,\Theta}_{1,2,3}$ and $\mathbf{C}^{u,\Theta}_{1,2,3}$ by studying one of the six spring-damper systems at a time, locking eleven of the twelve interface dofs and applying a unit force/momentum at the free dof. This approach neglects any coupling between the dofs acting in different directions, as seen by the zero terms

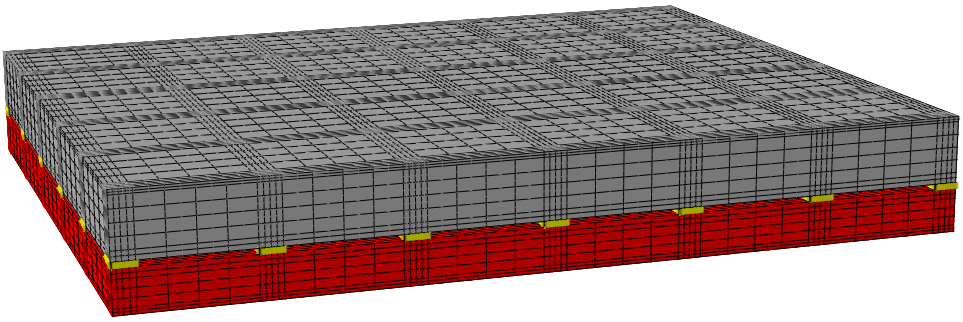

Figure 5: The FE mesh for the model of the floor-ceiling structure. The floor is shown in grey, the ceiling in red and the elastomer blocks in yellow.

E_1	E_2	E_3	G_{12}	G_{13}	G_{23}	ν_{12}	ν_{13}	ν_{23}	ρ
8500	350	350	700	700	50	0.2	0.2	0.3	432

Table 1: The material parameters used for the wooden beams, the stiffness parameters being given in terms of MPa and the density in kg/m^3.

in the system matrices in Eq. (26). The full matrices can be determined by applying a unit displacement at one dof at a time, where the corresponding column of the stiffness and damping matrices are determined from the real and imaginary parts of the reaction forces/momentums, respectively. Involving the full matrices would require user implemented elements to be employed in commercial FE software. The spring-damper systems can, however, be employed directly in such software, a practical advantage when dealing with models involving many different coupling elements. The validity of employing the spring-damper approach for modelling the elastomer blocks was checked in the test model presented in the following section.

4 Test model

A model of a floor-ceiling structure in wood, the FE mesh being shown in Figure 5, was investigated in order to compare the accuracy of different methods for interface reduction. The structure is $3690 \times 3045 \times 510$ mm^3 large, with the floor and ceiling consisting of five load-bearing wooden beams each, the floor having a particle board surface and the ceiling having a plaster board surface. Both the floor and the ceiling have beams placed at the ends of the load-bearing beams, perpendicular to these, creating box-like structures. The orthotropic material properties in Table 1 was employed for the wood beams and the isotropic properties in Table 2 was employed for the particle board and the plaster board. The floor and ceiling structures are connected through elastomer blocks with dimensions $95 \times 100 \times 25$ mm^3, having the frequency-dependent viscoelastic material properties determined in [18]. The blocks were placed at a centre-to-centre distance of 600 mm around the flanks and provide the only connection between the floor and the ceiling.

	E	ν	ρ
Particle board	3000	0.3	767
Plaster board	2000	0.2	692

Table 2: The material parameters used for the particle board and the plaster board, the modulus of elasticity being given in terms of MPa and the density in kg/m^3

The floor-ceiling structure was analysed by steady-state analyses for frequencies up to 200 Hz, applying a vertical unit load at the middle of the floor surface and having the displacements at the four corners of the ceiling surface locked. In order to investigate the vibration transmission from the floor to the ceiling when employing different methods for reducing the interface surfaces to the elastomer blocks, the vibration amplitudes in the nodes at the ceiling surface was evaluated by a root-mean-square (RMS) value of the complex magnitudes of the displacements. Due to symmetry, the displacements were evaluated in a forth of the ceiling surface. For each frequency step in the steady-state analyses, the RMS value was calculated as

$$u_{RMS}(f) = \sqrt{\frac{1}{n}\sum_{i=1}^{n} U_i(f)^2}, \tag{27}$$

where U_i is the magnitude of the three complex displacement magnitudes in node i, n is the number of nodes in a forth of the ceiling surface and f is frequency. The model employing interface reduction was compared to the full model by calculating a relative error in RMS-values according to

$$u^{\text{error}}_{RMS}(f) = \frac{\left| u^{red}_{RMS}(f) - u^{full}_{RMS}(f) \right|}{u^{full}_{RMS}(f)} \cdot 100, \tag{28}$$

where u^{red}_{RMS} is the RMS value of a model employing interface reduction and u^{full}_{RMS} is the RMS value of the full model. The quotient is multiplied by 100 to obtain the relative error in percent. In the result figures presented here, green, blue and red dashed lines are included to indicate the 0.1 %, 1 % and 10 % error levels.

First, the validity of employing the spring-damper approach for modelling the elastomer blocks was checked. This was carried out by modelling the interface surfaces between elastomer blocks and wood components as rigid in the full model. A model employing the spring-damper systems for the elastomer blocks, with the interface surfaces of the wood components being modelled as rigid, was compared to the full model with rigid interface surfaces. In case the spring-damper systems would represent the full model of an elastomer block exactly, the two models would yield precisely the same results since the properties of the spring-damper systems were evaluated assuming rigid interface surfaces. The relative error of the model employing the spring-damper systems, compared to the full model with rigid interface surfaces, is shown in Figure 6. It can be observed that the error is lower than 1 % for most frequencies, the exception being frequencies between 30-100 Hz where the error reaches a maximum of 4 %. Consequently, the spring-damper systems offer a fairly good representation of the full model of an elastomer block. In the results presented below, where different interface reduction meth-

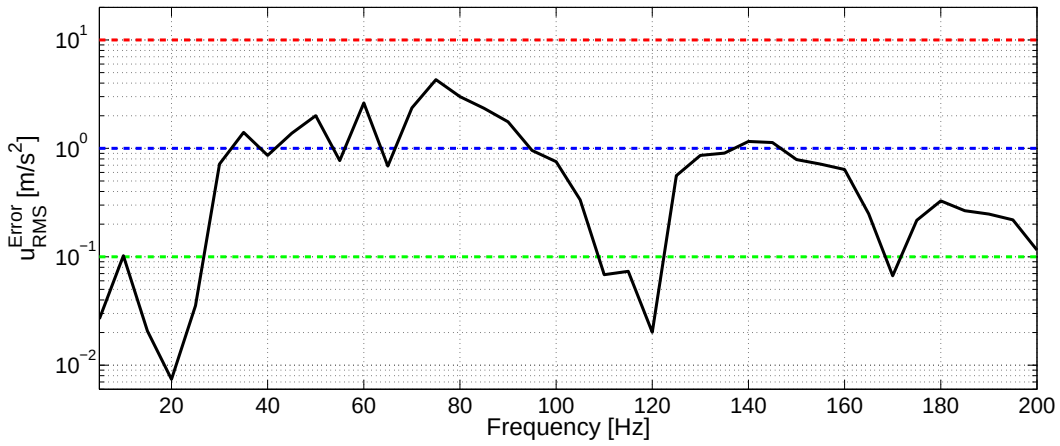

Figure 6: Relative error in RMS values when employing the spring-damper representation of an elastomer block, compared to a full model with rigid interface surfaces.

	Distributed Uniform	**Distributed linear**	**Distributed quadratic**	**Distributed cubic**	**Rigid**
Maximum error (%)	4.47	4.51	4.52	4.56	5.86
Average error (%)	1.00	1.06	1.01	1.25	1.66

Table 3: Maximum and average values of the relative errors in RMS values when employing the five different methods for interface reduction.

ods are compared, the spring-damper systems were employed in the models (the full model of course involving the full elastomer block models, without assuming rigid interface surfaces).

The five different methods for interface reduction (rigid coupling and four variants of distributed coupling) were employed at the interface surfaces of the floor and the ceiling. In Figure 7, the spectra of relative errors obtained when employing the five methods, compared to the full model, is shown and in Table 3, the maximum and average values of the error spectra are presented. It can be observed that a rigid coupling for the interface surfaces is the least accurate method, especially at lower frequencies (< 60 Hz). The different variants of distributed coupling provide similar results, a lower degree of the weighting polynomial in general resulting in lower errors, with uniform weighting providing the best accuracy regarding both maximum and average errors. Rigid coupling can, however, be the most suitable method in certain situations, depending on the frequencies of interest. It can be observed in Figure 7 that the errors obtained when employing rigid coupling is significantly lower than that of the distributed coupling methods for frequencies between 130-150 Hz.

Finally, it was investigated how employing distributed coupling for the interface surfaces of the elastomer blocks affects the accuracy. The properties of the spring-damper systems replacing the full models of the elastomer blocks were, consequently, evaluated when employing distributed coupling. The relative errors obtained when employing distributed coupling with

uniform weighting for the elastomer blocks are shown in Figure 8, using both rigid coupling and distributed coupling, also with uniform weighting, for the interface surfaces of the floor and the ceiling. It can be observed how the errors levels are very high in comparison to the results shown in Figure 7, where rigid couping was employed for the interface surfaces of the elastomer blocks. As discussed in Section 3, where rigid coupling was assumed to be suitable for interface reduction of the elastomer blocks, this can be explained by the large difference in stiffness between the wood components and the elastomer blocks, resulting in relatively small strains at the interface surfaces compared to the strains in the rest of the elastomer blocks.

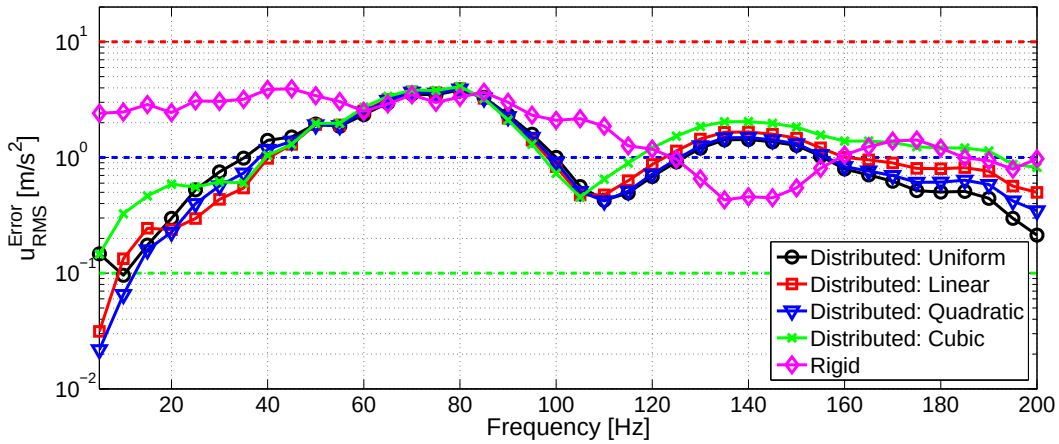

Figure 7: Relative error in RMS values when employing the five different methods for interface reduction.

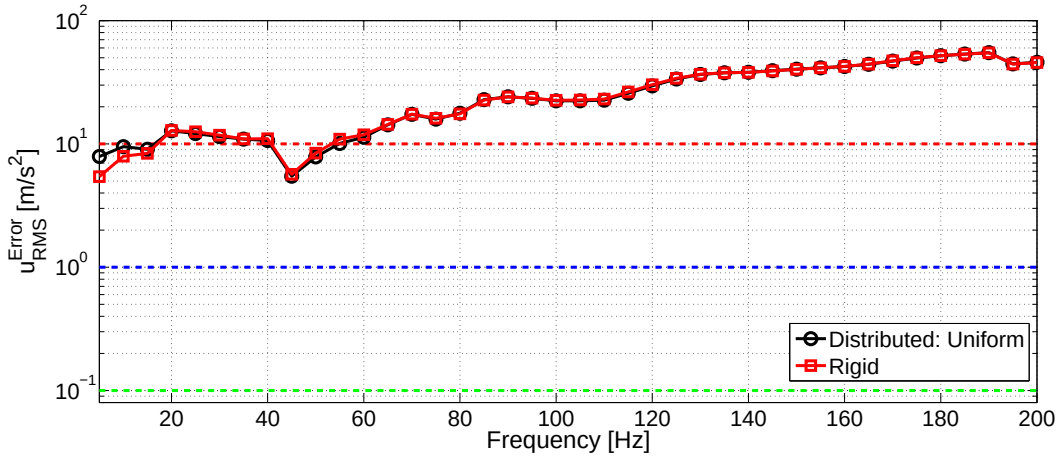

Figure 8: Relative error in RMS values when employing distributed coupling with uniform weighting for the interface surfaces of the elastomer blocks. The two plots show the errors when employing rigid coupling and distributed coupling with uniform weighting for the interface surfaces of the floor and the ceiling.

5 Conclusions

The results presented in the paper provide important information in the process of establishing efficient substructure models of multi-storey buildings in wood. It was investigated, by numerical studies on a test model, how the interface surfaces should be treated when employing the methodology of condensation nodes for interface reduction.

The frequency-dependent spring-damper systems, employed as simplified coupling elements representing the elastomer blocks, proved to model the coupling between the two condensation nodes of the elastomer blocks fairly good. Depending on the required level of accuracy, it may, however, be necessary to include the full matrices coupling all dofs of the two condensation nodes and not only the corresponding dofs of each node, as is the case when employing the spring-damper systems. The reasons for not including the full coupling matrices are purely practical, simplifying the modelling process when working with commercial FE software.

For the elastomer blocks, rigid coupling at the interface surfaces was superior to distributed coupling, the latter resulting in very large errors. For the interface surfaces of the wood components (the floor and the ceiling in the test model) distributed couplings was the most accurate method, a lower degree of the weighting polynomial in general resulting in lower errors. Depending on the frequencies of interest, however, a rigid coupling can be the most suitable alternative in certain cases.

Acknowledgements

The financial support for this work provided by the Silent Spaces project, a part of the EU program Interreg IV A, is gratefully acknowledged.

References

[1] Stehn L., Rask L.O., Nygren I. Östman B., Byggandet av flervåningshus i trä – Erfarenheter efter tre års observation av träbyggandets utveckling. Technical Report, Luleå University of Technology, Sweden, 2008.

[2] Gustavsson L., Pingoud K., Sathre R. Carbon dioxide balance of wood substitution: comparing concrete- and wood-framed buildings. Mitig Adapt Strateg Glob Change, 2006;11:667–691.

[3] Craig R.R., Bampton M. Coupling of substructures in dynamic analysis. AIAA J, 1968;6:1313–1319.

[4] Arnold R.R., Citerley R.L. Application of Ritz vectors for dynamic analysis of large structures. Comput Struct, 1985;21(5):901-907.

[5] Floden O., Reduction methods for the dynamic analysis of substructures of lightweight building structures, Unpublished results.

[6] Fehr J., Eberhard P. Simulation process of flexible multibody systems with non-modal model order reduction techniques. Multibody Syst Dyn, 2011;25(3):313-334.

[7] Nowakowski C., Kürschner P., Eberhard P., Benner P. Model reduction of an elastic crankshaft for elastic multibody simulations. J Appl Math and Mech, 2013;93(4):198-216.

[8] Koutsovasilis P., Beitelschmidt M. Comparison of model reduction techniques for large mechanical systems. Multibody Syst Dyn, 2008;20(2):111-128.

[9] Witteveen W. On the modal and non-modal model reduction of metallic structures with variable boundary conditions. World J Mech, 2012;2(6):311-324.

[10] Heirman G.H.K., Desmet W. Interface reduction of flexible bodies for efficient modeling of body flexibility in multibody dynamics. Multibody Syst Dyn, 2010;24(2):219–234.

[11] Albers A., Emmrich D., Haeussler, P. Automated structural optimization of flexible components using MSC.Adams/Flex and MSC.Nastran Sol200. 1th Europ MSC.ADAMS Users Conf, London, 2002.

[12] Albers A., Ottnad J., Weiler H., Haeussler P. Methods for lightweight design of mechanical components in humanoid robots. IEEE-RAS 7th Int Conf Humanoid Robots, Pittsburg, USA, 2007.

[13] Peeters J. Simulation of dynamic drive train loads in a wind turbine. PhD thesis, Katholieke Universiteit Leuven, Belgium, 2006.

[14] Helsen J., Heirman G., Vandepitte D., Desmet W. The influence of flexibility within multibody modeling of multi-megawatt wind turbine gearboxes. Proc ISMA 2008 Int Conf Noise Vibr Eng, 2008.

[15] Helsen J., Vandepitte D., Desmet W., Peeters J., Goris S., Vanhollebeke F., Marrant B., Meeusen W. From torsional towards flexible 6 dofs models for dynamic analysis of wind turbine gearboxes. Proc Europ Wind Energy Conf Exhib, Marseille, France, 2009.

[16] Kuratani F., Okuyama M., Yamauchi T, Washio S. Finite element modeling of spot welds for vibration analysis. 5th Asian Conf on Multibody Dyn, 2010;1:981-988.

[17] Ricci S. Model reduction techniques in flexible multibody dynamics with application to engine cranktrain simulation. PhD thesis, University of Bologna, Italy, 2013.

[18] Negreira J. Vibrations in lightweight buildings – Perception and prediction. Licentiate dissertation, Division of Engineering Acoustics, Lund University, Sweden, 2013.

[19] Ljunggren F., Ågren A.. Potential solutions to improved sound performance of volume based lightweight multi-storey timber buildings. Appl Acoust, 2011;72:231–240.

[20] Bathe K.J. Finite element procedures. Prentice Hall, New York, 1996.

[21] Guyan R.J. Reduction of stiffness and mass matrices. AIAA J 1965;3:380.

[22] O'Callahan J. A procedure for an improved reduced system (IRS) model. Proc 7th Int Modal Anal Conf, 1989;17–21.

[23] Craig R.R., Chang C.J. A review of substructure coupling methods for dynamic analysis. Adv Eng Sci, 1976;2:393-408.

[24] Lohmann B., Salimbahrami B. Introduction to Krylov subspace methods in model order reduction. Methods Appl Autom, 2003;1-13.

[25] Reis T., Stykel T. Balanced truncation model reduction of second-order systems. Math Comput Model Dyn Syst, 2008;14(5):391-406.